Breach Flow Modeled as Flow over a Weir

Master of Science Thesis

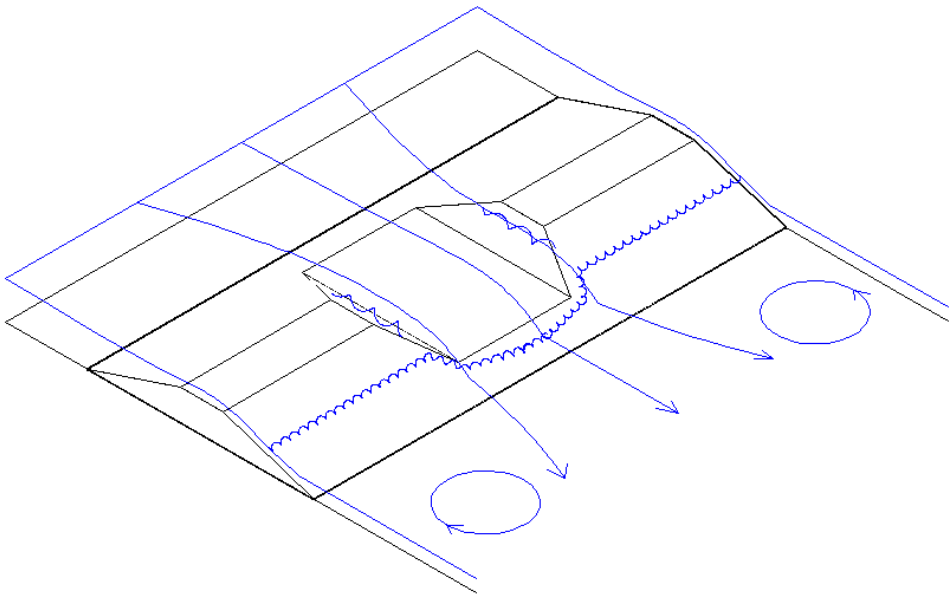

Yankai Ren

Department of Hydraulic Engineering
Faculty of Civil Engineering and Geosciences
Delft University of Technology

Graduation committee:

Prof. dr. ir. W.S.J. Uijttewaal	Section of Environmental Fluid Mechanics, TU Delft
Dr.ir. P.J. Visser	Section of Hydraulic Engineering, TU Delft
G. Zhao, MSc	Section of Hydraulic Engineering, TU Delft

January 2012

PREFACE

The thesis is written as a part of Master of Science Program in Hydraulic Engineering. The main goal of the report is to understand the effects of breach properties on the flow. A laboratory experiment was carried out in the Fluid Mechanics Laboratory of Delft University of Technology. Numerical model computations with Delft3D were done to compare the results with the experimental data.

I would like to thank the members of my graduation committee, prof. dr. ir. W.S.J. Uijttewaal, dr. ir. P.J. Visser and G. Zhao, for their thoughtful guidance and valuable suggestions. I am graceful to the staff members of the Fluid Mechanics Laboratory, S. de Vree and J.A. van Duin for their great support during the experiment. Also thanks to S. Ali and prof. dr. ir. G.S. Stelling for their practical advices. Finally, I would like to thank my parents for their support throughout my study in the Netherlands.

Yankai Ren

Delft, the Netherlands
January, 2012

ABSTRACT

The main objective of the study is to understand the effects of breach properties (e.g. the top width, the depth and the bottom width of the breach) on the breach flow. The breach flow was modeled as flow over a compound broad-crested weir. A laboratory experiment was carried out with a fixed weir model in a flume. Five cases with different breach properties were tested.

Firstly, the discharge coefficients for all cases were quantitatively determined. The calibrations were done under two flow conditions, namely emerged flow conditions (flow only through the breach) and overtopping flow conditions (flow through the compound cross-section of weir). In perfect weir situations, it turned out that the values of the discharge coefficient were below 1 and rather different in the two flow conditions. Particularly in the case of overtopping flow, the linear combination of traditional discharge equations was verified for predicting the discharge and the discharge distribution over the weir. In imperfect weir situations, submergence coefficient was introduced in emerged condition. Secondly, the dependence of the energy head loss caused by the weir on the upstream discharge and the downstream water depth was discussed in imperfect weir situations. The Form Drag model for estimating the energy head loss was proved to be applicable for the modeled breach flow. Thirdly, the local hydraulic characteristics of breach flow were described by means of velocity distribution, water level elevation and flow patterns appearing behind the weir. At last, the numerical model (Delft3D) was verified on the modeling of the present experiment by comparing with the experimental data.

The report provides the information for the breach flow which can be of use in the development of breach models, inundation models and compound weir design.

CONTENTS

LIST OF FIGURES

LIST OF TABLES

LIST OF SYMBOLS

(a). Latin Symbols

Symbol	Definition	Dimension
a	Depth of breach	$[m]$
A_1	Flow area in section of weir	$\left[m^2\right]$
A_2	Flow area in downstream	$\left[m^2\right]$
A_c	Flow area of critical flow	$\left[m^2\right]$
A_p	Piping flow area	$\left[m^2\right]$
b	Width of breach bottom	$[m]$
b_{top}	Top width of breach	$[m]$
b_i	Instantaneous width	$[m]$
$\bar{b}$	Depth-averaged width of breach	$[m]$
B	Width of the crest of the dam or weir	$[m]$
B_0	Flow width in upstream	$[m]$
B_1	Flow width in section of weir	$[m]$
B_2	Flow width in downstream	$[m]$
B_c	Width of dam (weir) crest	$[m]$
c_f	Friction coefficient	$\left[s/\sqrt{m}\right]$
C	Chézy coefficient	$\left[\sqrt{m}/s\right]$
C_1	Numerical coefficient of broad-crested weir flow	$\left[\sqrt{m^3}/s\right]$
C_2	Numerical coefficient of broad-crested weir flow	$\left[\sqrt{m}/s\right]$
C_d	Discharge coefficient	$[-]$
C_{db}	Discharge coefficient in the breach	$[-]$
C_{dc}	Discharge coefficient over the crest	$[-]$
C_{de}	Discharge coefficient in emerged condition	$[-]$
C_{do}	Discharge coefficient in overtopping condition	$[-]$
C_r	Dimensional coefficient for rectangular part	$\left[\sqrt{m}/s\right]$
C_s	Submergence coefficient	$[-]$
C_t	Dimensional coefficient for triangular part	$\left[\sqrt{m}/s\right]$

E	Specific energy	$[m]$
E_0	Upstream energy head	$[m]$
E_1	Energy head in section of weir	$[m]$
E_2	Downstream energy head	$[m]$
d	Water depth	$[m]$
d_0	Upstream water depth	$[m]$
d_1	Water depth over weir	$[m]$
d_2	Downstream water depth	$[m]$
d_b	Water depth in breach	$[m]$
d_c	Critical depth	$[m]$
d_t	tailwater depth immediately downstream of dam	$[m]$
D	Hydraulic diameter	$[m]$
f	Darcy–Weisbach friction factor	$[-]$
Fr	Froude number	$[-]$
Fr_m	Model value of Froude number	$[-]$
Fr_p	Prototype value of Froude number	$[-]$
g	Gravitational acceleration	$\left[m/s^2\right]$
g_m	Model value of gravitational acceleration	$\left[m/s^2\right]$
g_p	Prototype value of gravitational acceleration	$\left[m/s^2\right]$
h_0	Upstream water level above weir crest	$[m]$
h_1	Water level over weir	$[m]$
h_2	Downstream water level above weir crest	$[m]$
h_b	Elevation of breach bottom	$[m]$
h_p	Water level in polder	$[m]$
Δh	Water level difference	$[m]$
H	Total energy head	$[m]$
H_0	Upstream energy head above weir	$[m]$
H_{0b}	Upstream energy head above breach bottom	$[m]$
H_{0c}	Upstream energy head above weir crest	$[m]$
H_2	Downstream energy head above weir	$[m]$
ΔH	Energy loss	$[m]$

ΔH_{bed}	Energy loss caused by bed friction	$[m]$
ΔH_{wall}	Energy loss caused by wall friction	$[m]$
k_s	Friction height	$[m]$
l	Breach length	$[m]$
L	Characteristic length	$[m]$
L_m	Model value of characteristic length	$[m]$
L_p	Prototype value of characteristic length	$[m]$
L_w	Length of weir crest in direction of flow	$[m]$
m	Breach (side) slope	$[-]$
M	Weir slope	$[-]$
n	Manning coefficient	$\left[s/\sqrt[3]{m}\right]$
N	Scale parameter	$[-]$
N_L	Scale parameter of characteristic length	$[-]$
N_V	Scale parameter of flow velocity	$[-]$
N_v	Scale parameter of kinematic viscosity	$[-]$
p	Pressure	$[pa]$
P	Weir height	$[m]$
q	Discharge per unit width	$\left[m^2/s\right]$
Q	Total discharge	$\left[m^3/s\right]$
Q_b	Discharge through breach	$\left[m^3/s\right]$
Q_s	Discharge through spillway outlet	$\left[m^3/s\right]$
R	Hydraulic radius	$[m]$
Re	Reynolds number	$[-]$
Re_m	Model value of Reynolds number	$[-]$
Re_p	Prototype value of Reynolds number	$[-]$
S	Flow resistance slope	$[-]$
t	Time	$[s]$
u	Depth-averaged velocity in direction of flow	$[m/s]$
u_0	Upstream depth-averaged velocity in direction of flow	$[m/s]$
u_2	Downstream depth-averaged velocity in direction of flow	$[m/s]$
u_c	Critical flow velocity	$[m/s]$

V	Mean flow velocity	$[m/s]$
V_m	Model value of flow velocity	$[m/s]$
V_p	Prototype value of flow velocity	$[m/s]$
W	Width of flume	$[m]$
x	Longitudinal coordinate of flume	$[m]$
X	Parameter	$[-]$
X_m	Model value of parameter	$[m]$
X_p	Prototype value of parameter	$[m]$
y	Lateral coordinate of flume	$[m]$
z	Height above an arbitrary datum	$[m]$
z_b	Height of channel bottom above an arbitrary datum	$[m]$
z_c	Center-line elevation of initial breach	$[m]$
z_w	Elevation of breach bottom	$[m]$

(b). Greek Symbols

Symbol	Definition	Dimension
α_0	Energy coefficient in upstream	$[-]$
α_1	Energy coefficient in section of weir	$[-]$
β_1	Critical slope angle (Chapter 2) / Momentum coefficient in the section of weir (Chapter 3)	$[-]$
β_2	Momentum coefficient in downstream	$[-]$
ε	Relative crest length	$\left[m^2/s\right]$
ζ	Energy loss coefficient	$[-]$
θ	Angle between the breach side and the vertical	$[\deg]$
ν	Kinematic viscosity of the liquid	$\left[m^2/s\right]$
ν_m	Model value of kinematic viscosity	$\left[m^2/s\right]$
ν_p	Prototype value of kinematic viscosity	$\left[m^2/s\right]$
ρ	Flow density	$\left[kg/m^3\right]$
φ	Oblique angle of the weir	$[\deg]$
χ	Wet perimeter of the flow	$[m]$

CHAPTER 1. INTRODUCTION

1.1 Background

1.1.1 Flooding Events in the World

Flooding is one of the most frequent disasters that threaten human lives and habitats around the world. The history of mankind is full of events in which people struggled with floods. In some countries, the history of flooding can be even dated back to thousands years ago. The Netherlands, sometimes referred to as the 'sink' of Europe, has 26% of its area below mean sea level and 70% of the area would be flooded without coastal defense. Besides, three major European rivers, the Rhine, Meuse and Scheldt flow through the Netherlands. Due to the special geographic situation, the country is prone to storm surge and river flood. The history of Dutch water management dates from approximately 1000 AD, when people began to encircle their settlements with embankments (Visser, 1998). However, the history tells that more efforts were needed to reduce threatens of floods. For centuries, floods claimed many victims and losses, for instance, the great St. Elizabeth Deluge in 1421 caused tens of thousands of people died due to dike break. During the 20th century, in order to fulfill the objectives of being protected from the open sea and creating new agricultural land, one of the largest hydraulic engineering projects undertaken by the Dutch is the Zuiderzee Works consisting of dams, land reclamation and water drainage works. Nevertheless, the flood disaster in 1953 must be mentioned, the biggest natural disaster event in Dutch history and one of the worst floods in modem times in Europe. During the event, over 1800 people have died and about 4500 buildings were destroyed and seriously damaged with an enormous economic loss. Therefore, in response to the flood of 1953, the most well-known Delta Works including the Oosterschelde storm surge barrier were built. Nowadays, although the current defense systems are stronger than ever, the Dutch are facing the challenge of sea level rise and making efforts to improve the systems by the latest technology. Figure (1-1) shows the area vulnerable to flooding in the Netherlands and area drowned in 1953.

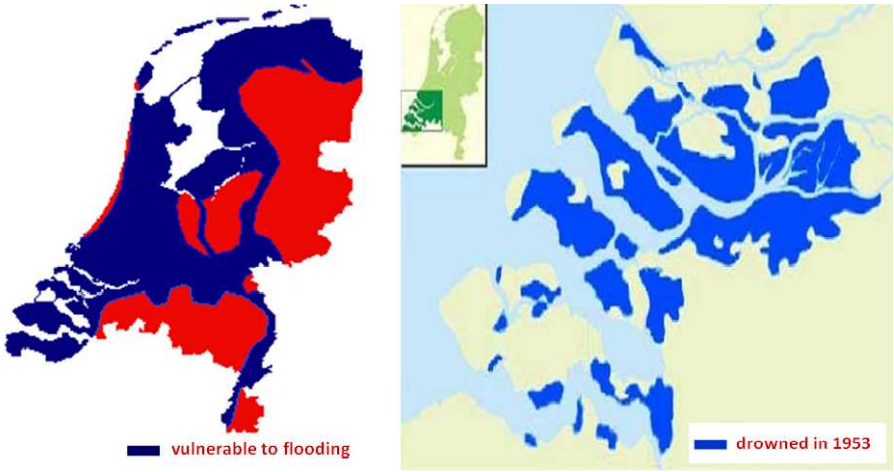

Figure (1 - 1): The Netherlands: Area vulnerable to flooding and area drowned in 1953 (Source: internet)

Besides the Netherlands, China also has a long history of flooding. The earliest historical document about flooding can be dated back to at least 4000 years ago when Great the Yu teaching the people techniques to tame rivers and lakes during an epic flood. According to historical data, around 1000 significant flood events were recorded in the period between 206 B.C. and 1949, averaging once in every two years (Zhang and Wen, 2001). The frequent occurrence of floods gave people the impulse to build flooding defense structures. The fatuous hydraulic project Dujiangyan was constructed in 256 BC in Sichuan province, China and it aimed for controlling the annual flooding of Min River combining the functions of irrigation and navigation. Surprisingly, it is still in use today to irrigate over 5,300 square kilometers of land in the region. In recent history, major rivers such as Yangtze and Yellow River (Figure (1-2)) in China were struck by a number of serious disastrous floods. Yangtze River is the longest river in China with a length of 6418 km and its river basin is home to one-third of China's population. The casualties of the Yangtze River flood in 1931 reached 145,000 people and affected 28.5 million. Afterwards, efforts were made to improve the flooding defense system, but the floods of 1954 and 1998 were still highly destructive and killed some 30,000 and 3,650 people respectively. Most recently in the summer of 2010, thanks to the accomplishment of Three Gorges Dam project in the Yangtze River, the flood was alleviated effectively but still killed several hundred people and caused extensive loss of property. The Yellow River, the second longest river in China with a length of 5464 km, has flooded 1,593 times in the last 3,000–4,000 years. The Yellow River floods (1887, 1931 and 1938) were three of the deadliest natural disasters ever recorded. These were caused by the overflow of dikes due to days of heavy rain and years of siltation. The result was devastating: around 900,000, 1,000,000 and 800,000 people were killed, respectively. These floods had catastrophic agricultural, economic and social impact in the history of China.

Figure (1 - 2): China: Yangtze River and Yellow River (Source: internet)

Floods also devastated many other areas in the world. In New Orleans, US, the city is protected by hundreds of miles of levees and flood gates. During Hurricane Katrina in 2005, the defense system failed and resulted in the inundation of approximately 50% of the metropolitan area and the death of 1,464 people. In Pakistan, in late July 2010, a flood caused by heavy monsoon rains affected about 20 million people with a death toll of close to 2,000. A series of floods hit Australia, at the beginning of December 2010, primarily in the state of Queensland and at least seventy towns and over 200,000 people were affected. In Thailand, a disastrous flooding took place from around July 2011 to December 2011, over 12.8 million people were affected and about six million hectares of land was inundated.

1.1.2 Inundation Modeling

Dams, dikes and weirs generally serve the primary purpose of retaining water for flood control, water supply, electricity generation, etc. However, at the same time, the potential of failure risks people's life. For the purpose of defending and predicting flood or storm surge, inundation models have been developed to obtain relevant information about the flood events, such as flood extent, flood propagation, water depth, etc. These provide people the basis for flood control, defense system design, catchment management and evolving of evacuation plans, etc. Figure (1-3) shows the elements that need to be analyzed in an inundation modeling. A flood inundation model can be one-dimensional, two-dimensional and three-dimensional. 1D models have the advantages of ease of calculation, parameterization and representation of hydraulic structures. 2D and 3D models are able to simulate minute hydraulic details but with the requirement of large computational times and sufficient data (Kuiry *et al.*, 2010). For instance, Ervine and MacCleod (1999) applied a steady-state one-dimensional river model to a river channel with distant flood banks by combining with channel-floodplain interaction methods. Beffa and Connell (2000) proposed a two-dimensional model to simulate flood plain flow with the help of a finite volume scheme. In the study of Li *et al.* (2006), a three-dimensional flood model was developed based on complete Reynolds-averaged Navier–Stokes equations including hydrodynamic pressure. Besides many inundation models are designed to simulate the flooding of natural lowland floodplains in a wide valley, in case of the inundation caused by breaching of dam, weir or dike (Han *et al.*, 1998; Ying and Wang, 2005; Li *et al.*, 2006).

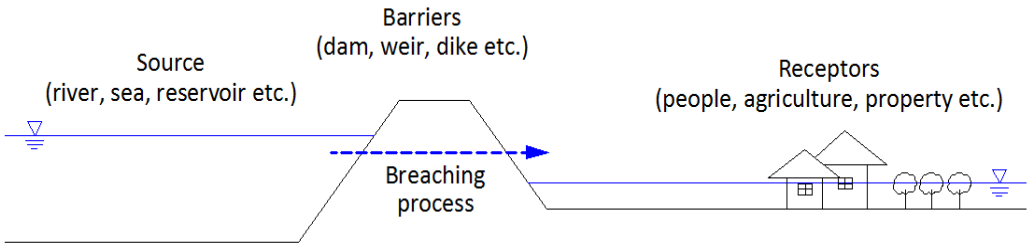

Figure (1 - 3): Description of elements in the flood defense system

1.1.3 Breach Modeling

Breach modeling is significant to understand the threats due to the potential failures of dams, dikes and weirs. The aims of predictions of dam failure are the outflow hydrograph of reservoir and the downstream routing hydrograph (Wahl, 2010). Predictions of the downstream flood inundation resulting from a failure of a dam, a dike or a weir first require investigation of the process of breaching as it has a significant influence on the flood, the discharge, hence the inundation. The breaching process is of great complication and uncertainty. The dam failures are of great complications and uncertainties which require the knowledge of hydraulics, hydrodynamics, sediment erosion, and geotechnical aspects (Singh *et al*, 1988). Many researchers have contributed to breach modeling (Fujita and Tamura, 1987; Wurbs 1987; Fread, 1988; Singh *et al*., 1988; Visser, 1998; Zhu, 2006; Macchione, 2008; Schmocker and Hager, 2009; Chang and Zhang, 2010). In general, the predicted key parameters in the models are the breach formation time and breach geometry including the maximum breach width, breach height, and the breach side slopes. The models have been developed based on different failure mechanisms, e.g. overtopping, piping and seepage, in addition, combinations of them. The target structure material could be sand, earth and clay or a mixture. In many models, an initial breach is assumed to be located at the crest and the shape of breach is usually schematized as triangular, rectangular, trapezoidal or parabolic. Thanks to these breach models, people have better understanding of breaching process and prediction of flood events has made rapid progress in recent years. Future sea level rise and river discharge increase due to climate change will increase the necessity of having good and reliable breach models.

1.1.4 Weir Flow

Experimental and field observations have indicated that flow over and through the breach can be simulated by the hydraulics of broad-crested weir flow (Chow, 1986). Weir flow is the basic topic in fluid mechanics and many investigations have been carried with regards to the weir flow (Bos 1985; Ramamurthy *et al.* 1988; Rijn 1990; Fritz and Hager 1998; Nguyen 2006; Sargison and Percy 2009; Ali and Uijttewaal 2009 & 2010). Weir flow can be considered rapidly varied and energy dissipated. Generally, an idealized equation is used to calculate the discharge over the weir, but in reality, the influence of energy losses, non-uniform velocity distribution and streamline curvature cannot be neglected. To account for these effects, discharge coefficient is introduced. Besides, some topics, such as critical flow, energy loss, velocity distribution over the weir etc., give people deep insight to the flow characteristics. The sketch of flow over a trapezoidal weir is shown in Figure (1-4) and more details about weir flow would be discussed in Chapter 3.

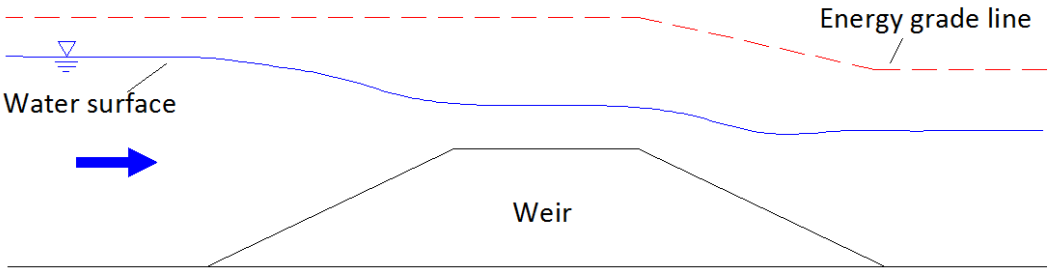

Figure (1 - 4): Sketch of flow over a broad-crested weir

1.2 Problem Description

Based on the above introductions, the necessity of breach flow study is clear. Although a considerable amount of investigations have been carried out on the breach models (see Chapter 2) and weir flow (see Chapter 3), the knowledge and information related to breach flow is incomplete. There are still questions about the effects of breach geometries to the flow. These are significant for studying the breaching process and the inundation process. To that end, further research of breach flow over weirs is required.

1.3 Objectives and Research Methods

The objectives of the study are:

(a). Understanding of the effects of breach properties (the top width, the depth and the bottom width of the breach) of broad-crested weirs on the flow.

(b). Qualitative description of hydraulic phenomena related to the breach flow.

(c). Improved tools on prediction of breach flow.

In order to achieve these purposes, weirs with various breach properties are to be accessed under different flow conditions. Firstly, the discharge coefficient needs to be quantitatively determined and the discharge distribution over the weir is about to be studied in overtopping condition. Secondly, the dependence of the energy head loss caused by the weir on the upstream discharge and the downstream water depth will be discussed. Thirdly, the characteristics of breach flow is to be described by means of velocity profiles, water level elevation and hydraulic phenomena occurring behind the weir, such as eddies and hydraulic jumps. In the study, the analytical solutions in literatures and numerical solutions based on a computer model (Delft3D) will be presented for predictions and comparisons.

1.4 Research Scope

The scope of the study is:

(a). The breach flow can be modeled as flow over a compound broad-crested weir. An idealized shape of breach is assumed to be located at the weir crest and only the breach properties would be varied for different cases.

(b). The attention of the study is focused on the hydraulic behavior and characteristics of the breach flow.

(c). The flow condition is considered steady and the dynamic processes (e.g. erosion and sediment transport) are not taken into account.

1.5 Outline of Thesis

Chapter 2 provides the background about the breach modeling including the information about the evolution of breach and discharge through the breach, etc. In Chapter 3, the literatures about flow over broad-crested weir are reviewed. The knowledge related to weirs with breach (compound weir) is included. Chapter 4 deals with the set-up and conduction of the experiment. Chapter 5 is presented to interpret and analyze the discharge through the weir, such as discharge coefficient. In Chapter 6, the energy head loss related to breach flow is discussed. The local hydraulic characteristics are presented in Chapter 7, including the velocity profiles, water level elevations and hydraulic phenomena occurring behind the weir. Chapter 8 gives the set-up and verifications of the numerical model (Delft3D). The comparisons of numerical and experimental results are stated in the chapter. Chapter 9 draws the conclusions and recommendations.

CHAPTER 2. BREACH GROWTH PROCESS

2.1 Introduction

Based on materials, dams or weirs can be classified into be homogeneous or zone-filled. The natural filled materials are usually rocks, earth or clay. The manmade materials are concrete, steel or timber. Different materials may lead to different failure mechanisms. In the particular case of earth dikes or dams, the most common failure modes are (Singh, 1996):

(a). Overtopping caused by extreme floods (hydraulic failure)

(b). Structural failure due to internal erosion or piping (hydraulic or geotechnical failure)

(c). Structural failure due to shear slide or foundation problems (geotechnical failure)

(d). Failure due to natural or induced seismicity

The mathematical models can be classified into parametric based or physically based models. Parametric based models frequently use key parameters (e.g. final breach geometry and breach formation duration) to simulate the breach growth as a simplified time-dependent process (e.g. linear increase of breach dimensions). This kind of models is generally simple and easy to use but weak in accuracy due to the lack of a solid foundation. On the other hand, physically based models tend to be more accurate but complicated to understand because the breach growth process is simulated by an erosion model based of hydraulics, sediment transport and soil mechanics. (Zhu, 2006)

In order to understand the process of breaching, some physical models and physically based mathematical models are illustrated in the following sections.

2.2 Physical Models

The physical models generally include small-scale laboratory experiments and large-scale field tests. Many physical models have been set up for the purposes of breaching study during the last several decades. In this section, some of these the physical models will be reviewed.

2.2.1 Laboratory Experiments

Caan (1996), see also Visser (1998), performed a laboratory experiment on sand dike breaching in a basin of 34 m long, 16.6 m wide and 0.7 m deep. The dike was built normal to 9 m long and 0.75 high glass-wall on a 0.5 m thick sand bed. The dike model had a height of 0.15 m and a width of 0.2 m. The inclination of outer slope was 1:2 and inner slope was 1: 4. The initial breach

had a more or less rectangular cross-section with a width of 0.1 m and a depth of 0.03 m. In the experiment, the water level (upstream), velocity (upstream and breach) and breach width were measured.

Andrews *et al.* (1999) carried out experiments on small-scale homogeneous embankments constructed with three types of noncohesive sediments. The flume was 2.4 m wide, 12 m long and 0.3 m deep. All the embankments had a height of 0.3 m, a crest length of 0.065 m and an embankment slope 2.7H: 1V. In the experiment the breach failure was found to evolve through the stages of initiation and deepening (primarily vertical erosion), deepening and widening, and finally widening (predominantly lateral erosion) only after the foundation level has been reached. The general shape of the breach channel cross-section was found to be parabolic. Andrews *et al.* (1999) proposed a method of predicting the evolution of breach shape and an equation to estimate the discharge through breach.

Zhu (2006), see also Zhu *et al.* (2006), conducted laboratory experiments on embankment breaching. The tests were carried out in a straight flume of 35.5 m long, 0.8 m wide and 0.85 m deep. The tested embankments all have a height of 0.75 cm and a width of 0.6 m at the crest. The slopes were 1H: 2V. Five embankments built with different materials including pure sand and sand-silt-clay mixtures were tested. Headcut erosion played an important role in the process of breach growth in the embankments built of cohesive soil mixtures. According to the tests, erosion usually initiated at locations close to the toe of the embankment when overflowed and then extended to the entire slope. Phenomena such as flow shear erosion, fluidization of the headcut slope surface, undermining of the headcut due to impinging jet scour and discrete soil mechanical slope mass failure from the headcut were observed. In the case of the embankment constructed with pure sand, the breach erosion process was dominated by shear erosion, which led to a gradual and relatively uniform retreat of the downstream slope. Although head cut occurred, no large slope mass failure was observed.

Under the IMPACT project (see Morris *et al*, 2007) three series of laboratory tests (in total 23 tests) were performed at HR Wallingford (UK). The first series simulated breach growth resulting from overtopping failure of embankments built from non-cohesive material. The second test series was done to investigate overtopping induced beach formation through cohesive material. The third series focused on breaching induced by piping in a small flume.

Bukreev *et al.* (2008) measured the discharge and energy loss coefficients of breach flow based in a fixed weir model. In the experiment, the real conditions of a partial dam break were modeled by a weir with a polygonal profile and lateral contraction. They concluded that the values of these coefficients for a trapezoidal weir with a slope ratio of 1: 3 differ insignificantly from their values for a rectangular weir.

2.2.2 Field Tests

Also under the IMPACT project, 5 large-scale field tests carried out at the downstream from the Røssvass Dam in northern Norway (see Morris *et al.,* 2007). The variables included embankment heights (4.5 m, 5 m, and 6 m), materials (cohesive, non-cohesive and composite) and failure mechanisms (overtopping and piping). Figures (2-1) shows photos of two field tests.

Figure (2 - 1): Field tests undertaken in the IMPACT project (Morris et al., 2007)

Zhang *et al.* (2009) carried out a field test with the prototype to study the effects of cohesive strength of the filling of a cohesive homogeneous earth dam on the breach formation. Three breach mechanisms were considered in the research as they defined: the source-tracing erosion of dam body with the form of "multilevel headcut", "two-helix flow" erosion of dam crest and collapse of breach sidewalls due to instability. They concluded that the cohesive strength of filling of earth dam has great effect on breach formation. When the cohesive strength is big, the main character of the breach formation is head cutting and dumping collapse (Figure 2-2, left). If it is small, the main character of the breach formation is single level head cutting and shearing collapse (Figure (2-2), right).

Figure (2 - 2): Damping failure (left) and shear failure (right) (Zhang et al., 2009)

2.3 Mathematical Models

2.3.1 DAMBRK Model

The DAMBRK model is a dam break flood forecasting model developed by Fread (1984). The model consists of three components: a breach component for providing a temporal and geometrical description of the breach, a component for computing the reservoir outflow hydrograph and a component for modifying flood wave to route through the downstream valley. The failure time and the temporal breach parameters are given as input for the model. The total outflow (Q) consists of broad-crested flow through breach (Q_b) and flow through any spillway outlet (Q_s):

$$Q = Q_b + Q_s \tag{2-1}$$

The outflow through the breach (Q_b) is calculated by:

$$Q_b = C_1 \left(d_0 - h_b \right)^{1.5} + C_2 \left(d_0 - h_b \right)^{2.5} \tag{2-2}$$

In case of piping induced break, then the orifice flow equation is used:

$$Q_b = 4.8 A_p \left(d_0 - d_t \right)^{1/2} \tag{2-3}$$

where h_b is the elevation of breach bottom, d_0 is the upstream (reservoir) water surface elevation, the coefficients of C_1 and C_2 which taking into account the coefficient of approach velocity and the influence of submergence can be calculated by the equations given by Fread (1984), A_p is the piping flow area and d_t is the tail water depth (elevation) immediately downstream of the dam. Discharge coefficient is not included in the discharge equations. The model was tested by two historical dam break events and the predicted results are satisfied with the observed values in outflow volume, peak discharge and peak flood elevation.

2.3.2 BREACH Model

Fread (1988, revised in 1991) developed the breach erosion model BREACH for an earthen dam to predict the breach size, shape, time of formation and the breach outflow hydrograph. He assumed that the breach has an initial rectangular shape and then according to the stability of soil slope, it changes to trapezoidal-shaped channel, forming an angle with the vertical, until the critical value has reached. The evolution of the breach is as shown in Figure (2-3). In the model, breach enlargement is governed by the rate of erosion which is assumed to occur equally along the bottom. Further downwards erosion is not allowed after reaching the valley floor. The flow into the breach is calculated by the discharge equation of broad-crested weir flow for overtopping failure and orifice flow for piping:

Overtopping: $$Q_b = 3b_i \left(d_0 - h_b\right)^{1.5} \quad (2\text{-}4)$$

Piping: $$Q_b = 0.98\left(2g\right)^{0.5} A\left(d_0 - z_c\right)^{0.5} \quad (2\text{-}5)$$

where Q_b is the flow through the breach channel, b_i is the instantaneous width of initially rectangular-shaped channel , d_0 is the upstream (reservoir) water surface elevation, h_b is the elevation of breach bottom and z_c is the center-line elevation of the initial breach. The dam may be homogeneous or consist of two different materials. The predicted outflow hydrograph and breach size and shape agree well with the values of four failure dams.

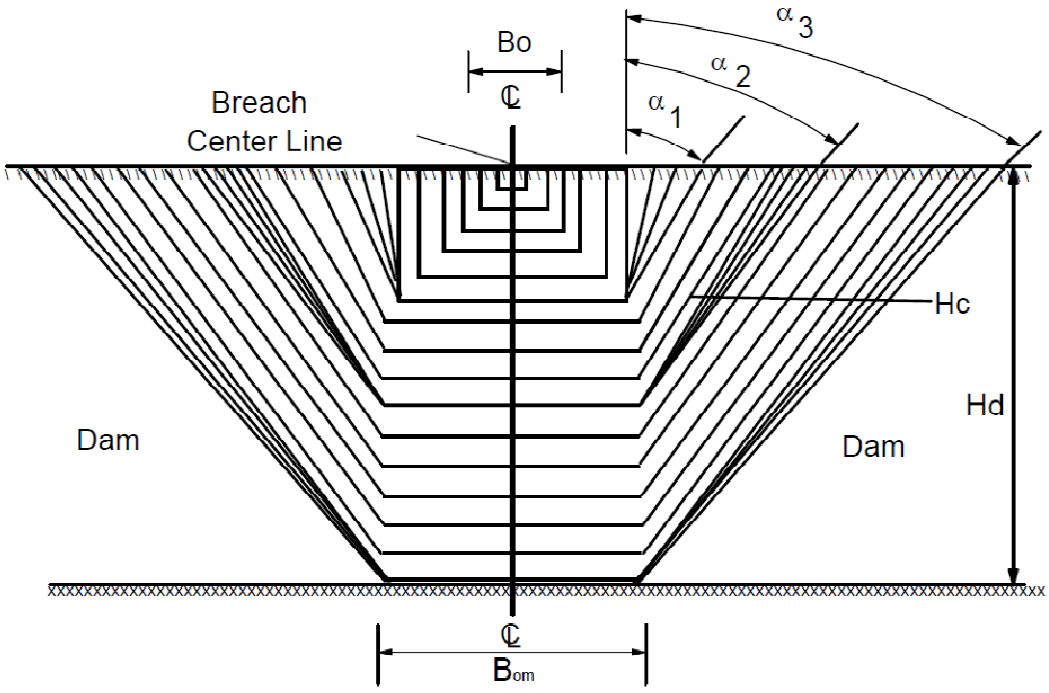

Figure (2 - 3): Front view of dam with breach formation sequence (Fread, 1988)

2.3.3 BEED Model

The BEED model (Singh and Quiroga 1987; Singh *et al.*, 1988) was developed for the simulation of gradual erosion of earth-fill dams. It describes the dynamic water sediment interaction during dam failure and incorporates both surface erosion and side slope sloughing. The model applies the mass conservation equation for the depletion of reservoir water and assumes that the breach behave as a broad-crested weir. The breach evolution sketch resulting from application of the BEED model to the historical dam failure (South Fork Dam) is shown in Figure (2-4). By utilizing quasi-steady state conditions near the breach, the discharge over the dam crest and through a trapezoidal breach can be expressed respectively as: (Singh *et al.*, 1988)

Over the crest: $$Q_c = C_r \left(B - b_{top}\right)\left(d_0 - P\right)^{3/2} \quad (2\text{-}6)$$

In the breach: $$Q_b = \left[C_r b + C_t \left(d_0 - h_b\right)\tan\theta\right]\left(d_0 - h_b\right)^{3/2} \quad (2\text{-}7)$$

where C_r , C_t are dimensional coefficients, B is the width of the dam crest, b_{top} is the top width of the breach, d_0 is the upstream (reservoir) water surface elevation, h_b is the elevation of the breach bottom measured from reference datum, θ is the angle between the breach side and the vertical. The theoretical value of C_r is 1.7 which is derived from the discharge equation of broad-crested weir with rectangular section and C_t is 1.35 which accounts for the triangular part.

By testing the model with two dam failure events, the model predicted well for timing, shape, and magnitude of the outflow hydrograph.

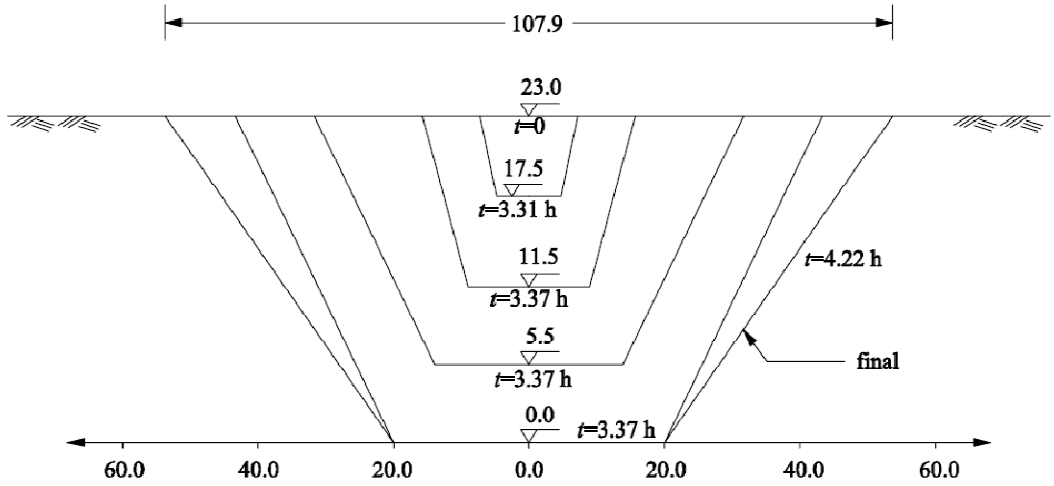

Figure (2 - 4): Breach evolution for the South Fork Dam simulated by the BEED model (Singh, 1996)

2.3.4 BRES Model

In the BRES model developed by Visser (1998), a relatively small initial breach is assumed in the top of the dike that is so large that water flows through it starting the breach erosion process. By assuming a trapezoidal shape of initial breach with the angle of repose, he distinguished the process of breach erosion for sand-dike into five stages (Figure (2-5)):

I. Steepening of the inner slope from the initial value.

II. Yielding a decrease of the width of the crest of the dike in the breach.

III. Lowering of the top of the dike in the breach, with constant angle of the critical breach side slopes, resulting in an increase of the breach width.

IV. Critical flow stage, in which the flow is virtually critical throughout the breach, and the breach continues to grow mainly laterally.

V. Subcritical stage, in which the breach continues to grow, mainly laterally due to the subcritical flow in the breach.

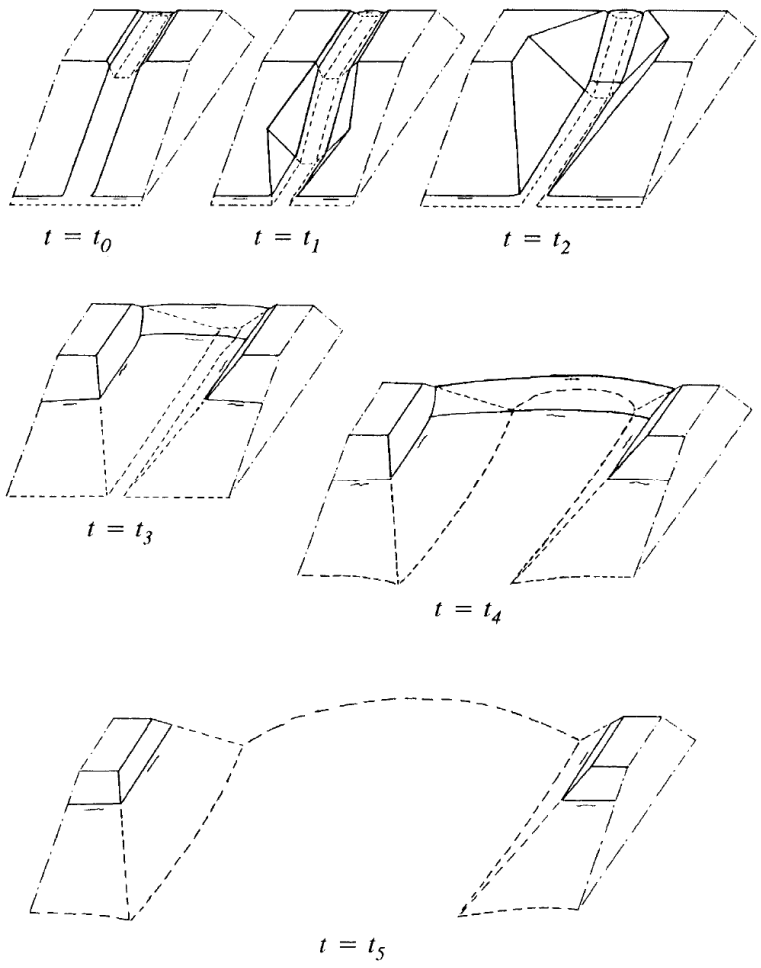

Figure (2 - 5): Schematic illustration of breach growth in a sand dike (Visser, 1998)

In the first three stages the initial breach cuts itself into the dike and in stages IV and V, most discharge through the breach happens and three types of breach are distinguished depending on the erodibility of the foundation. In the model, the discharge through the breach for different stages reads:

$$Q_b = C_d \left(\frac{2}{3}\right)^{3/2} \sqrt{g}\,\bar{b}\left(d_0 - h_b\right)^{3/2} \qquad \text{for } t_0 < t \le t_4 \tag{2-8}$$

$$Q_b = C_d \bar{b}\left(2g\right)^{1/2}\left(d_0 - h_p\right)^{1/2}\left(h_p - h_b\right) \qquad \text{for } t_4 \le t \le t_5 \tag{2-9}$$

where C_d is the discharge coefficient (≈ 1), $\bar{b}$ is depth-averaged width of the breach, d_0 is the upstream (reservoir) water surface elevation, h_b is the height of the bottom of the breach and h_p is the water level in polder. The BRES model simulate fairly well in the tests of a field experiment (Zwin, 94) and a laboratory experiment (Caan, 1996).

2.3.5 BRES-Zhu Model

Corresponding to the study of sand-dike breaching by Visser, Zhu (2006) investigated the breach process of clay dike. The distinct difference from the sand dike breaching is the headcut erosion occurring in the first stage of the clay-dike breaching process. Similarly, by assuming that the initial breach is relatively small, trapezoidal-shaped and located in the top of the dike, Zhu (2006) also classified the breach erosion process in clay-dikes into five stages: (see Figure (2-6))

I. Stage I ($t_0 < t < t_1$): Floodwater flows through the initial breach in the dike crest erodes soil away from the inner slope of the dike. Both flow shear erosion as well as small-scale headcut erosion can occur along the inner slope (see Figure (2-7)).

II. Stage II ($t_1 < t < t_2$): The steepened inner slope of the dike holds the critical slope angle β_1 throughout Stage II and acts like a headcut during the erosion process owing to its large steepness (see Figure(2-7)).

III. Stage III ($t_2 < t < t_3$): The headcut still maintains the critical slope angle β_1. The breach enlarges rapidly, accordingly also the breach flow rate, which in turn accelerates the breach erosion process in the dike. At the end of the stage, the dike body in the breach has been washed away completely down to the dike foundation or to the toe protection on the dike outer slope (sees Figure (2-9)).

IV. Stage IV ($t_3 < t < t_4$): In this stage the flow through the breach is critical. Breach erosion takes place mainly laterally, with flow shear erosion along the side-slopes of the breach and the resulting discrete side slope instability being the main mechanisms for the breach enlargement. Vertical erosion in this stage relies mainly on the geometrical and material features of the dike.

V. Stage V ($t_4 < t < t_5$): In this stage the flow through the breach is subcritical. The breach erosion still occurs mainly laterally and at the end, the velocity of the breach flow is reduced to such an extent that it can no longer erode away soil material from either the dike body or the dike foundation. Hence the breach growth process stops.

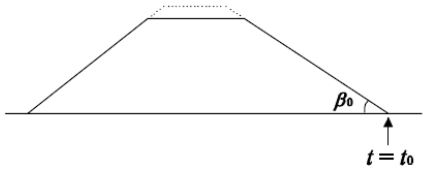

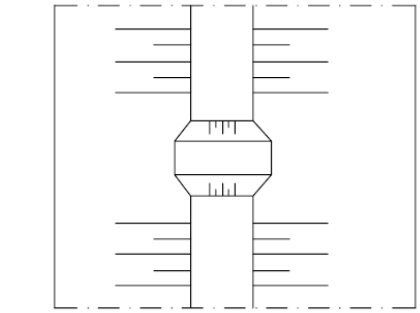

$t = t_0$

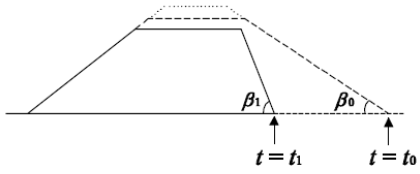

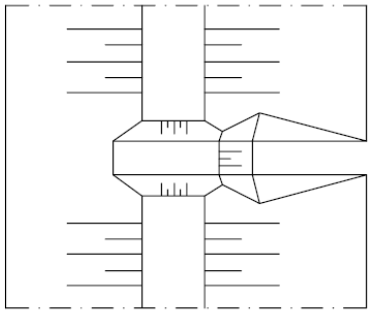

$t = t_1$

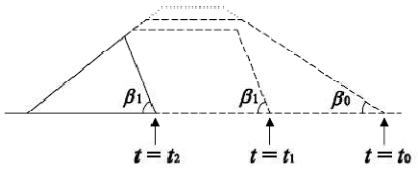

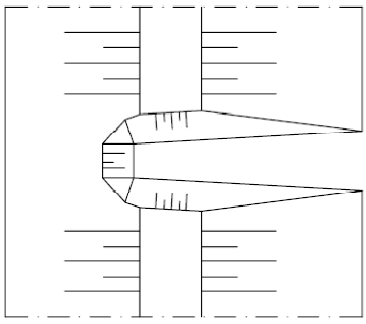

$t = t_2$

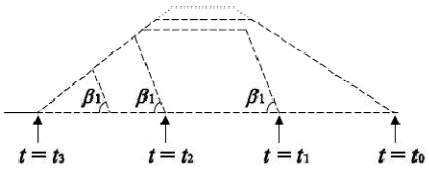

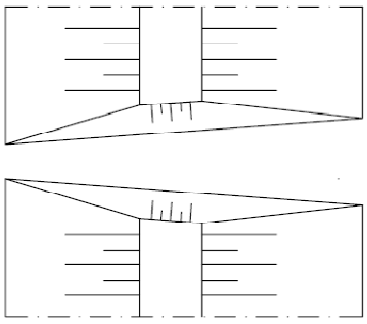

$t = t_3$

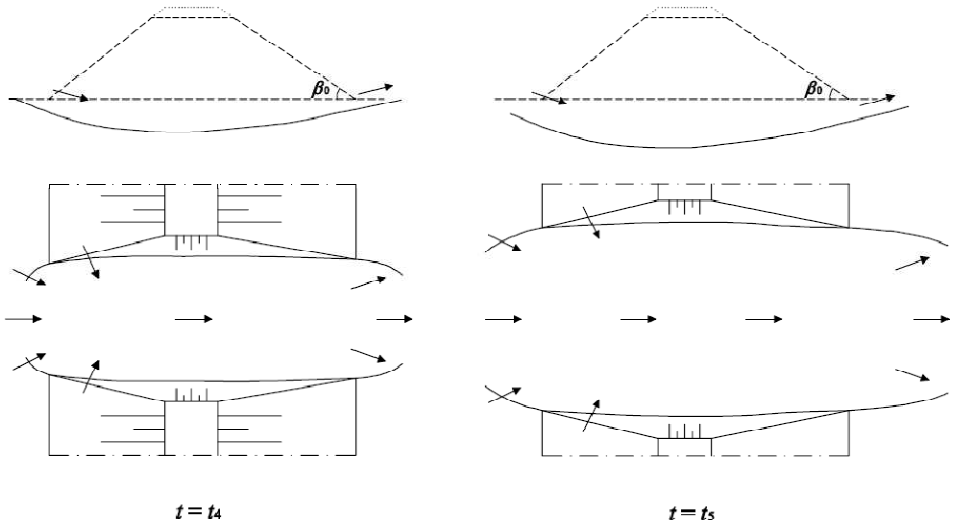

Figure (2 - 6): Sketch of breach development process in clay-dikes (Zhu, 2006)

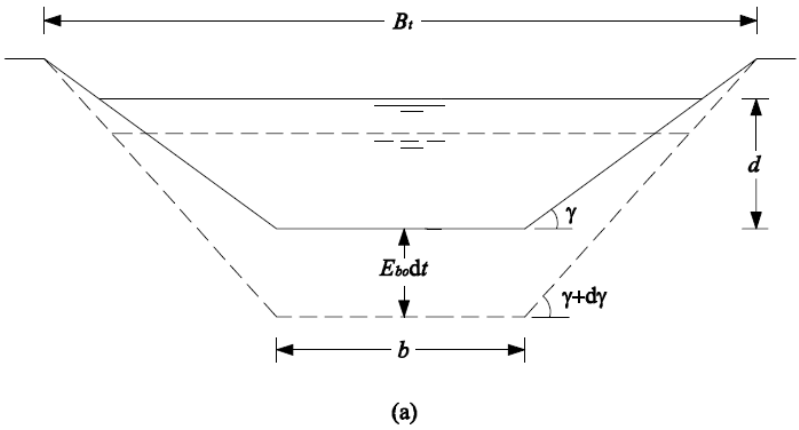

Figure (2 - 7): Process of breach enlargement in the dike crest in Stages I: (a) steepening of breach side-slopes. (Zhu, 2006)

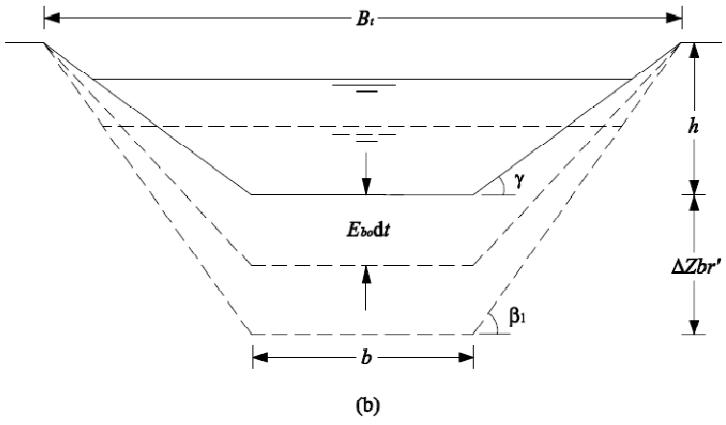

Figure (2 - 8): Process of breach enlargement in the dike crest in Stages II: (b) reaching of β_1 by the side-slope gradient. (Zhu, 2006)

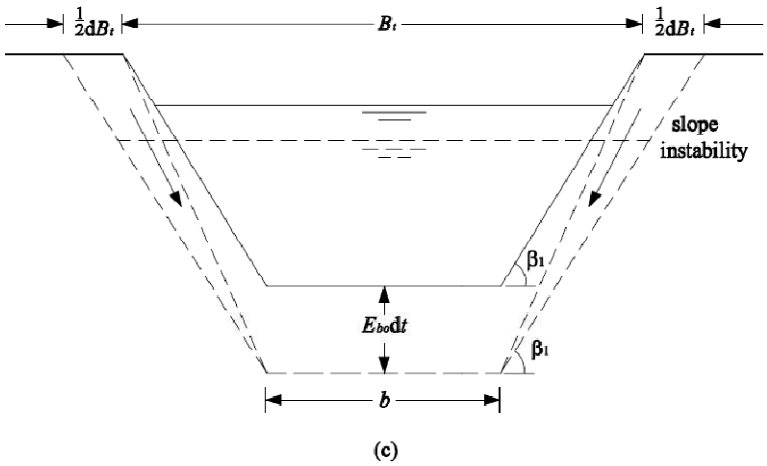

Figure (2 - 9): Process of breach enlargement in the dike crest in Stages III: breach widening after β_1 is reached. (Zhu, 2006)

Similar to the BRES Model, three types of breach shapes are distinguished in stage IV and V depending on erodibility of the foundation. The discharge equations (2-8) and (2-9) are still applicable for the flow though the breach in the clay dike. The model has been calibrated with some laboratory tests showing a good agreement with experimental data. Further, the model confronted with a prototype dike failure in China in 1998 with an about 40% smaller final breach with than the observed one and close predicted diverted floodwater volume.

2.3.6 Chang and Zhang Model

By considering the variations in soil erodibility along depth and the steepening of the downstream slope, Chang and Zhang (2010) studied the erosion process of landslide dams and divided the evolution of breach development into three stages (Figure (2-10)):

I. The side slopes below the water level will be eroded and the side slopes above the water level will collapse. The breach channel bed will also be eroded. This process will continue until the side slopes reach a critical value. The top breach width does not change during this stage, whereas both the breach depth and breach bottom width increase gradually.

II. The side slopes continues to be eroded keeping the critical slope. The breach top width, bottom width, and breach erosion depth increase during this stage.

III. The breach slopes will recede laterally keeping the same side slope angle. During this stage, the breach erosion depth keeps constant, whereas both the breach top width and bottom width increase. In the vertical direction, the breach cannot develop any further until a hard layer with its erosion resistance larger than the shear stress induced by the water flow has been encountered.

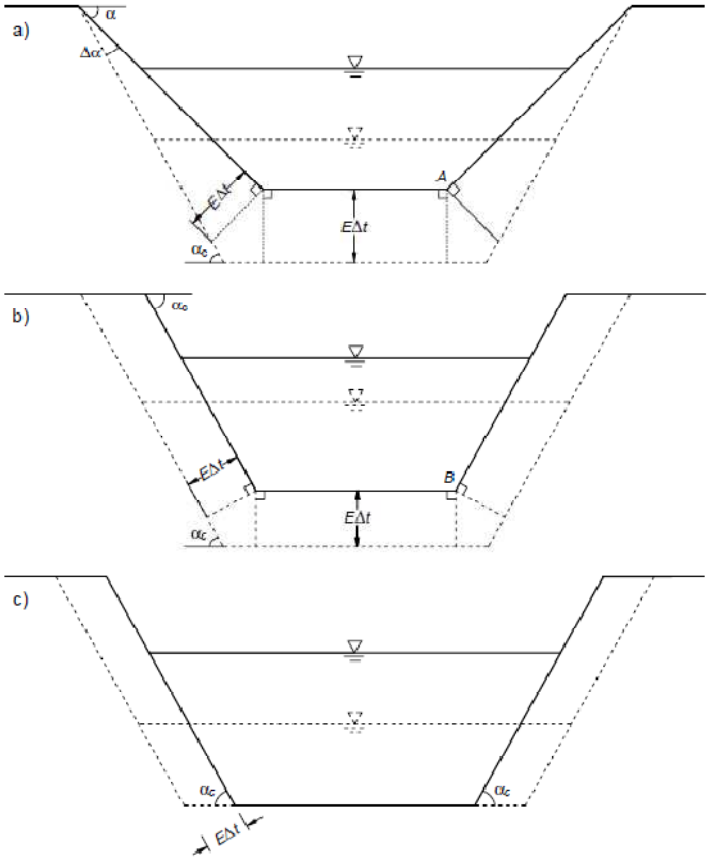

Figure (2 - 10): Breach enlargement process, a) Stage I, b) Stage II, c) Stage III (Chang and Zhang, 2010)

The discharge through the breach in the model is calculated as:

$$Q_b = 1.7\left[b + \left(d_1 - h_b\right)\tan\theta\right]\left(d_1 - h_b\right)^{3/2} \qquad (2\text{-}10)$$

Where b is the width of the breach bottom, d_1 is the water surface elevation in the section of the weir (in the breach), h_b is the height of the breach bottom, θ is the angle between the breach side and the vertical. The averaged width of breach of trapezoidal shape has been substituted into the broad-crested weir with a rectangular control section and a unit value of discharge coefficient is assumed. The historical cases of Tangjiashan Landslide Dam and Xiaogangjian Landslide Dam have be simulated by the mode and the results show good agreement with the observe values.

2.4 Conclusions

A number of physical models have been built to simulate the breaching process, which has provided a better understanding of the process and data for calibration and validation of physically based mathematical models. It can be found that most of these tests were conducted with mobile models which are made of sand, clay or mixtures of them and only a few (e.g. Bukreev *et al.* (2008)) were tested on fixed models. Both types of physical models have advantages and disadvantages (see (Table 4-1)).

In view of the breach hydraulics, it can be concluded from above that in many mathematical models the broad-crested weir equation has been applied to calculate discharge through the breach. The discharge coefficient is either assumed to have the unit value or not taken into consideration. In some cases (e.g. BEED model), the situation of a flow both over the crest and through the breach is considered. As for the evolution of the breach geometry, the breaching is generally assumed to start from a small initial breach at the crest to final shape experiencing the stages of steepening, deepening and widening. The initial breach shape is usually assumed as trapezoidal or rectangular but with the breaching process proceeding, trapezoidal breach is generally applied. The process is of great uncertainty and complexity which involving aspects as breach evolution, erosion and sediment transport. Depending on erodibility of the foundation, further erosion will occur or not. For clay dam or dike, headcut plays a significant role.

In conclusion, these models have been tested by either experiments or historical breaching events which provide the confidence and reliability for the models. Therefore, the process of breaching can be described by mathematical equations with simplifications. However, the research based on the fixed models needs more efforts by which the breach flow can be studied in detail for particular stage of breaching process. The theoretical study for the weirs with fixed shapes of breach can be done by reviewing the literatures on the weir flow.

CHAPTER 3. REVIEW OF LITERATURE ON WEIR FLOW

3.1 Introduction

Experimental and field observations have indicated that flow over and through the breach can be simulated by the hydraulics of broad-crested weir flow (Chow, 1986). As stated before, this principle has been widely used in breach models. The literature related to weir flow particular for compound weirs is to be reviewed in this chapter.

3.2 Basic Concepts in Open Channels

3.2.1 Specific Energy and Critical Depth

For steady frictionless flow, the equation of motion can be expressed (Bernoulli equation):

$$z + \frac{p}{\rho g} + \frac{V^2}{2g} = H \qquad (3\text{-}1)$$

in which H is the total energy head, z is the height above an arbitrary datum, V is the mean velocity of fluid, g is gravitational acceleration, p is the pressure, ρ is the water density. On the left-hand side of the equation, $\frac{V^2}{2g}$ is the velocity head representing the kinetic energy and $\frac{p}{\rho g}$ is the pressure head. Figure (3-1) shows the definition sketch of horizontal channel flow.

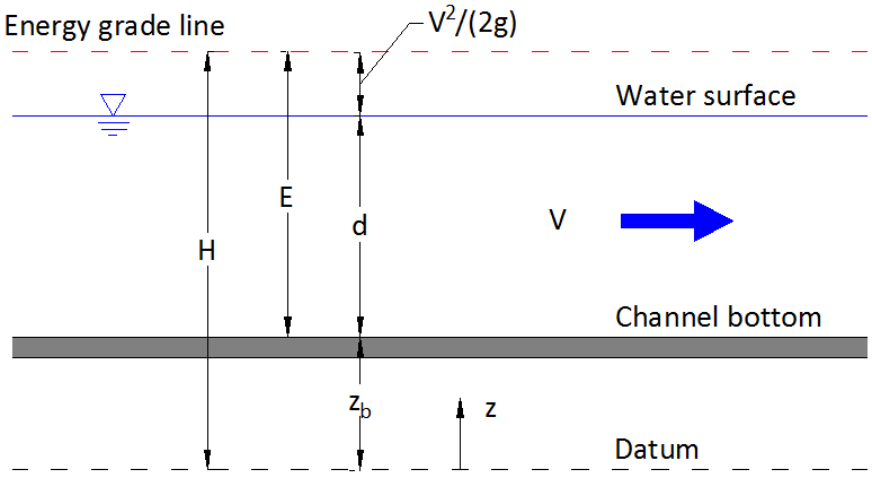

Figure (3 - 1): Definition sketch of horizontal channel flow

By assuming a uniform velocity distribution and hydrostatic pressure distribution (e.g. $p = \rho g\left(d + z_b - z\right)$), Equation (3-1) can be rewritten as:

$$z_b + d + \frac{V^2}{2g} = H \tag{3-2}$$

in which z_b is the height of channel bottom above an arbitrary datum and d is the water depth. Define the bed as the datum, then $z_b = 0$ and Equation (3-2) is reduced to:

$$d + \frac{V^2}{2g} = E \tag{3-3}$$

in which E is the so called specific energy. Considering a rectangular cross section with uniform velocity distribution, $V = \frac{q}{d}$ is valid and Equation (3-3) becomes:

$$d + \frac{q^2}{2gd^2} = E \tag{3-4}$$

In order to find out the extreme value, by differentiating Equation (3-4) with respect to d, it yields:

$$\frac{\partial E}{\partial d} = 1 - \frac{q^2}{gd^3} \tag{3-5}$$

E is minimum when

$$\frac{\partial E}{\partial d} = 1 - \frac{q^2}{gd^3} = 0 \tag{3-6}$$

By definition, the depth at which E is minimum is called the critical depth:

$$d_c = \sqrt[3]{\frac{q^2}{g}} \tag{3-7}$$

Rewrite Equation (3-7) and it gives:

$$q^2 = gd_c^3 \tag{3-8}$$

or

$$\frac{V_c^2}{2g} = \frac{1}{2}d_c \tag{3-9}$$

It indicates that the velocity head in critical flow is one-half of the critical depth. Hence, if critical depth has been reached, the specific energy becomes:

$$E = d_c + \frac{1}{2} d_c \tag{3-10}$$

or

$$d_c = \frac{2}{3} E \tag{3-11}$$

It shows that the critical depth is equal to two-thirds of the specific energy. If the flow over weir is critical, then the depth over the weir can be expressed as a function of upstream energy head.

3.2.2 The Froude Number

The Froude number is a measurement of flow characteristics at a cross section and useful in the calculation of hydraulic jumps and the design of hydraulic structures. In scale models it is an important parameter in similarity between model and real-world prototype (see section 4.1.3). The Froude number is defined as:

$$Fr = \frac{V}{\sqrt{gd}} \tag{3-12}$$

In which, V is the mean flow velocity and d is the flow depth. This equation is defined by assuming uniform velocity distribution and it can be interpreted as the ratio of the inertial forces to the gravitational forces in the flow. According to Equations (3-9) and (3-12), when the flow is critical, the Froude number $Fr = 1$. The upper end of the wave remains stationary, and only the downstream end travels in the downstream direction. If $Fr < 1$, the flow is subcritical and the gravitational forces are dominant. However, when $Fr > 1$, the flow becomes supercritical and the inertial forces play an important role.

3.2.3 The Reynolds Number

The ratio of viscous and inertial forces is defined as the Reynolds number:

$$Re = \frac{VL}{\nu} \tag{3-13}$$

In which, L is the characteristic length and ν is the kinematic viscosity of the liquid. The Reynolds number can be used to determine if flow is laminar, transient or turbulent. In open channel flow, at low Reynolds number ($\mathrm{Re} < 1000$) laminar flow occurs, where viscous forces are dominant, and is characterized by smooth, constant fluid motion; while at high Reynolds number

($\mathrm{Re} > 1000$), the flow is turbulent and is dominated by inertial forces, which tend to produce eddies, vortices and other flow instabilities.

3.2.4 Resistance

The total resistance in a straight bedform-dominated channel consists of three sources of resistance: (Mark, 2009 and Mark *et al.*, 2009)

(a). Grain friction: resulting from resistance to flow due to individual grains on the river bed.
(b). Form drag: resulting from resistance to flow due to the pressure difference and energy loss in the flow separation zone located downstream of the bedform crest.
(c). Sidewall friction: resulting from resistance to flow due to sidewall.

Three most frequently used parameters describing resistance to flow are (Yen, 2001):

Chézy coefficient: $$C = \frac{V}{\sqrt{RS}} \quad (3\text{-}14)$$

Manning coefficient: $$n = \frac{1.49}{V} R^{2/3} S^{1/2} \quad (3\text{-}15)$$

Darcy–Weisbach friction factor: $$f = \frac{8gRS}{V^2} \quad (3\text{-}16)$$

in which, V is the mean flow velocity, g is the gravitational acceleration, is the hydraulic radius of the flow ($R = A/\chi$ is the ratio between the cross sectional area and the wet perimeter of the flow) and S is the flow resistance slope.

3.3 Weirs and Weir Flows

3.3.1 Classifications

Weirs are generally divided into two types: sharp-crested weirs and broad-crested weirs. More in detail, according to Govinda Rao and Muralidhar (1963, see also Jain, 2001), four types of finite-crest-width weirs can be identified based on the ratio of h_0 / L_w (see Figure (3-2)):

(a). Long-crested weir: $h_0 / L_w \le 0.1$
(b). Broad-crested weir: $0.1 < h_0 / L_w < 0.35$
(c). Narrow-crested weir: $0.35 < h_0 / L_w < 1.5$
(d). Sharp-crested weir: $1.5 < h_0 / L_w$

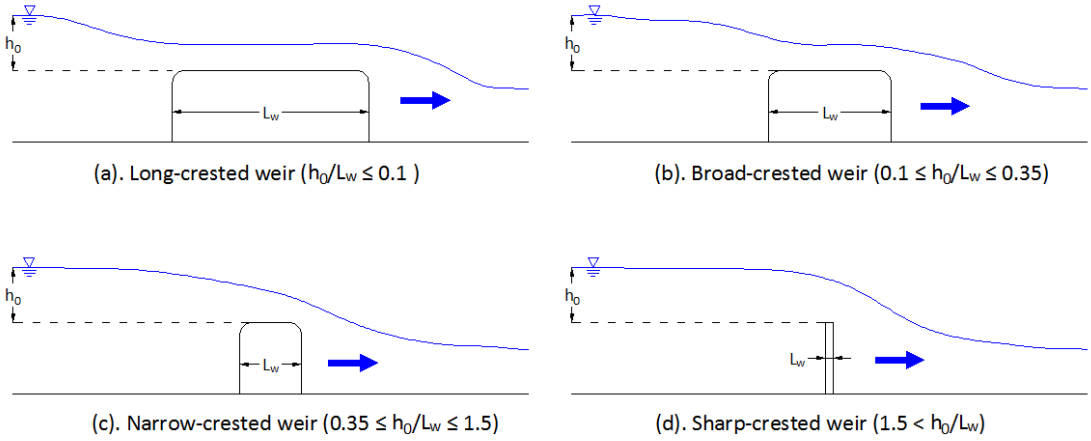

Figure (3 - 2): Four types of finite-crest-width weirs

Azimi and Rajaratnam (2009) agreed with the classification of the four types and described the distinction for all types. They defined the weir as broad-crested when parallel flow exists over the weir crest (critical flow). If the crest becomes even longer, long-crested weir is referred. Furthermore, narrowed (short) -crested weir is featured as curvilinear flow existing over the weir and the flow over sharp-crested weir separates from the upstream edge of the crest and runs away without reattaching to the weir.

Based on the profile of weir, the finite-crested weirs could be rectangular and trapezoidal. Generally, in case of broad-crested weirs, rectangular profile weirs refer to the standard broad-crested weir and trapezoidal profile weir is called embankment weir. Besides of that, some other types of weirs are also of great interest to researchers such as triangular weir and (semi-) circular weir (Figure (3-3)). The above classification is introduced by shape and dimension. According to the relative position of the weir and flow direction, the weirs can be placed obliquely to the flow (oblique weir, Figure (3-4)) and even on the side of it (side weir, Figure (3-5)). This report focuses on the broad-crested weirs in a rectangular channel with face perpendicular to the flow.

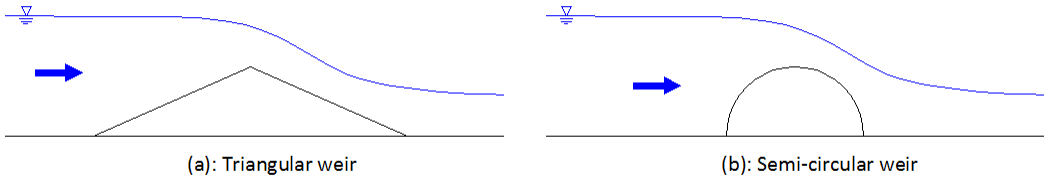

Figure (3 - 3): Triangular weir and semi-circular weir

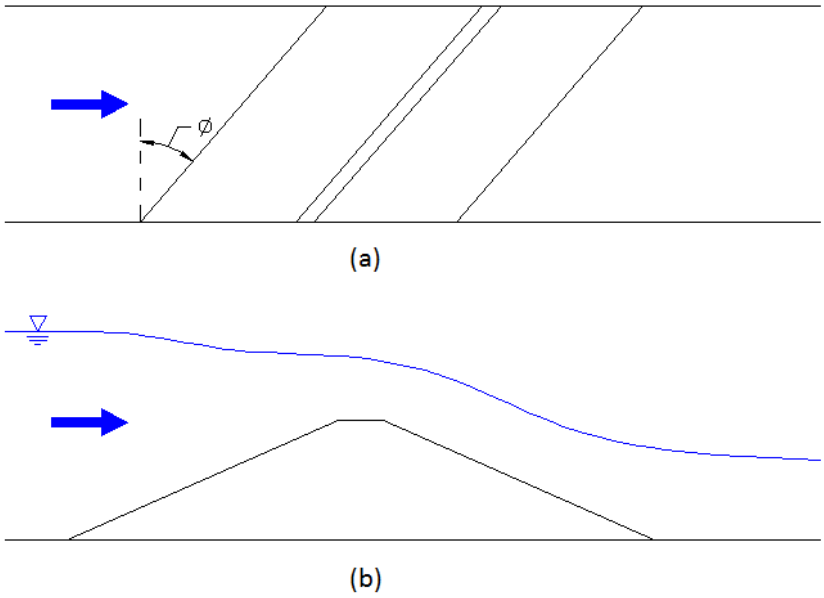

Figure (3 - 4): Oblique weir: (a). Plan view; (b). Side view

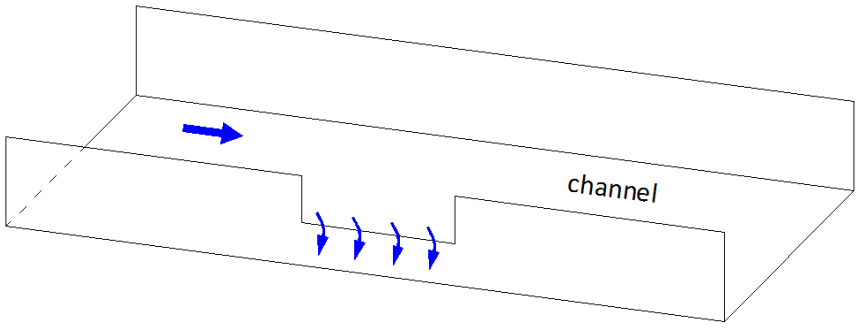

Figure (3 - 5): Layout of side weir and channel

3.3.2 Perfect and Imperfect Weirs

The imperfect weir refers to the situation that the discharge is dependent on the downstream water depth and if not, the weir is called perfect (Rijn, 1990). In some publications, the former is also defined as submerged flow condition and the latter is corresponding to free flow condition. For instance, when critical flow occurs over the broad-crested weir, the flow transforms from subcritical to supercritical, which means that the disturbances in downstream do not affect the upstream and the weir is so called perfect. However, if the downstream water depth rises to the level whereby the flow becomes subcritical, then it is named imperfect. Hence, the weir is perfect or not depends on the weir flow condition. Figure (3-6) shows the sketch of weirs in perfect and imperfect situations. In the report of Van Leeuwen (2006), the difference between the two situations is discussed regarding to flow over groynes. Note that in present

report, emerged flow refers to the flow only through the breach and overtopping flow refers to the flow through the full compound section. Both flow conditions could be either perfect or imperfect.

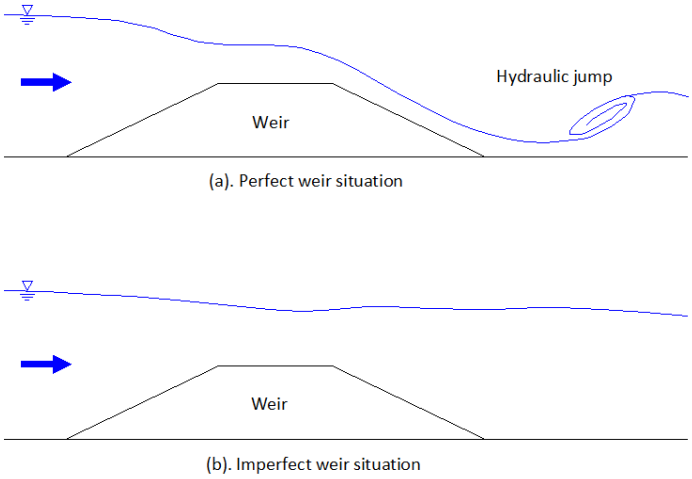

Figure (3 - 6): Sketch of perfect and imperfect broad-crested weir

3.4 Flow over Broad-Crested Weirs

3.4.1 Introduction

Considerable amount of research has been done on the properties of flow over broad-crested weirs. The main research objectives were to evaluate discharge coefficient, energy loss and the effect of the various weir geometries under different flow conditions. The significant difference between the perfect and imperfect weir situations is the applicability of critical flow assumption ($d_c = \frac{2}{3}E$) when deriving discharge formulae. The common analytical solutions of discharge will be discussed in this section as well as the main characteristics related to flow over broad-crested weirs.

Four types of flow over cylindrical-crested weir classified by Escande in 1939 (Fritz and Hager, 1998) has been applied to other types of weirs, such as trapezoidal embankment weirs and circular-crested weirs. In fact, it applies equally to all other overflow structures. The four flow types are (see Figure (3-7)):

(a). Hydraulic jump: with a surface roller behind the weir.

(b). Plunging flow: with the main flow along the downstream weir slope and a submerged roller behind the crest.

(c). Surface wave flow: with the main flow along the free surface and a bottom recirculation zone.

(d). Surface jet flow: with a nearly horizontal surface.

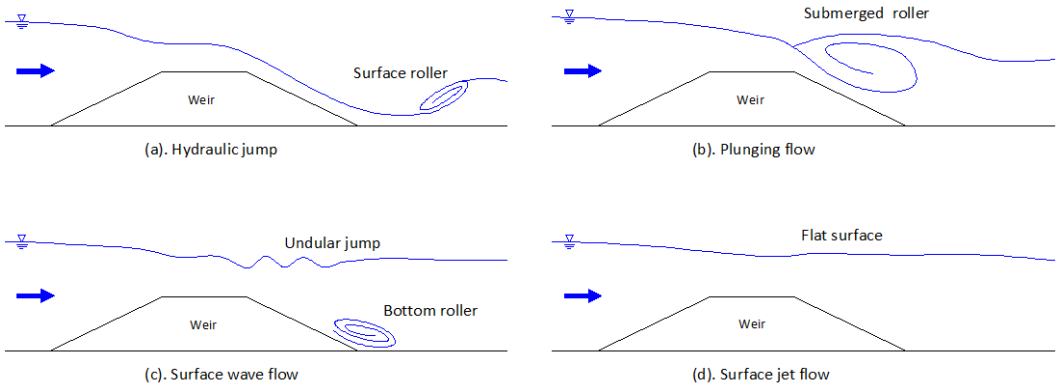

Figure (3 - 7): Four types of flow depending on tailwater depth (after Nguyen, 2006)

The position of hydraulic jumps is dependent on the tailwater condition (Chaudhry, 2008). For breach models, the position of hydraulic jumps also of great interest to know (see section 7.4), which is important for predictions such as energy dissipation, turbulence and scouring.

3.4.2 Discharge Equations

Perfect Weir Situation

By applying continuity equation and energy conservation between section 1 and 2 (See Figure (3-8)), the theoretical maximum discharge can be derived with $d_1 = \frac{2}{3} H_0$ over the weir crest:

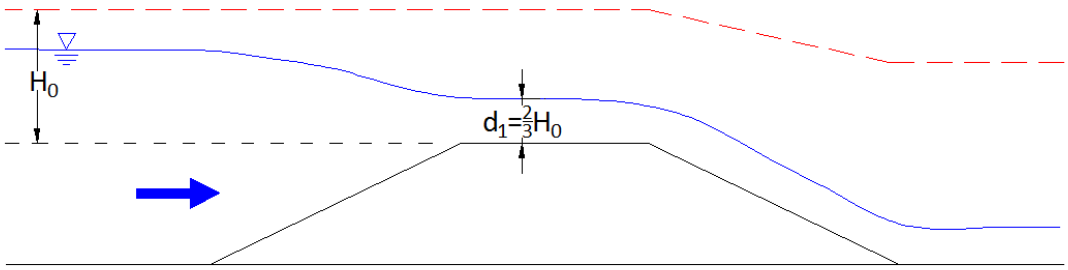

Figure (3 - 8): Definition sketch of flow over perfect broad-crested weir

$$Q = \frac{2}{3}\left(\frac{2}{3}g\right)^{1/2} B H_0^{3/2} = 1.7 H_0^{3/2} \qquad (3\text{-}17)$$

But in reality, energy loss due to bed friction and weir geometry cannot be neglected whereby the discharge coefficient is applied to account for these effects. Then the equation reads as:

$$Q = 1.7 C_d B H_0^{3/2} \qquad (3\text{-}18)$$

Bos (1985) proposed an empirical relation for to estimate the value of the discharge coefficient broad-crested weirs and long-throated flumes of all shapes and sizes. It is expressed as a function of H_0/L_w :

$$C_d = 0.93 + 0.1\frac{H_0}{L_w} \tag{3-19}$$

It can be seen from the theoretical estimation that the discharge coefficient linearly increases with the increase of the ratio of H_0 / L_w as is shown in Figure (3-9)

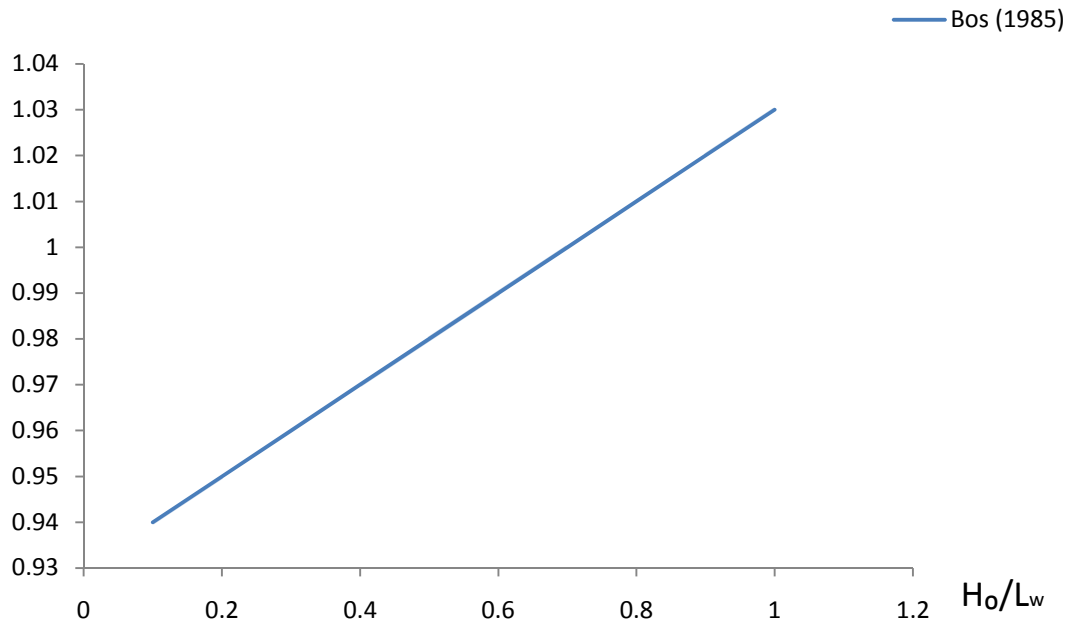

Figure (3 - 9): Discharge coefficient versus H_0 / L_w

Fritz and Hager (1998) conducted research on the flow hydraulics of embankment weir under the condition of free overflow. The weir they studied was broad-crested and with weir slopes of 1V:2H.

$$Q = C_d b\sqrt{2gH_0^{\,3}} \tag{3-20}$$

in which, Q is the discharge, C_d is the discharge coefficient, b is the width of flow, g is the gravity acceleration, and H_0 is the upstream total head above the crest.

Fritz and Hager (1998) also proposed an empirical formula for the discharge coefficient as a function of relative crest length.

$$C_d = 0.43 + 0.06\sin\left[\pi\left(\varepsilon - 0.55\right)\right] \tag{3-21}$$

where relative crest length $\varepsilon = \frac{H_0}{H_0 + L_w}$. The relation in Equation (3-21) is shown in Figure (3-10).

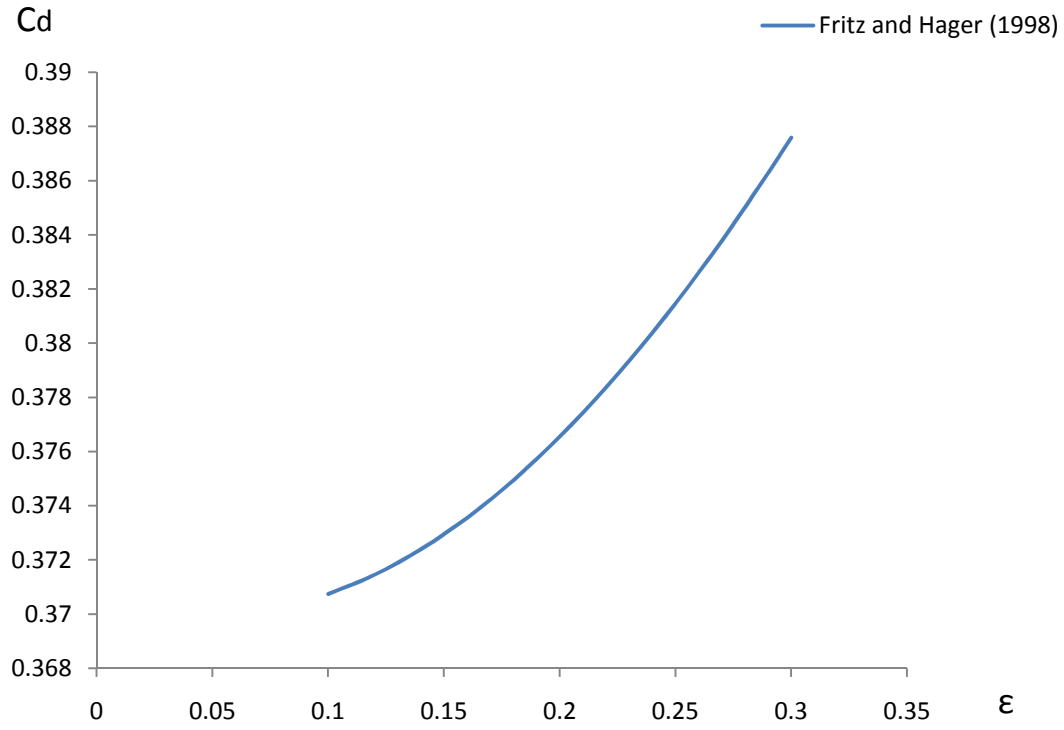

Figure (3 - 10): Discharge coefficient versus relative crest length

The formulae (3-20) and (3-21) were also applied by Sargison *et al.* (2009) whose measurements showed that the discharge coefficient was identical over the range of flow rates tested for 1V:1H upstream slope with 1V:2H or vertical downstream slope ,respectively and a lower value is generated for steep upstream slope (1V:1H) than gentle upstream slope (1V:2H). The discharge coefficient for a rectangular broad-crested weir was approximately 10 percent less than this value over the range of relative crest length $0 < \varepsilon < 1$ due to flow separation (Fritz and Hager (1998); Sargison and Percy (2009)).

Imperfect Weir Situation

The flow over the crest is not critical any longer in this case. One method is to apply the Bernoulli-equation between section 0 and 1 (see Figure (3-11)):

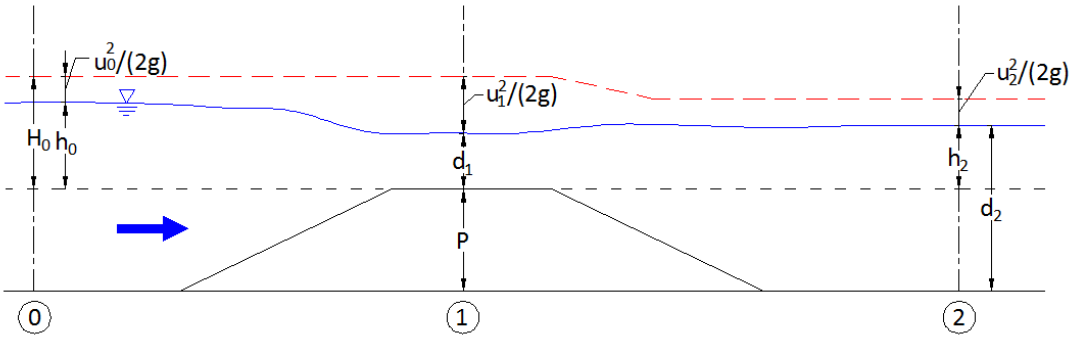

Figure (3 - 11): Definition sketch of flow over imperfect broad-crested weir

$$H_0 = \frac{u_1^2}{2g} + h_1 = \frac{Q^2}{2gh_1^2b^2} + h_1 \qquad (3\text{-}22)$$

or

$$Q = bh_1\sqrt{2g\left(H_0 - h_1\right)} \qquad (3\text{-}23)$$

For practical reasons, the equation is expressed as a function of h_2 :

$$Q = C_d bh_2\sqrt{2g\left(H_0 - h_2\right)} \qquad (3\text{-}24)$$

The discharge coefficient is introduced to account for contraction effects and energy losses due to expansion and bottom roughness. Van Rijn (1990) indicated that the discharge coefficient varied from 0.9 for a rough weir with sharp bottom transition to 1.3 for a smooth weir with rounded bottom transition. However, discharge coefficient may be further decreased due to the tail water effects if the flow over weir becomes subcritical. A reduction factor can be used to account for the effects. Nikolov *et al.* (1978) introduced the coefficient of submergence C_s into the discharge equation of broad-crested weirs (Equation (3-20)) and it reads:

$$Q = C_s C_d b\sqrt{2gH_0^3} \qquad (3\text{-}25)$$

By equating the right-hand side of Equations (3-23) and (3-25) with the conditions that if C_s = 1 (perfect weir condition), then $h_1 = \frac{2}{3}H_0$, the coefficient of submergence reads (Nikolov *et al.,* 1978):

$$C_s = 2.6\frac{h_1}{H_0}\sqrt{1-\left(\frac{h_1}{H_0}\right)} \qquad (3\text{-}26)$$

Based on the Equation (3-26), the coefficient of submergence C_s is plotted against the ratio of h_1 / H_0 (see Figure (3-12)). As can be seen, the reduction factor decreases with the increase of the ratio of h_1 / H_0.

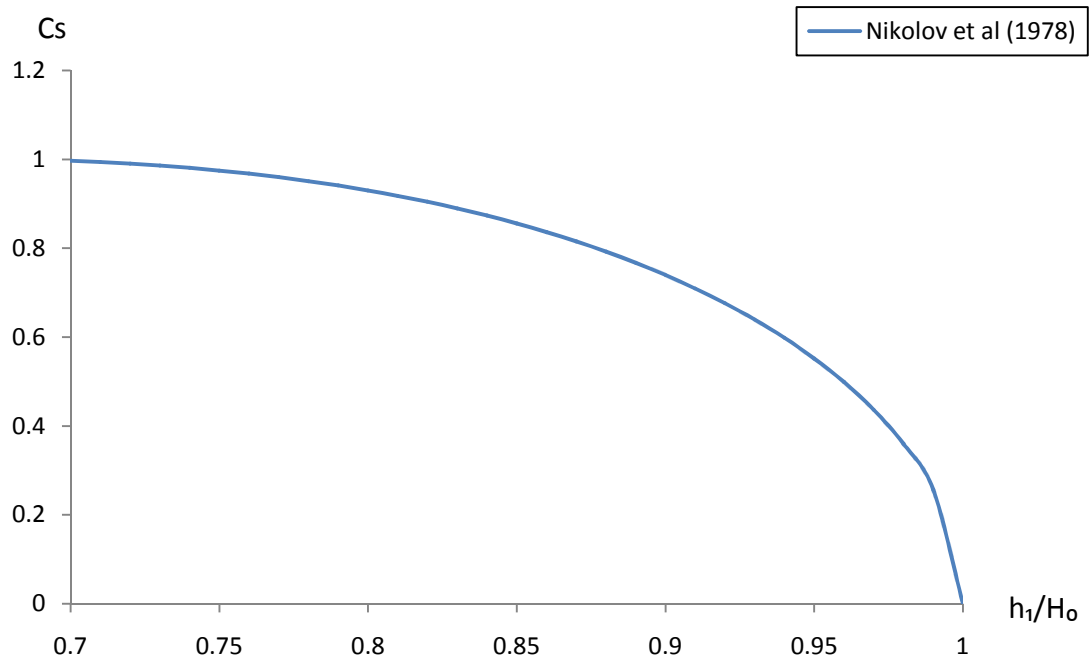

Figure (3 - 12): The coefficient of submergence versus the ratio of h_1 / H_0

3.4.3 Energy Loss

In order to know the conveyance capacity of the downstream outflow, the energy losses caused by a weir should be estimated to have a flooding prediction. Since the energy loss caused by a weir in perfect weir situation is difficult to interpret due to the complex phenomena (e.g. hydraulic jumps) which contribute significantly to the total loss, this section will only focus on imperfect weir situation and provide the analytical solutions and precious investigations related to energy loss caused by weir.

Analytical Solutions

The weir-like structure can be considered as a sudden rise in the channel, thus the flow over it can be considered as the rapidly varied flow. Phenomena as hydraulic jumps, eddies, turbulence and flow separation may occur caused by contractions and expansions of channel geometry, which would cause energy loss. Theoretically, by applying the energy conservation over the distance from the upstream of the weir (section 0) to the downstream (section 2), the total loss can be estimated as (see Figure (3-11)):

$$\Delta H = d_0 + \frac{u_0^2}{2g} - d_2 - \frac{u_2^2}{2g} \qquad (3\text{-}27)$$

It is of great interest to investigate and specify the contributors to the amount of energy loss. According to the literature (Mark 2009; Ali and Uijttewaal 2009 & 2010), in the case of channel with obstacle (weir-like structure), the energy loss mainly results from three sources:

(a). Form drag due to the local acceleration (contraction), deceleration (expansion) and stagnancy of the flow.

(b). Grain friction due to bed and weir surface.

(c). Sidewall friction due to sidewall of channel.

Note that form resistance is usually larger than the grain and sidewall resistance and the expansion accounts for the major part of form resistance (Bloemberg, 2001, see also Nguyen, 2006). Generally, the energy loss induced by a weir is considered by form resistance. There are two methods to estimate the amount energy loss during the process.

(a). Form Drag Model

One way is to apply the expansion loss form drag model (Ali and Uijttewaal, 2009) based on 1-D momentum conservation equation to account for the energy loss caused by the decelerating flow downstream of a sudden expansion. The theory behind the model is assuming that energy is conserved in the upstream of the weir and momentum is conserved in the downstream. By applying the two conservation laws respectively (Figure (3-11)), the equations are presented as below:

$$d_0 + \frac{\alpha_0 q^2}{2gd_0^2} = d_1 + \frac{\alpha_1 q^2}{2gd_1^2} \tag{3-28}$$

$$\frac{1}{2}\rho g\left(d_1 + P\right)^2 + \rho\frac{\beta_1 q^2}{d_1} = \frac{1}{2}\rho g d_2^2 + \rho\frac{\beta_2 q^2}{d_2} \tag{3-29}$$

In which α_1 and α_2 are the energy coefficients in the upstream and downstream, respectively. β_1 and β_2 are the momentum coefficients in the upstream and downstream, respectively. According to these two equations, the relation of d_0 and d_2 can be derived, hence, the energy loss due to weir can be expressed as a function of downstream water depth d_2. The energy loss caused by the other contributors, the bottom and the sidewall, can be estimated by a set of equations as below:

$$\Delta H_{bed} = c_f \frac{LV^2}{gD} \tag{3-30}$$

$$\Delta H_{wf} = c_f \frac{LV^2}{gW} \tag{3-31}$$

$$c_f = \frac{g}{C^2} \tag{3-32}$$

$$C = 18\log\left(\frac{12d}{k_s}\right) \tag{3-33}$$

where, k_s is the friction height, d is the water depth, c_f is the friction coefficient, C is the Chézy coefficient, L is the characteristic length, V is the mean velocity, D is the hydraulic diameter and W is the flume width. Based on given equations, the energy loss caused by weir can be calculated. Ali and Uijttewaal (2009 & 2010) carried out laboratory tests for flow over weirs with and without vegetation at high water. By comparing with data collected from experiments, the form drag model provided a good prediction of energy head loss for subcritical flow.

(b). Carnot Equation

Another way to determine the energy loss due to form resistance is to use the Borda-Carnot equation which is derived by applying the simplified one-dimensional momentum and energy conservation equations over the expansion region (Figure (3-11)). The equation reads (Van Rijn, 1990):

$$\Delta H = \frac{(u_1 - u_2)^2}{2g} = \frac{u_1^2}{2g}\left(1 - \frac{A_1}{A_2}\right)^2 \tag{3-34}$$

This is valid when $\Delta h = h_2 - h_1 << 2h_2$, if Δh is not negligible with respect to $2h_2$, the above equation yields:

$$\Delta H = \frac{(u_1 - u_2)^2}{2g} + \frac{2u_2(u_1 - u_2)}{2g}\frac{(d_1 + P - d_2)}{(d_1 + P + d_2)} \tag{3-35}$$

If the effect of the velocity profile is taken into account, the Carnot equation becomes:

$$\Delta H = \frac{(\beta_1 u_1 - \beta_2 u_2)^2}{2g} \tag{3-36}$$

Precious Investigations

Nguyen (2006) conducted experiments on the flow over a dike form weir and concluded with respect to the energy loss:

(a). The head loss decreases with the increase of the downstream water head for a constant discharge. In case of free overflow, the head loss increases as much as the downstream water head decreases. In the situation of high submergence, the weir can hardly cause any head loss.

(b). The higher discharge results in the bigger head loss with for a given downstream water head.

3.4.4 Related Investigations

Weir Slopes

The slopes of weirs can be gentle, steep or even vertical. Also the combination of upstream and downstream slopes can be various and has an influence on the hydraulics of the weirs. Sargison and Percy (2009) investigated the influence by varying the slopes of a broad-crested weir. They conducted experiments for four combinations (see Figure (3-11)). On the basis of results from experiments, they found that the upstream slope of the weir influenced the hydraulics of weir the most. Increasing the upstream slope to the vertical decreased the discharge coefficient, surface elevation and static pressure over the crest. However, the downstream slope had a negligible effect. For vertical face, leaping flow would occur, which prevents cavitations at high flow rates. In another investigation, Fritz and Hager (1998) also found that the sloped broad-crested weirs (1V:2H) has a larger flow capacity than those with vertical faces.

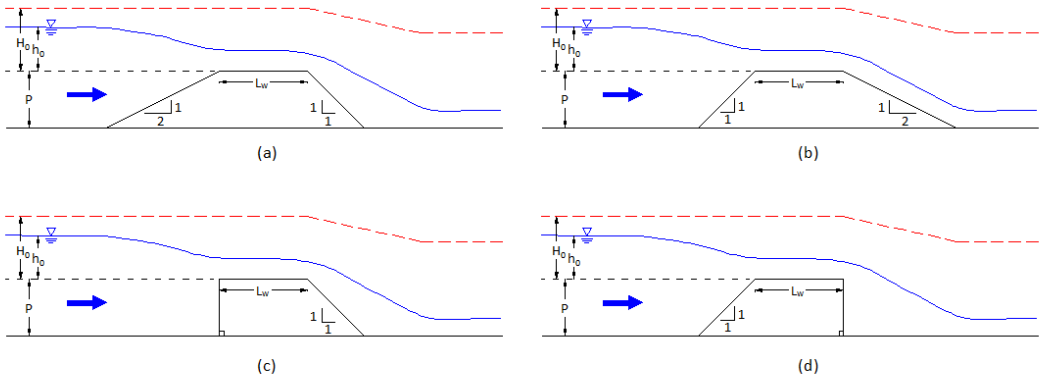

Figure (3 - 13): Four tests in the research of Sargison and Percy (2009)

Upstream Corner

Upstream corner of weirs can be round or sharp (Figure (3-14)). The significant difference between the round and sharp corner is that the flow separation over the crest is formed or not. For a sharp corner, the separation would occur and hence, the discharge coefficient would be smaller than for a round corner where the flow would smoothly flow over the crest without leaping. Ramamurthy *et al.* (1988) studied the two configurations and concluded that the characteristics of flow over a broad-crested weir with a square-edged or a round-nosed upstream corner depend on the ratios of H_0 / L_w and R / P. It was found that the effect of rounding the upstream corner of the square-edged broad-crested weir is to increase the coefficient of discharge. In addition, based on the degree of rounding of the upstream corner, three groups are indentified:

(a). Slightly rounded ($0 < R / P < 0.094$): the degree of rounding is small and it does not affect the flow.

(b). Moderately rounded ($0.094 < R / P < 0.25$): it reduces flow separation and is effective in increasing the discharge coefficient.

(c). Well-rounded ($0.25 < R / P < 1$): there is no flow separation and the discharge coefficient reaches the highest value.

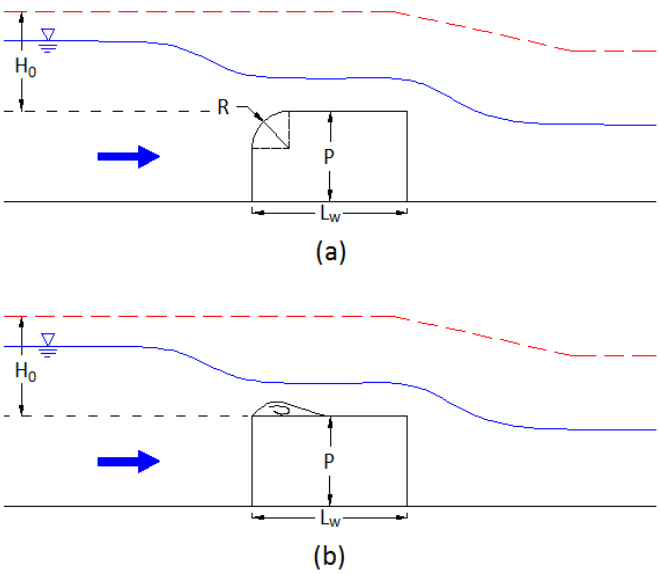

Figure (3 - 14): Upstream corner of weirs: (a) round corner; (b) sharp corner

Water Surface Profile

Sargison and Percy (2009) investigated the free-surface profile over four configurations of broad-crested weirs. The found:

(a). A reduction in surface height near the upstream corner of the crest.

(b). Horizontal streamlines over the weir crest.

(c). A reduction in profile near the downstream end of the crest to follow the downstream slope except for the vertical downstream face which exhibits leaping flow.

(d). Flow that departs the toe of the weir with a low head and high velocity.

Velocity Distribution

Nguyen (2006) conducted experiments on flow over oblique weirs and measured the distribution on the vertical of the horizontal velocity (see Figure (3-15)). The velocity profile was considered as a combination of a flow in an open channel (in the lower part) and a surface jet-flow (in the upper part). It can also be seen that the surface velocity is very large over the slope and gradually decreases along the downstream channel as well as the profiles become logarithmic.

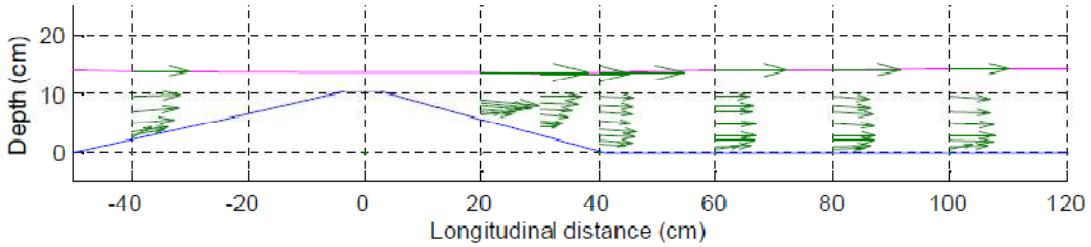

Figure (3 - 15): Velocity profiles on the downstream of the weir (Nguyen, 2006)

3.5 Flow over Broad-crested Weirs with Compound Cross-section

3.5.1 Introduction

As stated above, flow through the breach can be simulated by the hydraulics of broad-crested weir flow. Hence, the background related to the flow over compound broad-crested weirs is to be presented. The study of analytical solutions will be cataloged by two flow situations (perfect and imperfect) and each catalogue includes two types of cross-section geometry (rectangular and trapezoidal).

In addition to the flow patterns shown in Figure (3-7), because of the fact that the contraction and expansion will occur, some phenomena are expected. For instance, eddies, flow separation and shock waves (Figure (3-16)). In the case of channel with compound cross-section, the flow behavior and characteristics including the velocity distribution, interactions and vortices are shown in Figure (3-17).

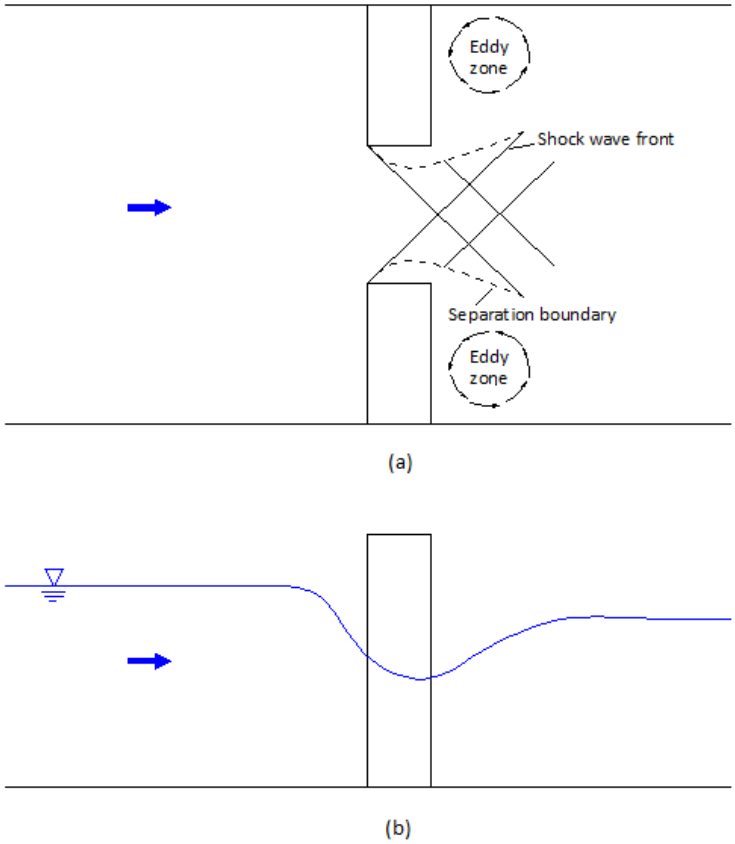

Figure (3 - 16): Definition sketch of flow through constriction: (a). Plan view; (b) Side view (after Chow, 1986)

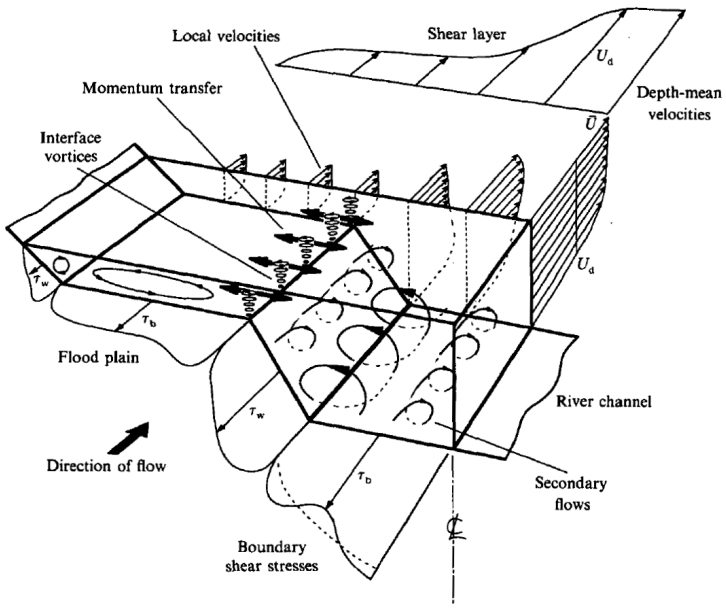

Figure (3 - 17): Hydraulic parameters associated with overbank flow in a two-stage channel (Shiono and Knight, 1991)

3.5.2 Discharge Equation

The literatures about rectangular and trapezoidal control sections will be reviewed in this section, including the emerged and overtopping flow conditions. Both the perfect and imperfect weir situations are to be discussed.

Perfect Weir Situation

Rectangular Compound Cross-section

Gögüs *et al*. (2006) studied the flow over the broad-crested weirs with rectangular compound cross-section. In their research, the discharge equations were given by two flow situations namely emerged and overtopping situations (see Figure (3-18)).

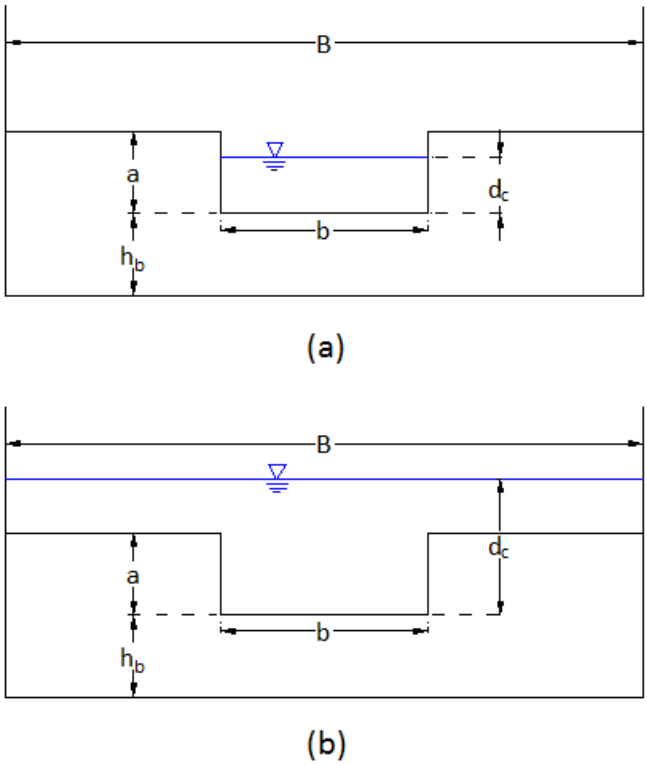

Figure (3 - 18): Two different flow situations through weir section

(a). Emerged Situation ($H_0 \le 1.5a$, $d_c \le a$)

Emerged situation refers to the flow only passing through the breach. In the study of Gögüs *et al.* (2006), the discharge equation obtained as a function of upstream water depth is Equation (3-17), i.e.:

$$Q = C_d \frac{2}{3} b \left(\frac{2}{3} g \right)^{1/2} H_0^{3/2} \qquad (3\text{-}37)$$

in which, b is the width of the lower weir crest, h_0 is the upstream water level and H_0 is energy head above the lower weir crest.

(b). Overtopping Situation ($H_0 > 1.5a$, $d_c > a$)

In this case, flow occurs through the compound cross section, the discharge equation can be expressed as a function of upstream water depth (Gögüs *et al.*, 2006):

$$Q = C_d \left(\frac{g}{B}\right)^{1/2} \left[ba + B\left(\frac{2}{3}H_0 - \frac{ba}{3B} - \frac{2a}{3}\right)\right]^{3/2} \qquad (3\text{-}38)$$

in which, B is the total width of the compound weir section and a is the step height of the weir. In this equation, the control section is considered as combination of two rectangular sections over the weir crest and in the lower part. Two critical depths as a function of upstream energy head are applied.

Based on Equations (3-37) and (3-38), Gögüs *et al.* (2006) studied the effects of width of the lower weir crest and step height of broad-crested weirs of rectangular compound cross section on the values of the discharge coefficient. Gögüs *et al.* (2006) concluded that increasing the lower weir crest width results in higher values of the discharge coefficient at a decreasing rate for a given value of H_0 / L_w, particularly when $H_0 / L_w < 0.4$. Besides, the step heights almost had no influence on the discharge coefficient except for some cases within certain conditions. Moreover, the values of the discharge coefficients are larger for emerged cases than for the overtopping cases. The sketch of the model is shown in Figure (3-19).

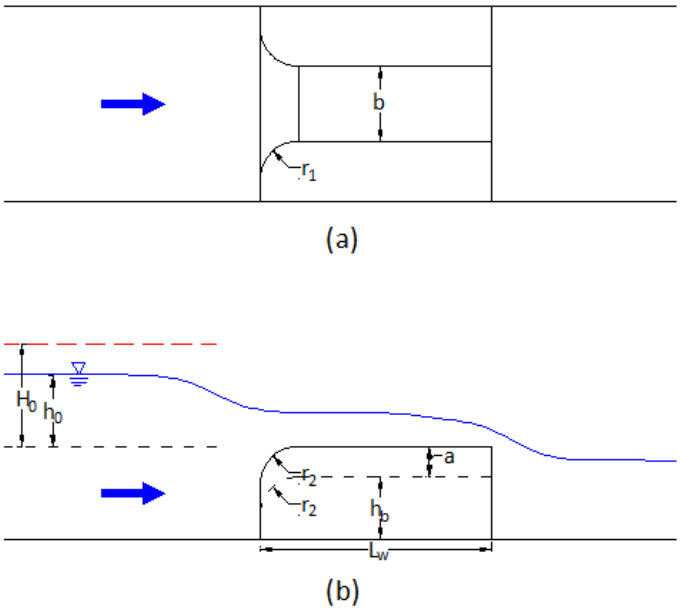

Figure (3 - 19): Definition sketch of models: (a). Plan view; (b). Side view

Trapezoidal Compound Cross-section

(a). Emerged Condition

Bos (1985) studied the flow over broad-crested weirs with trapezoidal control section (Figure (3-20)) and the discharge equation in emerged flow condition was given as below:

$$Q = C_d \left(bd_c + md_c^2 \right) \left[2g \left(H_0 - d_c \right) \right]^{1/2} \tag{3-39}$$

in which C_d is the discharge coefficient, b is the width of the lower weir crest, m is the side slope, d_c is the critical depth and H_0 is energy head above the lower weir crest.

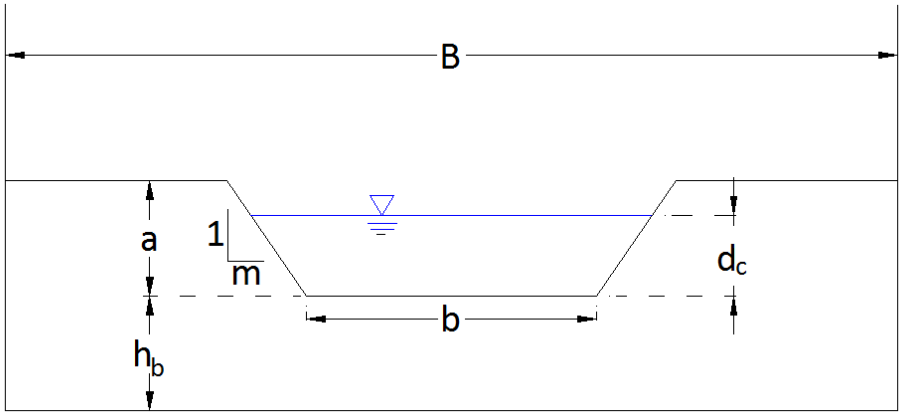

Figure (3 - 20): Sketch of broad-crested weir with trapezoidal compound-section in emerged condition

It should be noted that the superposition of the discharge equations of rectangular and triangular control sections is not valid in the case of broad-crested weir. According to Bos (1985), the combination would result in strongly variable values of discharge coefficient due to the fact that the critical water depths are different from each other ($\frac{2}{3}H_0$ for rectangular control section and $\frac{4}{5}H_0$ for triangular control section). In addition, the mean flow velocities through the rectangular and triangular portions are of significant difference. However, if the flow is critical (Fr =1), Equation (3-12) can be rewritten as:

$$\frac{u_c^2}{2g} = \frac{A_c}{2\bar{b}} = \frac{bd_c + md_c^2}{2b + 4md_c} \tag{3-40}$$

in which A_c is the flow area of critical flow and $\bar{b}$ is the depth averaged width. Since for ideal fluid flow $H_0 = H_1 = \frac{u_c^2}{2g} + d_c$, it yields:

$$H_0 = \frac{3bd_c + 5md_c^2}{2b + 4md_c} \tag{3-41}$$

which indicates that if b and m are known, the ratio $\frac{d_c}{H_0}$ is a function of m and $\frac{H_0}{b}$. The values regarding to this relationship are shown in Appendix C, Table (C-1).

(b). Overtopping Condition

For trapezoidal compound cross-section (Figure 3-21), the discharge equation has not been found in the literature. But in BEED model (see section 2.3.3), it shows that the discharge through the crest and in the breach is calculated separately. In the present study, a linear combination of Equations (3-18) and (3-39) is presented to describe the discharge equation for the trapezoidal control section in overtopping condition. The combination yields:

$$Q = C_{dc} 1.7 B_c H_{0c}^{3/2} + C_{db}\left(bd_c + md_c^2\right)\left[2g\left(H_{0b} - d_c\right)\right]^{1/2} \tag{3-42}$$

where, C_{dc} is the discharge coefficient over the crest, C_{db} is the discharge coefficient in the breach, H_{0c} is the energy head above the weir crest, H_{0b} is the energy head above the breach bottom. The first part on the right hand of the equation represents for the discharge over the crest and the second part for the discharge through the breach. If the weir geometry and the upstream energy head are known, then the discharge through the weir can be estimated with proper discharge coefficients.

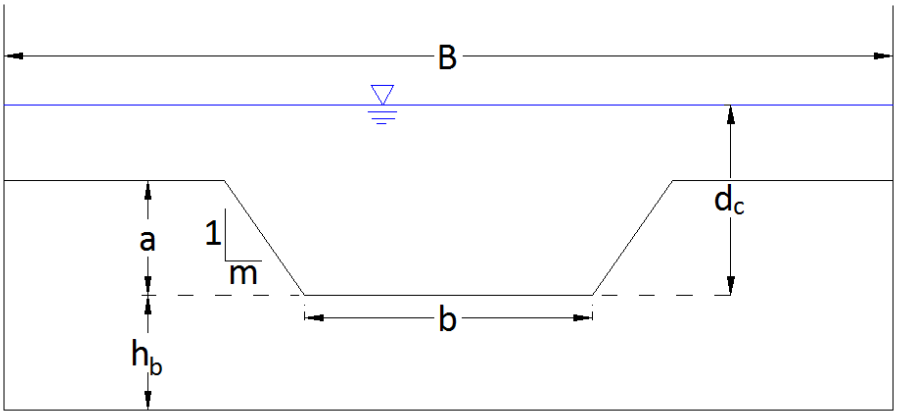

Figure (3 - 21): Sketch of broad-crested weir with trapezoidal compound-section in overtopping condition

Imperfect Weir Situation

Depending on the flow conditions, the weir breaching could happen in imperfect weir situations. Equation (3-24) can be applied in this case. But due to the tail water effects and energy dissipations, small values of discharge coefficient are expected in compound weir flow. Particularly in emerged condition, the validation of the coefficient of submergence (Equation (3-26)) on the discharge through breach needs to be evaluated.

3.5.3 Energy Loss

As in perfect weir situations the downstream has no influence on the upstream. Therefore, it is more interesting to investigate the energy loss in imperfect flow in which the downstream plays a role. The three sources for energy losses discussed in section 3.4.3 are considered valid for the weirs with compound cross-section. In this case, flow would experience the contraction and expansion which can be interpreted as a conversion from potential to kinetic energy followed immediately by a reconversion from kinetic to potential energy (Chow, 1986). Unlike the weirs without breach or straight channel with constant width that the contraction and expansion are only in vertical direction, for the weirs with compound cross-section the contraction and expansion might be both in vertical and horizontal. In addition, the Borda-Carnot equation in the case of compound weirs requires the velocity information which is not easy to be accurately collected. The form drag model needs to be modified in this case as the flow width is not constant along the channel.

Analytical Solution

For the expansion loss form drag model, Equation (3-27) is still valid as the width of channel is the same in the upstream and downstream. However, the discharge per unite width in the channel is not uniform due to the compound cross-section of the weir. In this case, the energy conservation in the upstream and momentum balance in the downstream give:

$$d_0 + \frac{\alpha_0 Q^2}{2gB^2 d_0^2} = d_1 + \frac{\alpha_1 Q^2}{2gB_1^2 d_1^2} \tag{3-43}$$

$$\frac{1}{2}\rho g\left(d_b + h_b\right)^2 + \rho\beta_1 \frac{Q}{B_1} u_1 = \frac{1}{2}\rho g d_2^2 + \rho\beta_2 \frac{Q}{B} u_2 \tag{3-44}$$

in which d_b is the water depth above the lower weir crest. In emerged condition, the flow width in section of weir B_1 equals to the averaged width of the breach $\bar{b}$. In overtopping condition, B_1 equals to the total width of the weir crest B. Therefore, according to Equations (3-27), (3-43) and (3-44), the energy loss can be estimated according to the downstream water depth d_2. The form model for the weirs with a breach (the compound weirs) is to be examined in the study.

Previous Investigation

Bukreev *et al.* (2008) defined energy loss coefficient as:

$$\zeta = \frac{E_1 - E_2}{E_2} \tag{3-45}$$

Bukreev *et al.* (2008) conducted experiments for the weirs with rectangular compound cross-section in emerged condition and found that the energy loss coefficient depends significantly on the initial tailwater depth and the smaller this depth, the greater the energy loss. Also, the energy loss decreases with increasing the submergence. By comparing with the loss at the entrance of the breach, Bukreev *et al.* (2008) also stated that the loss at the entrance of the weir makes a significant contribution to the total loss.

3.5.4 Related Investigations

Upstream Water Depth and Discharge

Gögüs *et al.* (2006) presented the upstream water depth-discharge relation for the broad-crested weirs with rectangular compound cross-section as is shown in Figure (3-22). Wahl *et al.* (2006) simulated the similar experiment with a numerical model (Winflume) as shown in Figure (3-23). According to Gögüs *et al.* (2006) and Wahl *et al.* (2006), it can be concluded that a break in the slope of the rating curve would be expected due to the sudden change in the flow area.

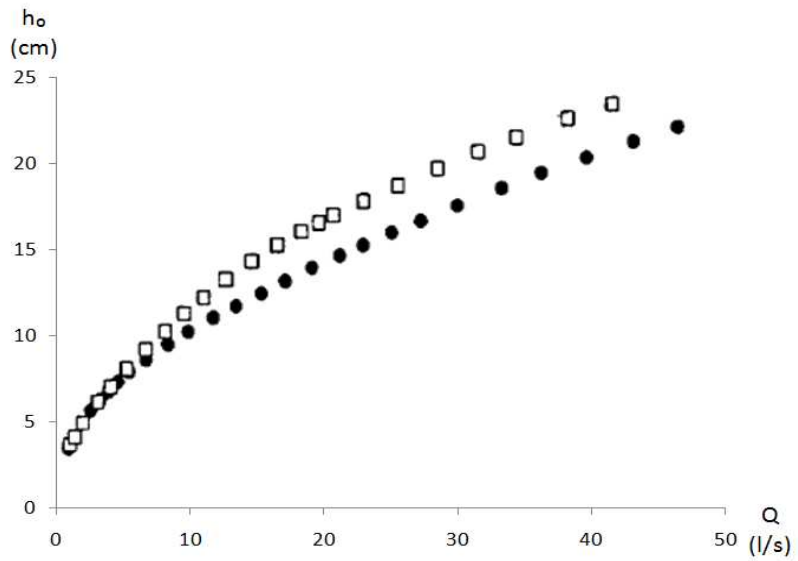

Figure (3 - 22): Depth-discharge rating curves (Göğüş et al. (2006))

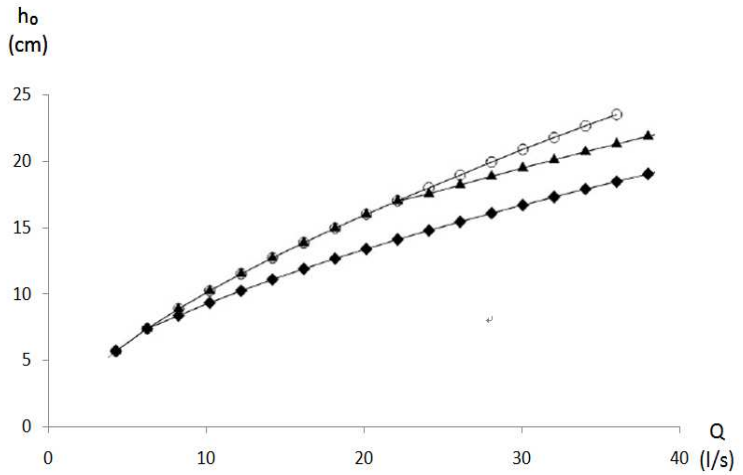

Figure (3 - 23): Water depth-discharge rating curves based on Winflume (Wahl et al., 2006)

3.6 Conclusions

The previous investigations have provided the information for understanding the behaviors and properties of breach flow. A large amount of researches based on laboratory experiment have been done on flow over normal broad-crested weirs. The flow characteristics for instance, discharge coefficient, energy loss and velocity distribution have been studied. As for compound weirs, some literatures regarding to the weir with rectangular section can be found. Nevertheless, the experiments on broad-crested weirs with trapezoidal compound cross-section are not complete compare to normal weirs. The information of the effects of the control section (breach properties) on weir flow is required. Also there is a question as to whether the linear combination method can be applied to estimate the discharge for overtopping condition. Besides, some other information which is useful for the study of breach flow such as the energy loss caused by weir and overtopping discharge distribution over the crest and the breach are still not clear. Therefore, these unknowns and some other hydraulic characteristics of breach flow are necessary to be further investigated by conducting laboratory experiment.

CHAPTER 4. LABORATORY EXPERIMENT

4.1 Introduction

4.1.1 Types of Models

According to Chanson (2004), three types of models are commonly used in hydraulics: analytical models, numerical models and physical models. Analytical models are theoretical solutions of the fundamental principles within a framework of basic assumptions, e.g. the discharge equations listed in Chapter 2. Numerical models are computer softwares which solve the basic fluid mechanics equations, e.g. Delft3D to be used in the present study. A physical model is a scaled representation of a hydraulic flow situation such as the laboratory weir model.

4.1.2 Interpretation of Laboratory Model

As stated in the literature review, a number of laboratory experiments were carried out by researchers before, but most of them were tested over mobile models were made of sand, clay and sand-clay mixtures which would be breached by flows acting as a "real" breaching event. However, fixed model is applied in the present study and some simple comparisons between fixed model and mobile model are made below.

Table (4 - 1): Comparison between fixed models and mobile models

Point of view	***Fixed models***	***Mobile models***
Assumption	Idealized breach shape as assumed in the numerical models. It corresponds to different stages of breaching. Dynamic processes such as erosion and sedimentation are not taken into account.	More close to the real breaching event, including the whole dynamic process during the breaching
Experiment preparation	The shape and size to be build according to literatures	Need well prepared and precisely design, such as discharges, breaching time and position, model materials etc.
Experiment duration	As it is fixed, there is no time limitation	The breaching takes place fast and the duration is short (hours)
Observation and measurement	Easy to observe and measure under different flow conditions (emerged, overtopped etc.). For every configuration, the test can be repeated	High requirement of equipments to collect data. Model is onetime and the flow conditions are limited

Research	Bukreev *et al.* (2008)	Fujita and Tamura (1987), De Looff *et al.* (1997), Andrews *et al.* (1999), Coleman *et al.* (2002), Mohamed *et al.* (2002), Chinnarasri *et al.* (2003), Zhu *et al.* (2006), Dupont *et al.* (2007), Yan and Cao (2008), Schmocker *et al.* (2010)
Overview	Help understand the flow properties in details at certain stage of breaching and with various flow conditions	Good understand of dynamic process of breaching for models made of different types of material

In conclusion, both types of models have advantages and disadvantages. Each offers different information about breaching. With the data from a mobile model, for particular stage, the breach can be shaped by a fixed model to collect more detailed information. With the data of a fixed model, the behavior of a mobile model under certain flow condition can also be predicted somehow. Hence, the information from both can help modeling breaching processes.

4.1.3 Dimensional Analysis of Physical Model

Basic Parameters

It is important to know the parameters that may have a significant effect on the results of an experiment. These basic parameters are useful for dimensional analysis. They can be simply divided into three aspects: flow properties, flume geometry and physical constants. The flow properties include discharge Q (m^3/s), water depth d (m), flow velocity V (m/s) and kinematic viscosity ν (m^2/s). The geometry parameters are flume width W (m), weir height P (m), weir crest length L_w (m), weir crest width B_c (m), weir slope M $(-)$, breach side slope m $(-)$, breach width b (m), breach length l (m) and breach height a (m). For physical constants, it consists of gravity acceleration g (m/s^2) and flow density ρ (kg/m^3).

Scale Rules

When a prototype is difficult to set up, a scale model with reduced dimensions is generally applied in hydraulic engineering. In order to keep the similarity between the physical model and real-world prototype, scale rules are required. Although geometrical dimensions can be changed, some properties, such as gravity and material properties (density, viscosity etc.) cannot be scaled (Schiereck, 2007).

The scale parameter is defined as:

$$N_X = \frac{X_p}{X_m} \tag{4-1}$$

In which, N_X is the scale of parameter X, X_p and X_m are its prototype value and model value respectively. The widely used scales in hydraulics are length scale and velocity scale:

$$N_L = \frac{L_p}{L_m} \tag{4-2}$$

$$N_V = \frac{V_p}{V_m} \tag{4-3}$$

In modeling of hydraulic engineering, two scale rules are commonly performed, namely Froude similitude and Reynolds similitude.

The Froude similitude requires:

$$Fr_p = Fr_m \tag{4-4}$$

or

$$\frac{V_p}{\sqrt{g_p L_p}} = \frac{V_m}{\sqrt{g_m L_m}} \tag{4-5}$$

If the gravity acceleration in both prototype and model is the same, then

$$N_V = \frac{V_p}{V_m} = \sqrt{\frac{L_p}{L_m}} = \sqrt{N_L} \tag{4-6}$$

It implies that the velocity scale is determined by the square root of the length scale and velocity in prototype is larger than that in scale model.

The Reynolds similitude holds:

$$Re_p = Re_m \tag{4-7}$$

or

$$\frac{V_p L_p}{\nu_p} = \frac{V_m L_m}{\nu_m} \tag{4-8}$$

By applying Equation (4-6), the scale of kinematic viscosity gives:

$$N_\nu = \frac{\nu_p}{\nu_m} = N_L^{3/2} \tag{4-9}$$

It indicates that the kinematic viscosity is larger in a model than in prototype if $N_L > 1$. In reality, condition (4-9) is quite difficult to be met.

Generally speaking, only the most dominant mechanism needs to be modeled. In free-surface flows (e.g. flows with free surface), gravity plays a dominant role. In this case, a Froude similitude is usually applied. In fully enclosed flows (e.g. pipe flows), viscosity effects on the solid boundaries are important. Hence, the Reynolds similitude can be used. (Chanson, 2004)

In present study, the research domain belongs to the free-surface flows, and then the Froude similitude is to be in use. However, the requirements of both Froude similitude and Reynolds similitude cannot be satisfied at the same time, which results in an application of Froude similitude with Reynolds number different in the physical model and prototype. In the case, gravity dominants over viscosity and the Froude similitude yields:

$$N_{Re} = \frac{Re_p}{Re_m} = N_L^{3/2} \tag{4-10}$$

Therefore, Reynolds number becomes much smaller in the model than in prototype. According to Chanson (2004), scale effects would arise due to the distortions caused by e.g. viscosity, whereas the effects are often small. In the case of flow over weirs, the flow above the crest can be treated as an ideal flow since the effects of resistance and viscosity are small.

4.2 Experiment Set-up

The dam break is modeled by a weir with a fixed profile and lateral contraction in a laboratory flume. The experiment is expected to fulfill the objective of getting insight into the characteristics and behaviors of breach flow over broad-crested weir with breach of various geometries. In order to achieve this, some tests were conducted by varying the breach geometry. The experiment was carried out in the Fluid Mechanics Laboratory of Delft University of Technology.

4.2.1 Layout of Flume

The experiment was carried out in a horizontal flume with a width of 2 m, a height of 0.2 m and a length of 19.2 m. The bottom is stick by gravels with diameter of 0.005 to 0.006 m. The flume is wide enough to minimize the effect of the side walls on the interacted area and turbulence induced by the entrance of the inlet. The sketch of layout is shown in Figure (4-1) and a picture of flume is shown in Figure (4-2).

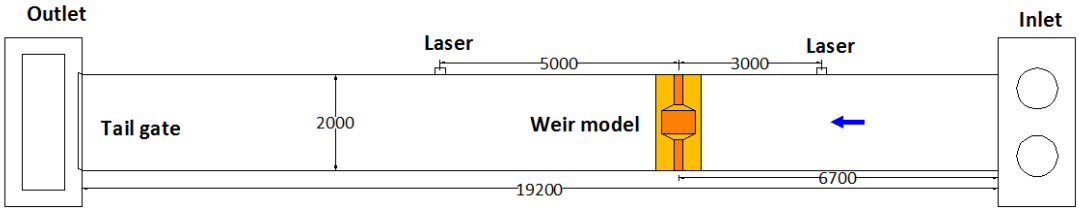

Figure (4 - 1): Sketch of flume layout (in mm)

Figure (4 - 2): Picture of flume layout

4.2.2 Weir Design

The weir model is built with a crest length L_w = 180 mm, a height P = 130 mm and a slope of 1V:3H in both upstream and downstream with the breach located in the middle of the weir crest (see Figure (4-3) and (4-4)).

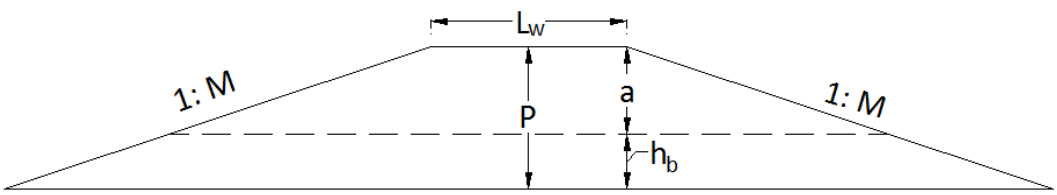

Figure (4 - 3): Side view of designed weir

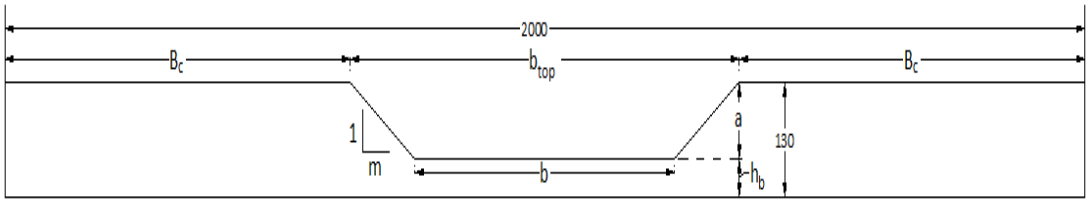

Figure (4 - 4): Control section of designed weir

The weir control sections were designed to test the effect of breach properties on the breach flow. In combination with the breaching process presented in Chapter 2, five cases with different control sections are to be tested Figure (4-5). By keeping some breach parameters constant, the effect of the specific stage can be evaluated. The detailed explanations are presented in Table (4-2).

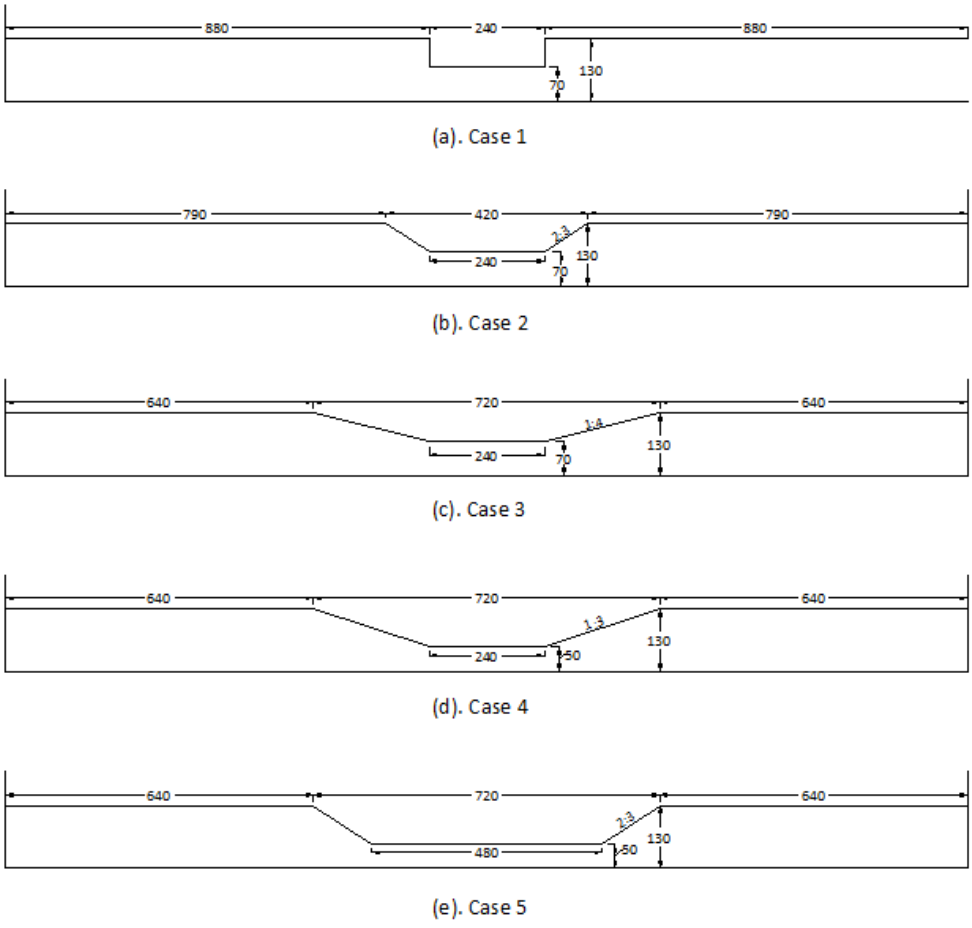

Figure (4 - 5): Control sections for 5 cases (in mm)

Table (4 - 2): Breaching stages to be tested

Stages	Constant Parameters	Tested Cases
Top width widening	Breach height and bottom width	1, 2, 3
Breach deepening	Top and bottom width	3, 4
Widening and deepening	Breach slope	2, 5
Bottom width widening	Breach height, top width	4, 5

The changes of breach size are illustrated in Table (4-3). Cases 1 and 2 are considered as the initial breaches as described in the mathematical models. Cases 3 and 4 represent the enlargement of the breach during breaching and case 5 represents the final shape of breach in the study.

Table (4 - 3): Changes of breach geometry

Cases	Relative Changes	Increased Area
1→2	Top width: (420-240)/240=0.75	37.5 %
2→3	Top width: (720-420)/420=0.71	45.5 %
3→4	Breach height: (80-60)/60=0.33	33.3 %
4→5	Bottom width: (480-240)/240=1	25 %

4.3 Instrumentation

4.3.1 Point Gauges

A point gauge is used to measure the vertical distance between two single points in the flume. The device consists of a solid probe with a vernier measuring the elevation of desired points (Figure (4-6)). Generally, the water depth can be calculated by measuring the elevation of the surface and the bottom at one point. The difference between two values is the water depth. It is usually mounted at a beam above the water surface and moveable along the beam. The device is quite handy without complicated electronic instruments, hence, widely used in laboratory experiments.

Figure (4 - 6): Point Gauge

4.3.2 Prosonic Flow Meter

The Prosonic Flow Meter consists of a transmitter and measuring sensors (Figure (4-7)). The transmitter is used to actuate the measuring sensors and the measuring sensors work bidirectionally as sound transmitters and sound receivers. Since there is transit time difference between the two sensors, the transit time difference is proportional to the flow velocity. Hence, based on this principle, the discharge through the pipe can be calculated for a particular cross-sectional area and then the data can be directly read from the transmitter.

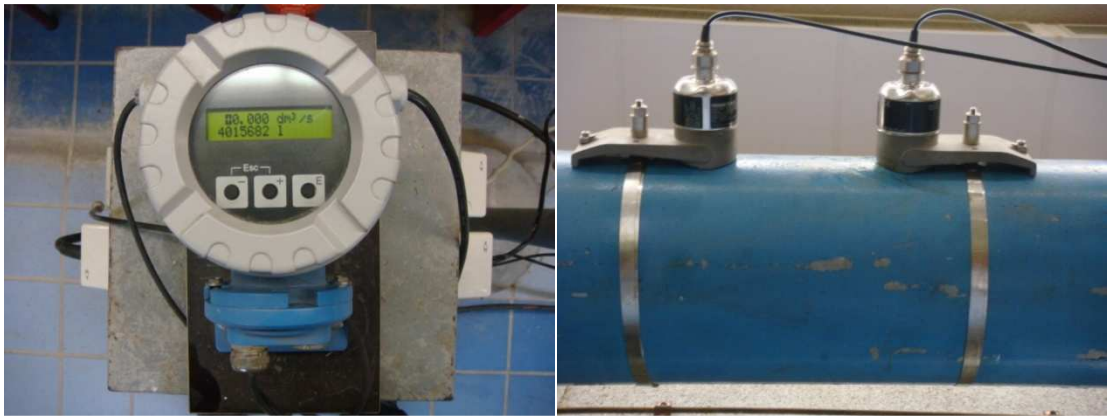

Figure (4 - 7): Prosonic Flow Meter: transmitter (left) and measuring sensors (right)

4.3.3 ADV – Acoustic Doppler Velocimeter

Acoustic Doppler Velocimeter (Vectrino) measures the flow velocity using the Doppler Effect. Ultra sound pulses are transmitted from the center transducer, and the four receivers sense the flections from particles that move along with the flow. The sampling volume of the Vectrino is place at 5 cm in front of the center transducer. The magnitude of instantaneous velocity can be presented via a computer and the data can be storaged within the recording time. In some cases, the signals are not good enough due to the turbulence and air bubbles around the probe; increasing the size of the sampling volume or adding china clay into the flow help to obtain reliable data. Usually, data is considered to be good when the correlation has at least 80% confidence. The system of ADV is shown in Figures (4-8) and (4-9).

Figure (4 - 8): Acoustic Doppler Velocimeter (Vectrino)

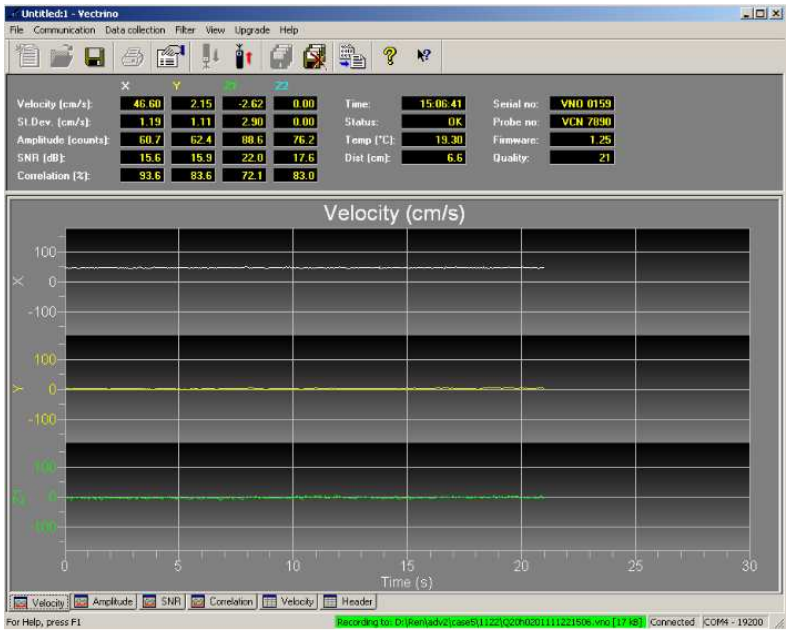

Figure (4 - 9): Screen view of ADV computer program

Two kinds of probes are available. One is downlooking and the other is sidelooking (see Figure (4-10)). In the present experiment, sidelooking probe is applied. When all four beams are covered with water (around 3-4 cm) all three velocity components can be collected. For shallow water, with the two lower horizontal receivers the velocity components, stream velocity and transverse velocity, can be obtained, which offers a way to collect 2D-data with only the lower receiver arms submerged.

Figure (4 - 10): Downlooking probe (left) and sidelooking probe (right)

4.3.4 Laser Distance Meter

The system of Laser Distance Meter mainly consists of three elements: beamer, floating plate and computer program. Particularly, the water level difference between two cross-sections can be calculated. The principle is that horizontal reference level needs to be set first and the distance between the water level and reference level can be calibrated via the reflection of the floating plate. Since the floating plate rises and falls with the instantaneous water level, by assuming the longitudinal distance is much larger than the width of cross-section, the reference based distance measured can represent the cross-section. Hence, the water level distance between two cross-sections can be calculated by the laser of each via the aid of the computer. This instrument provides an accurate and efficient way to calculate water level difference. (Figure (4-11))

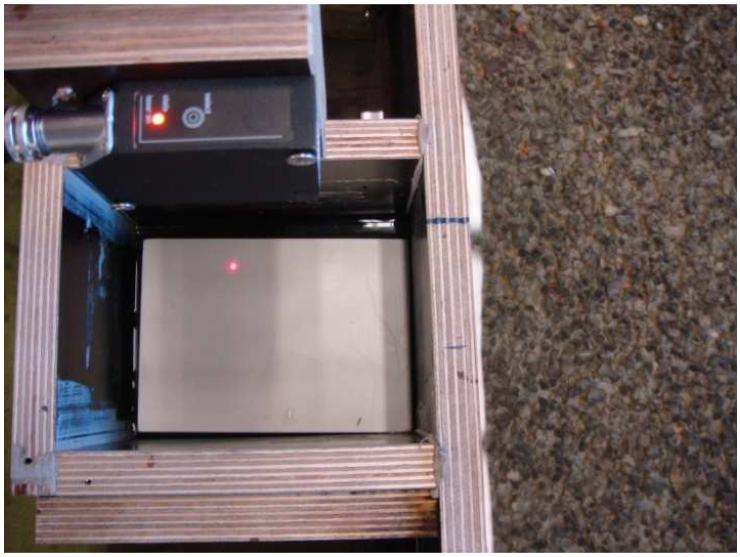

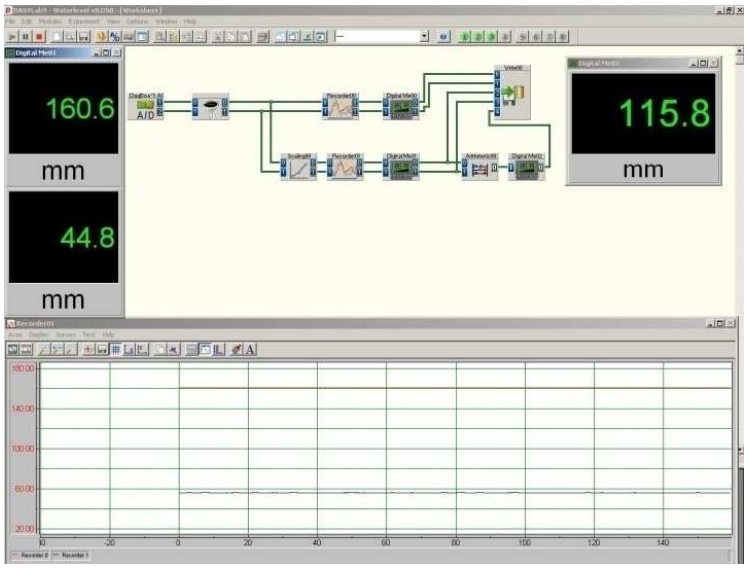

Figure (4 - 11): Laser Distance Meter (up) and computer program (down)

4.4 Measurements Elaboration

4.4.1 Head Measurement

The energy head consists of water depth and the velocity head. The water depth is preferred to be measured by the Laser Distance Meter with the advantages of high accuracy and efficiency. The velocity head difference can be calculated with the averaged velocity which equals to the discharge divided the flow area. By considering the influence of the weir model to the flow, the total energy head is measured by laser distance meter at about 3 meters in front of the weir. In order to obtain the relation of the upstream water depth and the discharges for different cases, a range of discharges from 3 l/s to 60 l/s were set by the valve in the inflow pipe and the tail gate was controlled low enough to get the perfect weir situation. The collected data can be found in Tables (5-1) and (5-3).

4.4.2 Energy Loss Measurement

In the experiment, the measurement reference level was set to the level of the flume bottom and two measurement sections were selected to calculate the energy head loss: one at about 3 meters in front of the weir and another is placed at 5 meters in the downstream of the weir. For given discharges, the head loss was measured by gradually raising the tail gate from low level (almost horizontal) to such a high level that the weir model was totally submerged (8 to 10 different heights). For given tail heights (3 to 4 different heights), a range of discharges (3 l/s to 60 l/s) was applied. Hence both the situations that perfect and imperfect weirs and overtopping and emerged were all included. The measurement was taken when the signal shown in computer was stable. In some cases, especially downstream of weir, fluctuations would occur, and then the data was collected by taking the average. The collected data can be found in Appendix B, Tables (B-1) and (B-2).

4.4.3 Discharge Coefficient

The investigation into the discharge coefficient is focused on the perfect weir situation. According to the theoretical analysis, the discharge for a compound cross-section can be expressed as a function of the upstream water depth for perfect weir situation. The upstream head, as stated before, was measured by the Laser Distance Meter at 3 meters upstream of the weir and the discharge could be read directly from the Prosonic Flow Meter.

4.4.4 Velocity Profile

Velocity profile was measured with the aid of the ADV (Vectrino), since it is interesting to find out the velocity profile in the breach in both transverse and vertical directions, which is not applicable in shallow water. Therefore, the measurement was only taken in relatively large discharge flow condition (e.g. 50 l/s in case 5).Over the crest, the flow velocity was measured only in one point in the vertical, assuming it was the depth averaged velocity. This was done since the water depth on the crest was very small. Special attention was given to assume that the two lower receivers of the Vectrino were submerged in the water. All the data had at least 80 % correlation confidence and even many 90% level. Besides, these were despiked by a matlab file to remove the unrealistic peak values. The collected data of measured velocities can be found in Appendix B, Table (B-3).

4.4.5 Discharge Distribution

In order to investigate the discharge distribution in the breach and over the crest, the flow velocity (ADV) and water depth (point gauge) were measured over the crest. Therefore, the discharge passing over the crest can be calculated by the product of them. As the total discharge can be calibrated from the Prosonic Flow Meter, the discharge through the breach was obtained by subtracting the amount of discharge through the crest. The reason for this is the fact that the flow over the crest is more uniform and streamlined, which could provide good velocity signals collected by the lower receivers of Vectrino. However, the flow in the breach was more complicated, with turbulence and bubbles etc., and usually the sampling signals around the border were weak. In other words, the discharge measurement over the crest is more accurate than that in the breach.

4.5 Accuracy Analysis

4.5.1 Discharge

The discharge flowing into the flume was measured by the Prosonic Flow Meter. The measured error of reading can be estimated (Appendix C, Figure (C-1)). As can be seen, the basic accuracy of the measuring system is 0.5%. With decreasing the flow rate, the accuracy decreases. In the present experiment, a range of discharges was specified. The largest error occurs at the lowest discharge (Q = 3 l/s) around 4 %. As for the highest flow rate (Q = 60 l/s), the error is approximated as 0.7 %. Due to the turbulence of flow in the pipe, there is a small fluctuation of reading around the desired value. Another factor influencing the measurement was the air in the pipe of incoming flow which can be reduced by flushing the pipe with a large discharge before doing the experiment.

4.5.2 Velocity

Velocity signal was collected via the ADV. The accuracy might be decreased when there were strong turbulences and air bubbles around the receivers. This could happen in the breach. It could be improved by adjusting the settings and adding the clay particles to the flume. In the study, most of the data was collected having over 80% correlation. For some cases, e.g. in the breach, some signals were within the 70% - 80% correlation. However, over the crest where the flow is stable and streamlined, signals with around 90% correlation could be obtained. In addition, matlab scripts were used to despite the unrealistic peak values in case it occurs.

4.5.3 Water Depth

The water depth was measured over the weir with the point gauge which has an accuracy of 0.1 mm. In the breach where turbulence and vortexes were generated, the accuracy could decrease due to the fluctuations of water level, but it was considered to be acceptable for just having qualitative description of the water level in the breach. The water depth measured by Laser Distance Meter in the upstream and downstream is with a measured error of ± 0.4 mm.

CHAPTER 5. ANALYSES OF RESULTS ON BREACHING DISCHARGE

5.1 Discharge Coefficient

The discharge coefficient is an important parameter for predicting the breaching discharge. In this section, the perfect weir situation is considered and both the emerged and overtopping conditions will be discussed. In order to have a clear impression, the breach geometries for the five cases are shown in Figure (5-1).

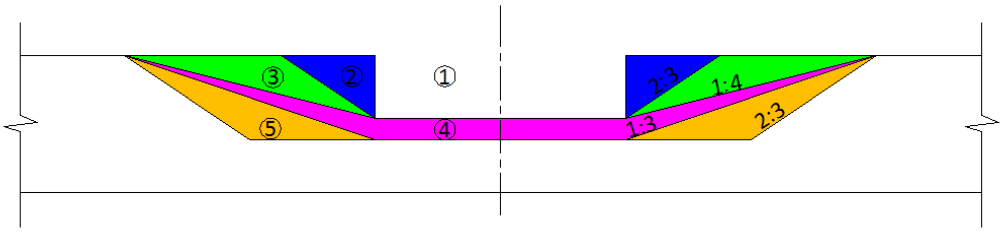

Figure (5 - 1): The design of weir geometries

5.1.1 Emerged Condition

Perfect Weir Situation

In the emerged condition (Figure (5-2)), the flow passes through the breach only. A contraction can be expected to occur due to the reduced width of the flow section.

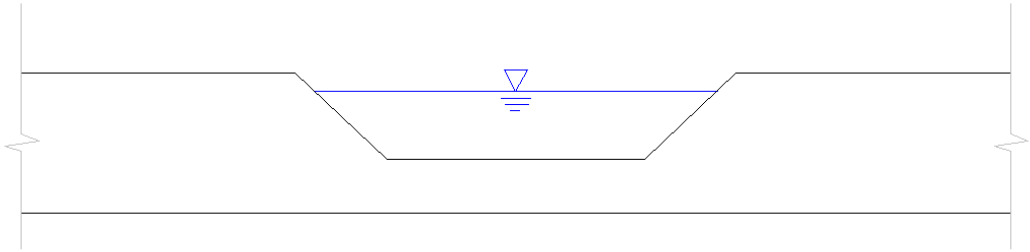

Figure (5 - 2): Weir sketch in emerged condition

By applying Equation (3-39) for all the cases including the weir with rectangular control section (m = 0), the discharge coefficient versus total energy head including error bars is plotted in Figure (5-3) and the corresponding data is shown in Table (5-1). By comparison, the conclusions are made as below:

(a). The discharge coefficients for the five cases are between 0.77 and 0.87. By increasing the upstream energy head (discharge), the values for each case are more or less constant. If increasing the discharge, the effects of the friction are reduced and the difference among the cases becomes less according to the trend.

(b). As can be seen, the discharge coefficients in cases 1 and 2 are smaller compared to the other cases. The cause of this phenomenon is the stronger contraction in these two cases which have smaller top widths.

(c). Although the cases 3, 4, and 5 which have the same top width are slightly different in the values of discharge coefficient, it still can be seen that the discharge coefficient increases during the processes of breach deepening and bottom widening. The combine effect of widening and deepening with constant breach slope is illustrated in cases 2 and 5. Figure (5-3) shows that the discharge coefficient is significantly increased due to the combined effect.

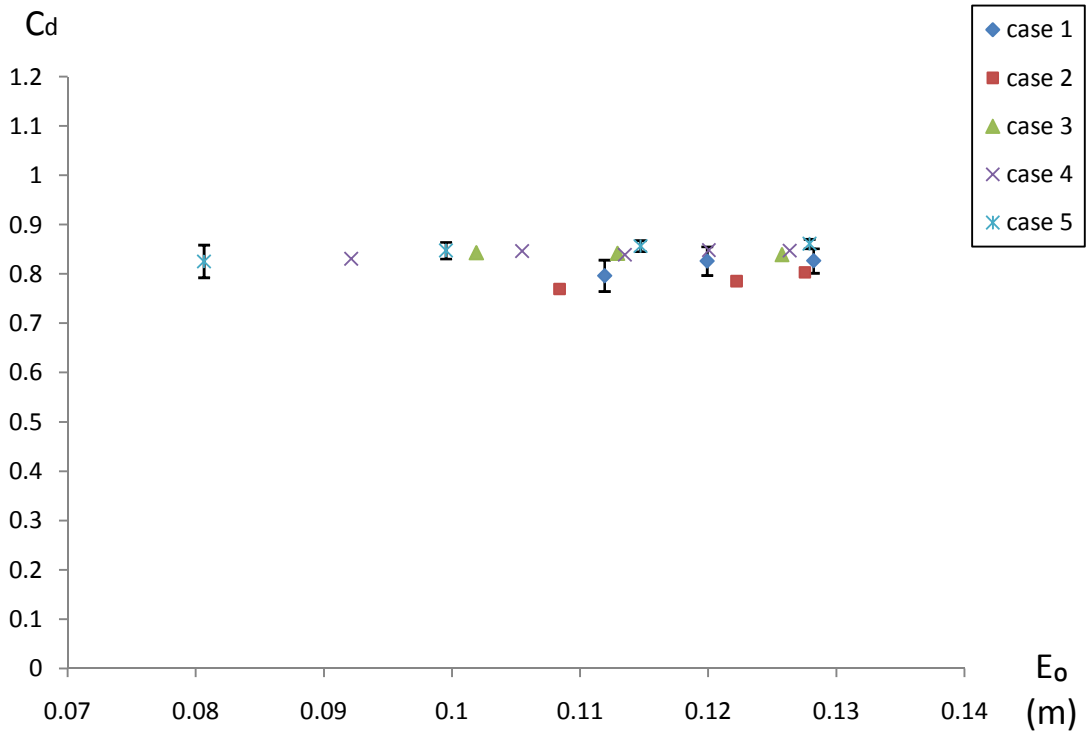

Figure (5 - 3): Discharge coefficient versus total energy head

Table (5 - 1): Data collected in emerged condition (perfect weir situation)

Case 1	Q (l/s)	3	4	5		
	d_o (mm)	111.9	119.9	128.2		
Case 2	Q (l/s)	3	5	6		
	d_o (mm)	108.4	122.2	127.5		
Case 3	Q (l/s)	3	5	8		
	d_o (mm)	101.9	112.9	125.7		
Case 4	Q (l/s)	5	8	10	12	14
	d_o (mm)	92.1	105.4	113.4	119.9	126.2
Case 5	Q (l/s)	5	10	15	20	
	d_o (mm)	80.6	99.4	114.5	127.6	

Particularly for rectangular control section, previous investigations (Bos, 1985 and Fritz and Hager, 1998) on the discharge coefficient can be used for comparison. The results of the present experiment in case 1 and predictions by Equations (3-19) and (3-21) are shown in Figure (5-4). It can be seen that the predictions are 12% - 18% higher than the discharge coefficients for case 1. Two main reasons may lead to the overestimations. First, the lateral contraction generating flow separation and curvature might reduce the discharge coefficient whereas the empirical formulas were proposed based on weirs without contraction in lateral. Second, the weir in case 1 belongs to long broad-crested weirs in which surface undulations may occur (Hager and Schwalt, 1992) and the discharge capacity is quite low that the friction might play a role.

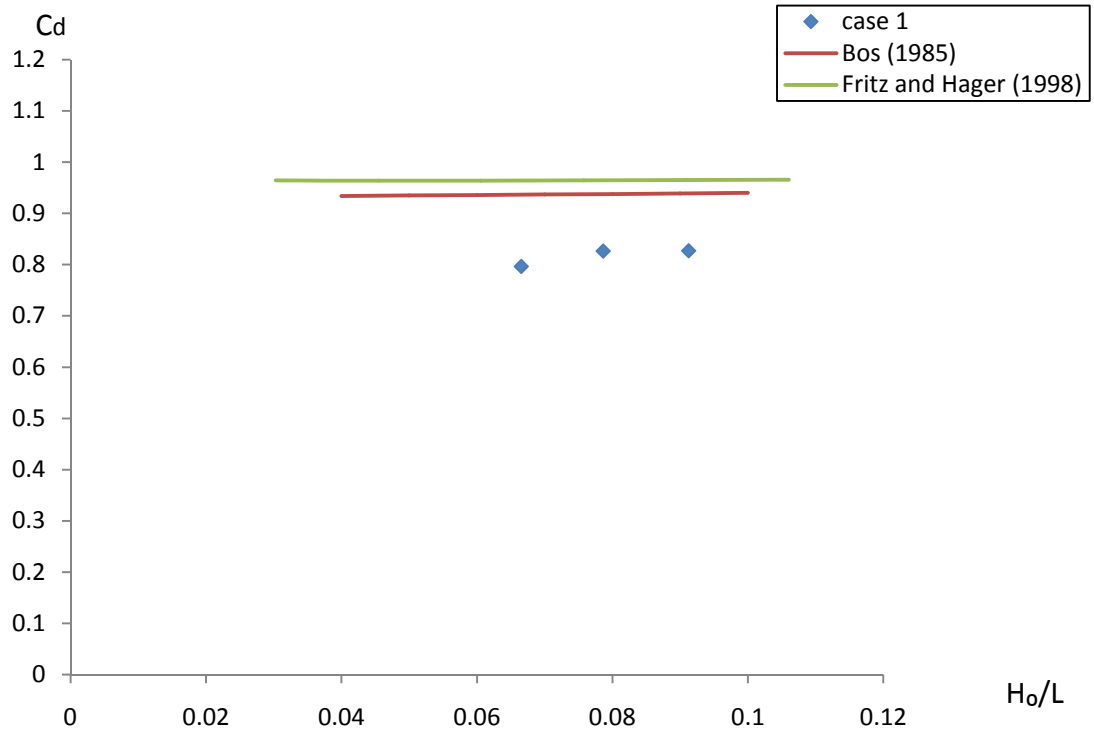

Figure (5 - 4): Comparison on discharge coefficient for rectangular control section

Imperfect Weir Situation

Based on the results in perfect weir situation, the coefficient of submergence is calculated for all cases in imperfect situation. For practical reasons, the downstream water depth is applied in Equation (3-26) instead of water depth in the breach. The comparison is made in Figure (5-5). As is shown, the calculated values based on laboratory measurement fit well with the theoretical predictions of Nikolov *et al.* (1978), especially at high ratio of h_2 / H_0. It also can be concluded that for highly submerged flow, the reduction of discharge coefficient is large.

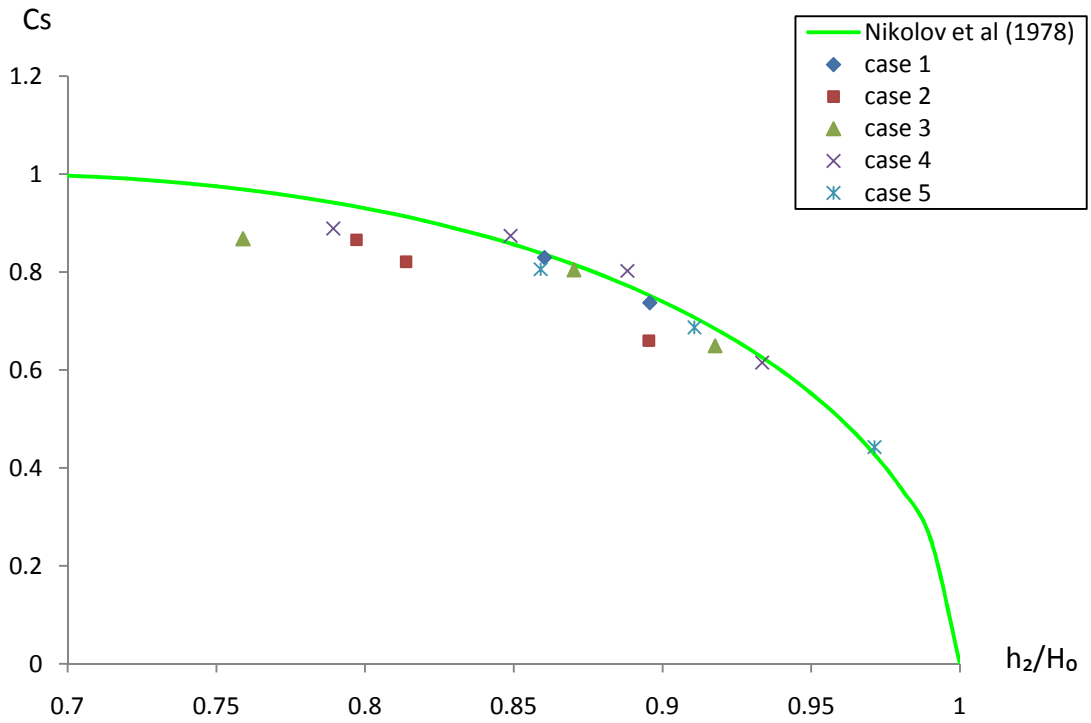

Figure (5 - 5): Comparison of calculation and prediction by Nikolov et al. (1978)

Table (5 - 2) Data collected in emerged condition (imperfect weir situation)

Case 1	Q (l/s)	3	4		
	d_0 (mm)	121.8	126.8		
	d_2 (mm)	116.2	118.6		
Case 2	Q (l/s)	3	5		
	d_0 (mm)	115.9	125		
	d_2 (mm)	110.9	114.4		
Case 3	Q (l/s)	3	5	8	
	d_0 (mm)	109.4	116.7	127.5	
	d_2 (mm)	106	110.4	113.2	
Case 4	Q (l/s)	5	8	10	12
	d_0 (mm)	106.6	113	118.5	124.7
	d_2 (mm)	102.5	105.4	107.4	107.9
Case 5	Q (l/s)	5	10	15	
	d_0 (mm)	104.8	113.8	124.4	
	d_2(mm)	103.1	107.7	113.3	

5.1.2 Overtopping Condition

Perfect Weir Situation

In this condition, the flow passes through the whole width of the weir. An interaction between the flow over the crest and the flow through breach would occur. As the discharge equation for the compound weirs with trapezoidal breach in overtopping condition has not been found in the literature, the discharges over the crest and through the breach will be studied separately. As is shown in Figure (5-6), the flow section is divided into three parts, the

discharge through the breach Q_b, and the discharges over the crest Q_1 and Q_2 which should be identical in theory. The observations during the present experiment show that the flow over the crest is thin and streamlined except close to the breach where transverse flow occurs. However, the flow in the breach is of great turbulence and with a lower water level compared to the flow over the crest.

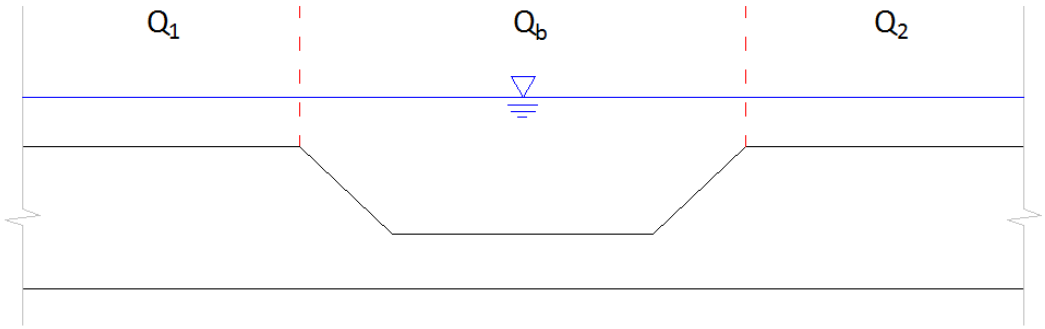

Figure (5 - 6): Weir sketch in overtopping condition

Discharge over the Crest

The discharge over the crest is measured by collecting the velocity signals and corresponding water depths. By neglecting the interaction between the weir crest and breach, the broad-crested weir equation for rectangular cross-section, Equation (3-18), is applied over the weir crest. The discharge coefficient is plotted against total energy head as is shown in Figure (5-7). Based on it some findings are:

(a). The values for all cases vary from 0.79 to 0.98. It can be clearly seen that the discharge coefficients of cases 1, 2 and 5 which have relatively low values increase gradually with the increase of energy head. For cases 3 and 4, the values do not change too much. As a result, the differences caused by the five weir geometries are evident in the range of low upstream energy head and become less by increasing the energy head. So it can be concluded that with the increase of the upstream head, the discharge coefficients approach to the same value and the effect of the breach is reduced.

(b). Besides of including the friction loss and contraction, the streamline curvatures due to contraction and interaction between the crest and breach are also taken into account in the discharge coefficient over the crest. As can be seen, case 1 (rectangular breach) and case 5 (largest breach size) have relatively low values. This is due to the fact that the case 1 owns sharp change in breach geometry which may lead to flow separations and turbulence, and case 5 generates strong curvature over the crest.

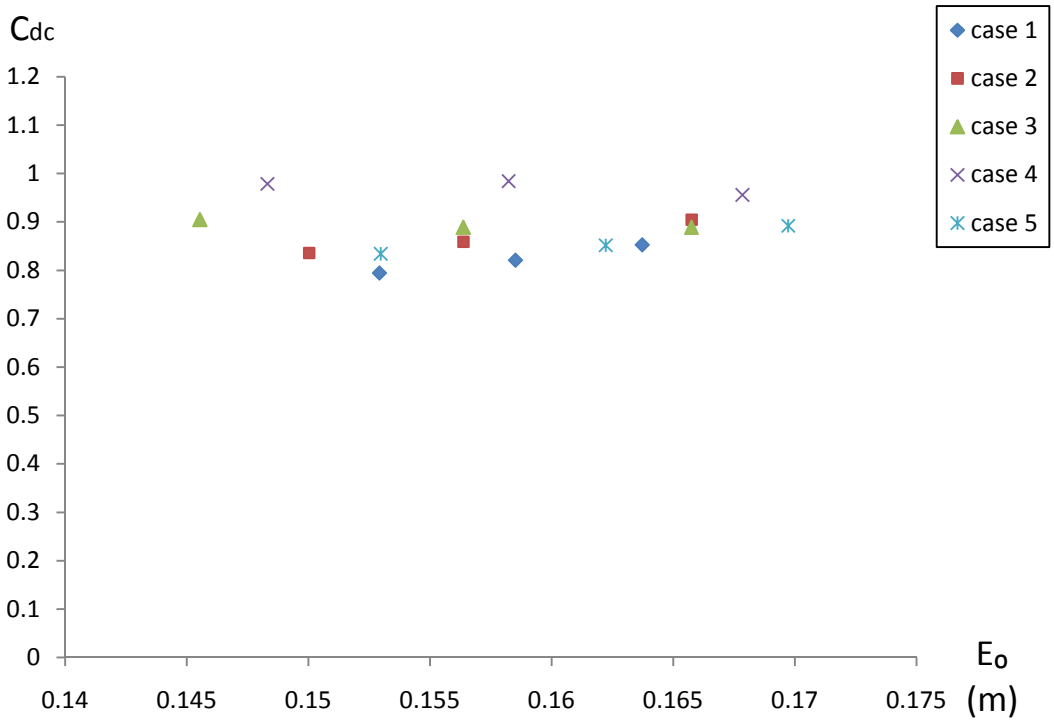

Figure (5 - 7): Discharge coefficient versus total energy head (over weir crest)

Discharge through the Breach

The discharge through the breach can be obtained by subtracting the amount of discharge over the crest from the total discharge. As for the discharge coefficient, the Equation (3-39) is used and the discharge coefficient is plotted against the total energy head in Figure (5-8). It can be concluded that:

(a). The discharge equation for a trapezoidal control section can predict the discharge through the breach rather accurately as the values vary closely around the unit value. According to Figure (5-8), the top width widening of breach reduces the discharge coefficient and in contrast, the breach deepening may result in higher values that come close to the unit.

(b). According to the trend, it can be predicted that the discharge coefficients would be similar for all cases at large flow stages, which is reasonable because the influence of the breach is reduced by increasing the discharge.

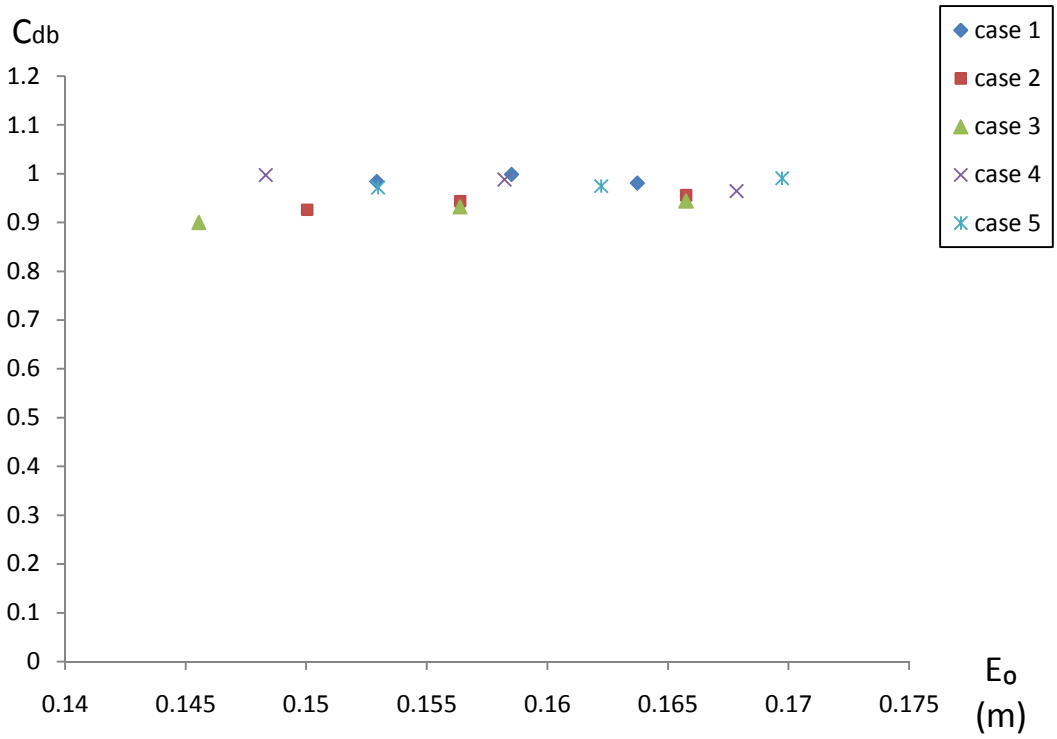

Figure (5 - 8): Discharge coefficient versus total energy head (through the breach)

By considering the flow section as a whole, the linear combination method is applied to express the discharge in overtopping condition. By neglecting the interaction between the flow over weir crest and the flow through the breach, the two equations applied over the crest and in the breach are combined linearly. Finally, including the discharge coefficient, the discharge equation in overtopping condition yields:

$$Q = C_{do}\left[1.7H_{0c}^{3/2} + \left(bd_c + md_c^2\right)\left[2g\left(H_{0b} - d_c\right)\right]^{1/2}\right] \qquad (5\text{-}1)$$

in which C_{do} stands for the discharge coefficient in the case of overtopping. The discharge coefficient versus total energy head is plotted in Figure (5-9). It can be concluded that:

(a). The overall trend for all cases is that C_{do} gradually approaching the unit value with the increasing upstream head. Compared with the emerged condition, the values are more close to 1 as the effect of the breach is reduced.

(b). By comparing the cases 1, 2, and 3, it can be stated that the effect of the top width widening is small and the rectangular breach leads to a slightly lower discharge coefficient than trapezoidal shapes of breach.

(c). The discharge coefficients increase significantly in case 4 compared with case 3, which indicates the process of deepening would have higher values

of the discharge coefficient.

(d). Based on the results from cases 4 and 5, the values decrease obviously in the process of breach bottom widening.

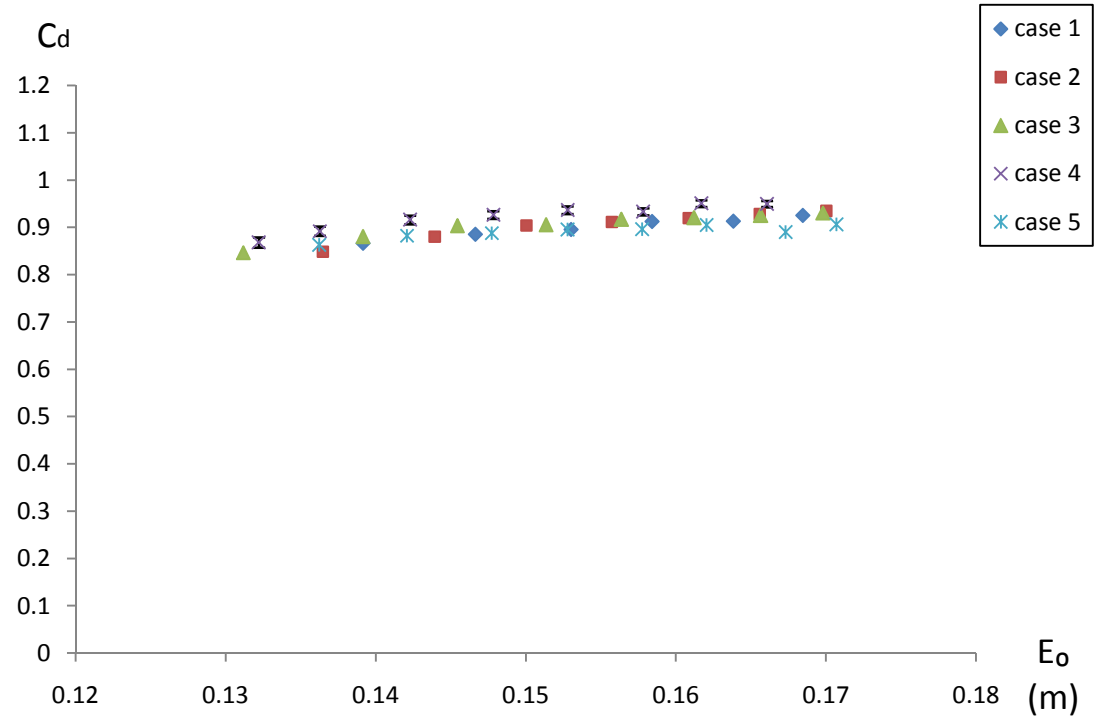

Figure (5 - 9): Discharge coefficient versus total energy head in overtopping flow condition

Table (5 - 3): Data collected in overtopping condition (perfect weir situation)

Case 1	Q (l/s)	10	15	20	25	30	35		
	d_o (mm)	139.1	146.5	152.8	158.1	163.4	167.9		
Case 2	Q (l/s)	10	15	20	25	30	35	40	
	d_o (mm)	136.4	143.8	149.8	155.4	160.4	165	169.3	
Case 3	Q (l/s)	10	15	20	25	30	35	40	45
	d_o (mm)	131.1	139	145.2	151	155.9	160.6	164.9	168.9
Case 4	Q (l/s)	17	20	25	30	35	40	45	50
	d_o (mm)	132	136	141.9	147.3	152.1	157	160.7	164.9
Case 5	Q (l/s)	25	30	35	40	45	50	55	60
	d_o (mm)	135.8	141.5	147	151.9	156.7	160.8	165.9	169.1

Overview

As the discharge equations for emerged and overtopping flows are both derived from the continuity equation and the energy conservation equation, the corresponding discharge coefficients based on them are comparable. In Figure (5-10) the transition of discharge coefficients from emerged condition to overtopping condition regarding to the upstream energy head is shown. The following conclusions can be made:

(a). The discharge coefficients are all below 1 and increase with the increase of the upstream energy head. In emerged flow, the bottom friction plays an important role and the discharge coefficient is relatively low. After overtopping, the discharge coefficients are more close to each other. The values for emerged flow are more scattered due to the complex three-dimensional characteristics of the flow there. However, the influence of the breach is reduced for overtopping condition.

(b). For the same case, the effects caused by breach are different in the emerged condition and overtopping condition. For instance, the discharge coefficient for case 5 is highest in emerged flow and lowest in overtopping flow, in addition, the difference is the smallest in the two flow conditions compared to others. This is caused by the fact that the large size of breach is dominant to breach flow. Therefore, it is reasonable to see that the values for the small-sized trapezoidal shape of breach, e.g. case 2, are of great difference under the two flow conditions.

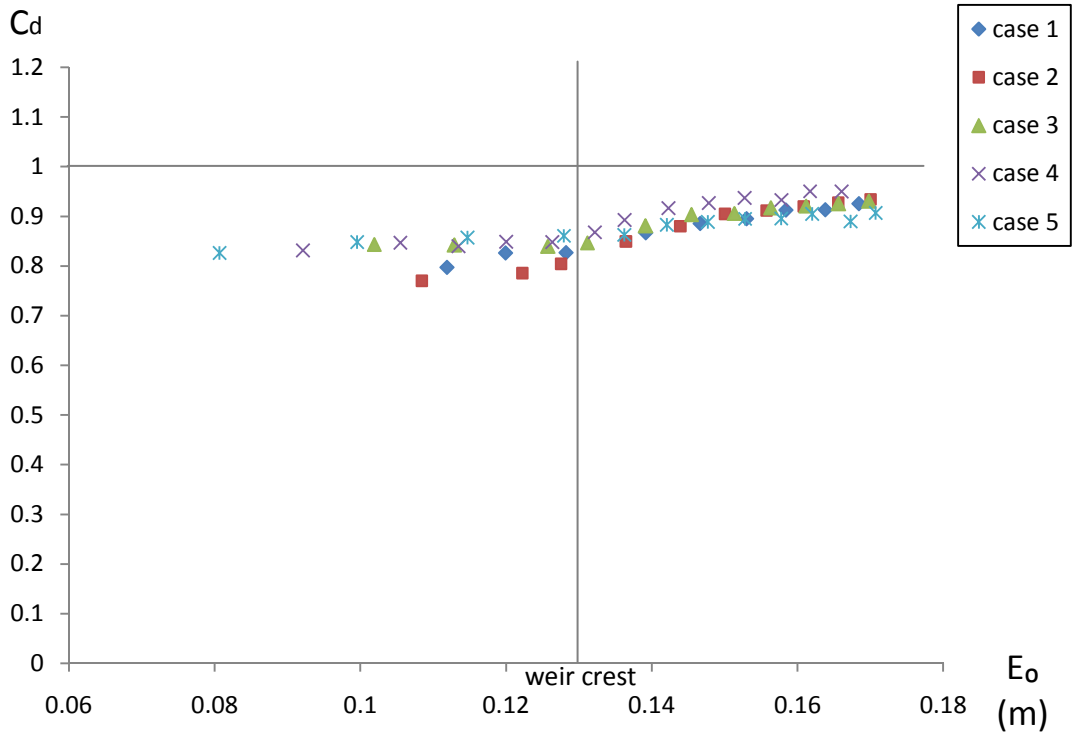

Figure (5 - 10): The overview of discharge coefficient from emerged condition to overtopping condition

5.2 Discharge Distribution

Particularly in the overtopping condition, it is of great interest to investigate how much water passes through the breach or over the crest. This is important to simulate the breaching process and to estimate the discharge contributing to the breaching. In the present study, each case is tested by three discharges. The total discharge is measured by the Prosonic Flow Meter and the discharge over the crest is measured with the aid of the Vectrino and the point gauge. Again, the discharge through the breach can be obtained by subtracting the discharge over the crest from the total discharge. The laboratory results are shown in Figure (5-11) and the theoretical predictions have been made with Equations (3-39) and (3-42) by applying the unit value for the discharge coefficients.

According to Figure (5-11), the analytical predictions for cases 1 and 5 slightly underestimate the experimental data and overestimate for case 3 at low discharges. As for the other cases, the theory and experimental results fit well. Overall, it can be concluded that the laboratory results for the five cases are in good agreement with the theoretical predictions. Based on the results of the theory and the experiment, it can be found that the breach conveys less compared to the total discharge with the increase of discharge for each case. It is quite logic that for the discharges the effect of the breach is reduced and at same discharge, the larger the breach size is, the more water flows through the breach.

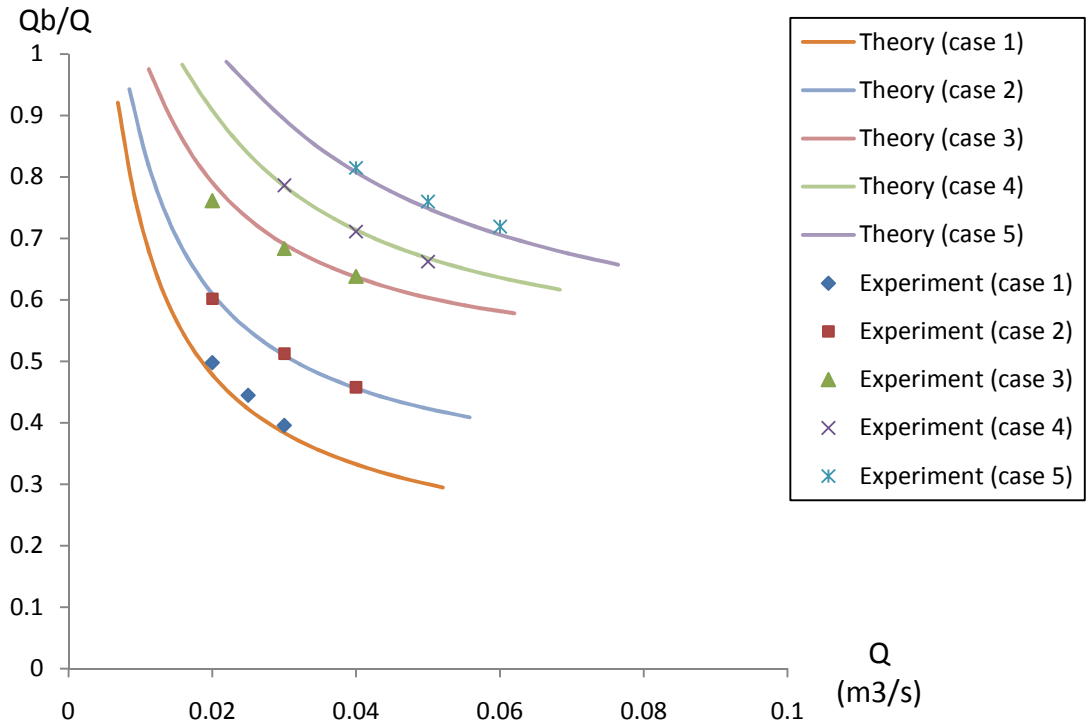

Figure (5 - 11): Comparison of theory predictions and laboratory measurements on discharge distribution

During the experiment, it can be found that the flow through the breach would become subcritical first and then the flow over the crest if gradually raising the tail gate from the low level. Hence, there is a situation that subcritical flow through the breach and critical flow over the crest at the same time. The discharge distribution in the situation is illustrated in Figure (5-12). Due to the small size for first two cases, the appearance the situation is not clear. So the results for last three cases are plotted. As can be seen that the difference on the discharge distribution is small between the perfect weir situation and the imperfect weir situation in cases 3 and 4, which indicates the influence of flow situations for these two cases is small to the discharge distribution. But in case 5 which owns larger size of breach, the difference is evident. Therefore, it can come to the conclusion that the discharge distribution is dependable on the downstream water depth in the case of relatively large breach in the situation of subcritical flow through the breach and critical flow over the crest.

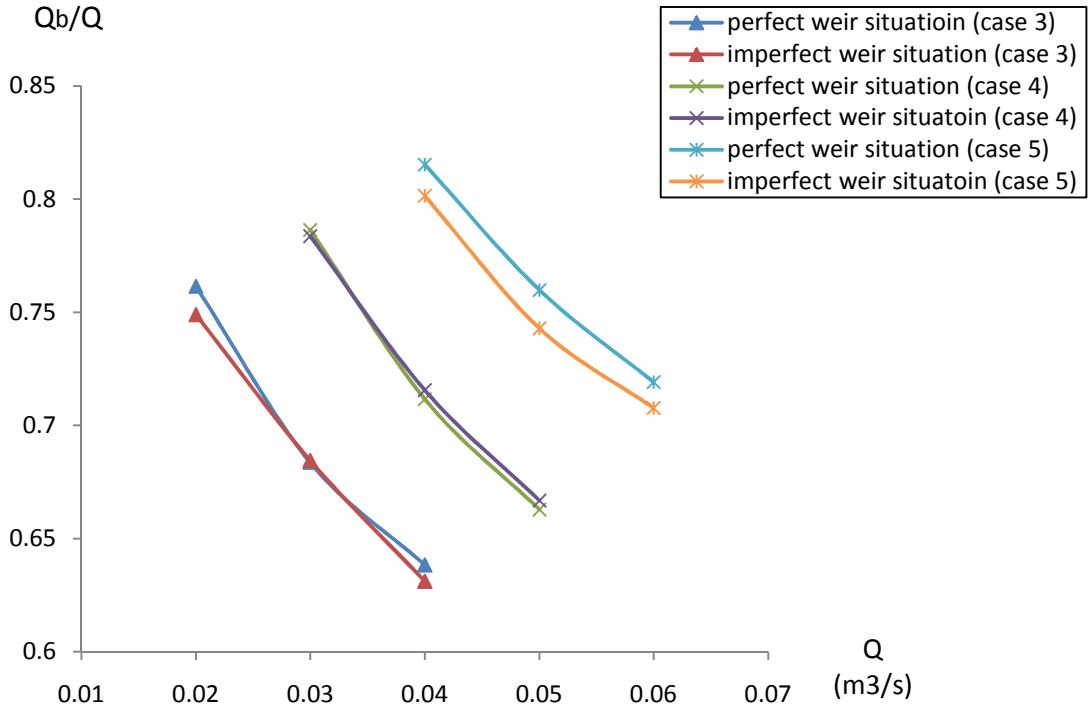

Figure (5 - 12): Discharge distribution in the case of subcritical flow through the breach and critical flow over the crest

CHAPTER 6. ANALYSES OF RESULTS ON ENERGY HEAD LOSS

6.1 Energy Head Loss and Upstream Flow Conditions

In an imperfect weir situation, the upstream flow conditions have a significant influence on energy head loss for given downstream water levels. According to the energy conservation in the upstream and momentum balance in the downstream, it can be found that the energy loss can be expressed as a function of the downstream water depth in imperfect weir situations. By applying a high tail gate for each case and gradually increasing the upstream discharge, the energy head loss against the upstream discharge is shown in Figure (6-1).

It can be seen from Figure (6-1) that the energy head loss increases with the increase of the discharge which is the same case for the flow over weirs in general. But in present study, there is an obvious break in slope for each curve. It is caused by the sudden change of flow control section when the flow starts overtopping. According to the curves, the slope break occurs one after the other from cases 1 to 5, which depends on the size of the breach. It is also worth mentioning that the energy loss increases with the increase of the discharge but at different rates before and after the overtopping. In emerged condition, the curve rate tends to decrease from cases 1 to 5. However, the rate drops significantly after overtopping and the curves seem to be parallel to each other. Therefore, one can draw the conclusion that the energy dissipation rate decreases during the enlargement of the breach in emerged condition and comes to the same constant value after overtopping for all the cases.

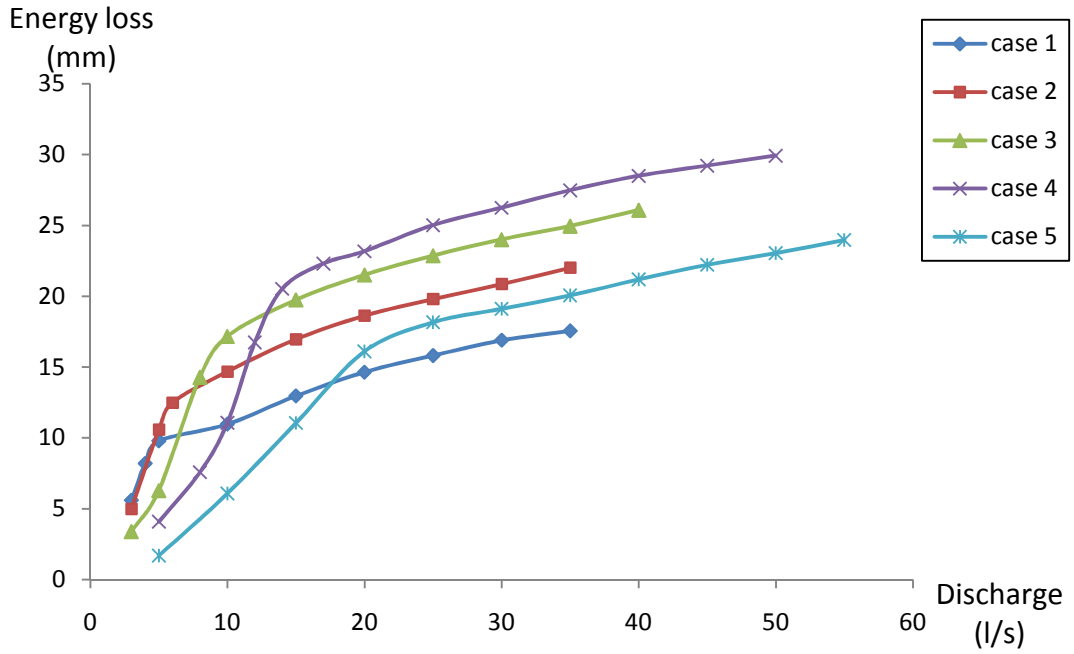

Figure (6 - 1): Energy head loss versus upstream discharge at given tail heights

As stated before, the energy head loss can be expressed as a function of the downstream water depth in highly submerged condition. In Figure (6-2) the relation between them is presented. Still, there is a break in the slope on each curve. In both the emerged and overtopping conditions, case 2 may have more energy loss than case 1 at the same downstream water depth, which indicates that the top widening from the rectangular to trapezoidal breach results in a higher loss. This also applies to cases 2, 3 and 4. Therefore, the processes of top widening and deepening of the breach have more energy dissipation. Nevertheless, at the same downstream flow condition, the energy loss drops less in case 5 after widening the breach bottom compared to case 4.

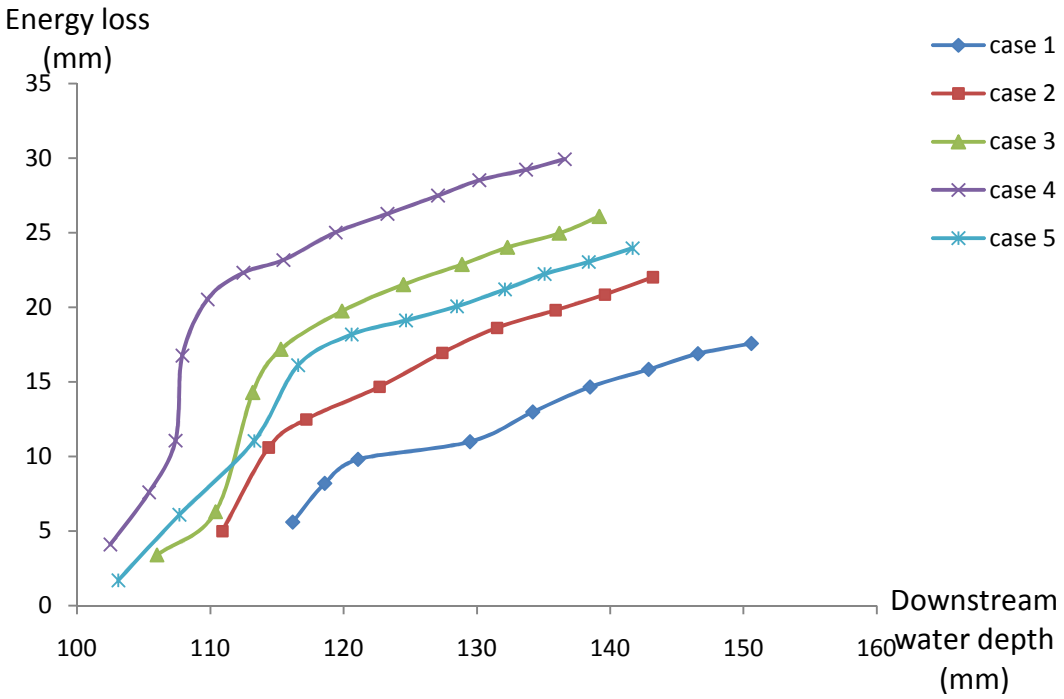

Figure (6 - 2): Energy head loss versus downstream water depth

6.2 Energy Head Loss and Downstream Flow Conditions

In imperfect weir situations, the downstream does have influence on the upstream. By applying certain discharges at the upstream boundary, the effects of downstream water depth on the energy head loss can be investigated by varying the tail gate. Figures (6-3) to (6-6) show the results regarding to the influence of downstream flow condition in imperfect situations.

As is shown for all cases, the energy loss decreases with the increase of the downstream water depth and the larger discharges imposed, the higher loss would be generated at the same downstream water depth. These are also in line with the flow over weirs in general. Particularly for the modeled breach flow, the decreases are at a decreasing rate from cases 1 to 5 during the enlargement of the breach.

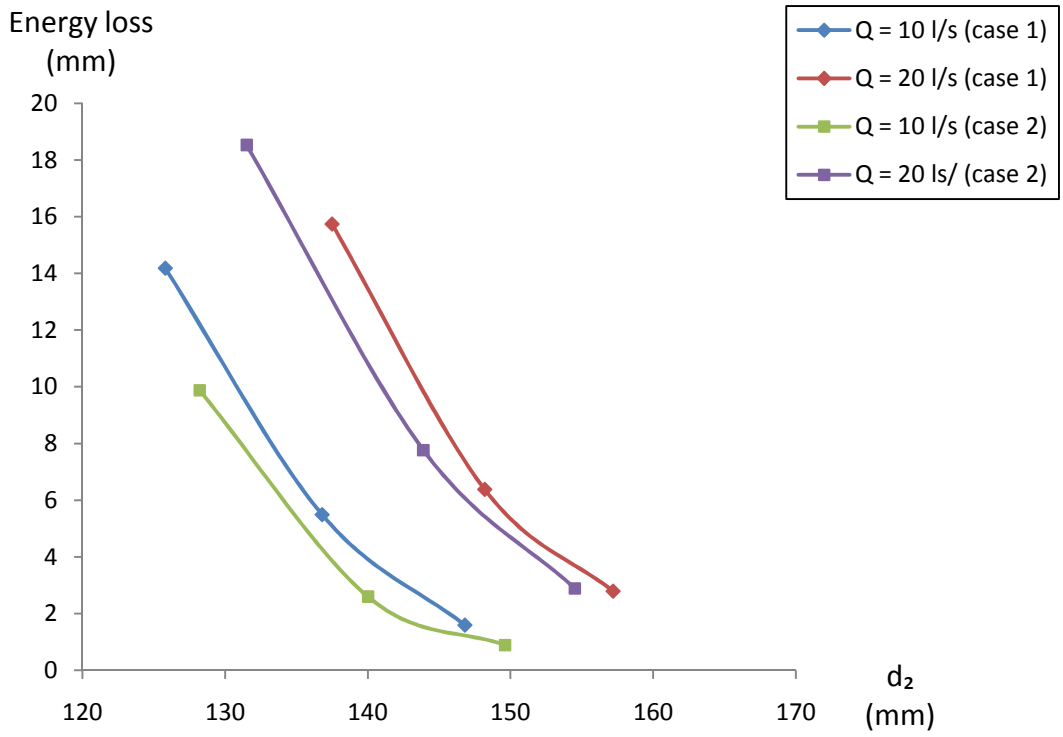

Figure (6 - 3): Energy head loss versus downstream water depth (case 1 and case 2)

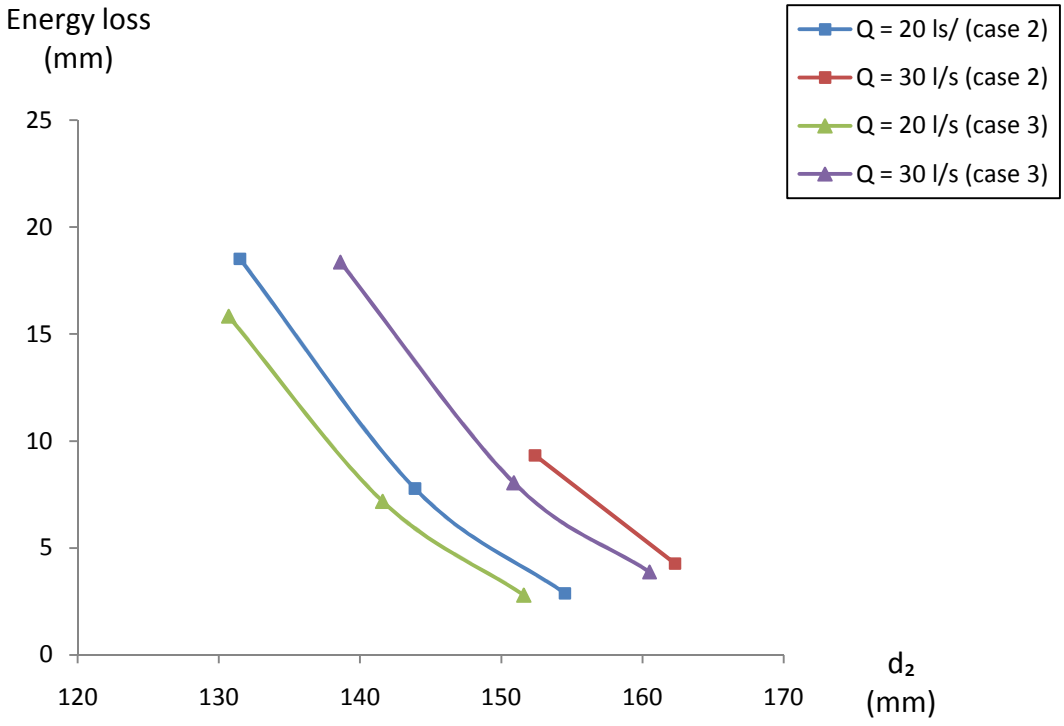

Figure (6 - 4): Energy head loss versus downstream water depth (case 2 and case 3)

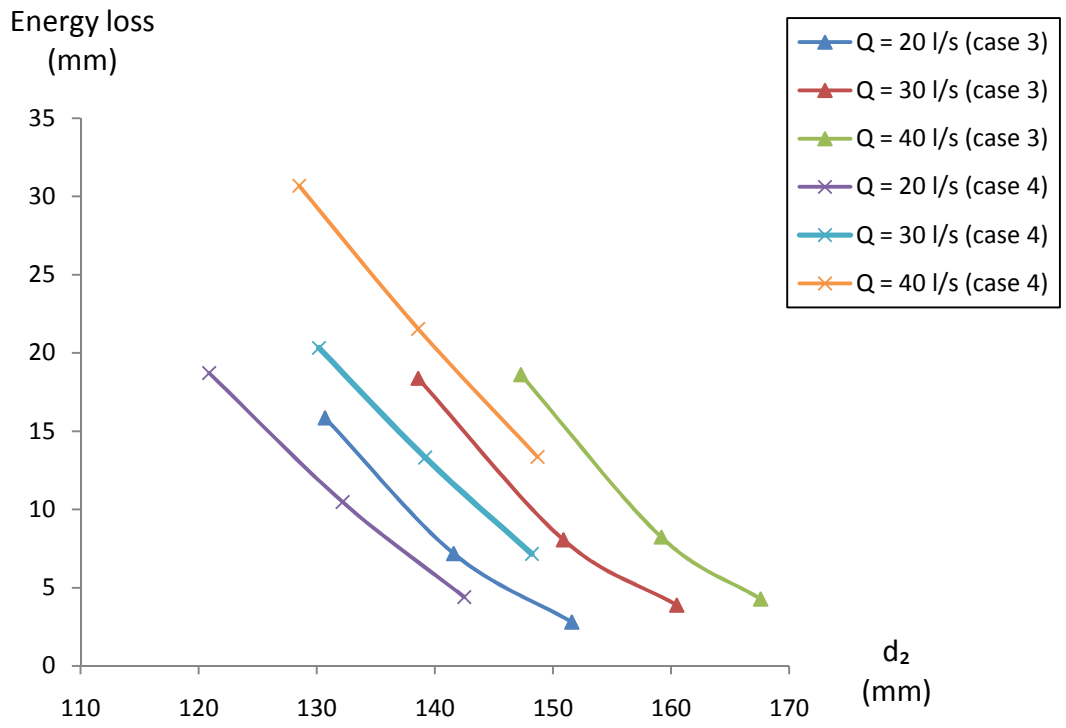

Figure (6 - 5): Energy head loss versus downstream water depth (case 3 and case 4)

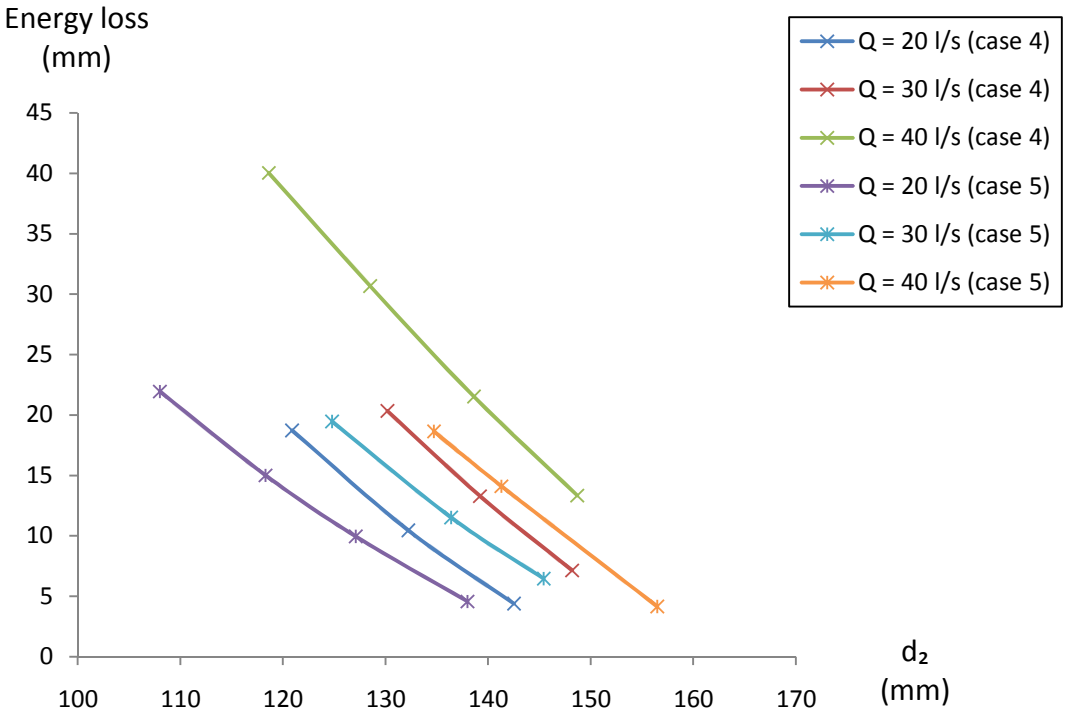

Figure (6 - 6): Energy head loss versus downstream water depth (case 4 and case 5)

In order to have an overview, the relation is plotted with the discharge Q = 20 l/s for all cases in Figure (6-7). It can be found that the rates of the curves decrease slightly from case 1 to 5. In the case of extreme highly submerged flow (a few millimeters loss), e.g. cases 1, 2 and 3, the rate may further decrease.

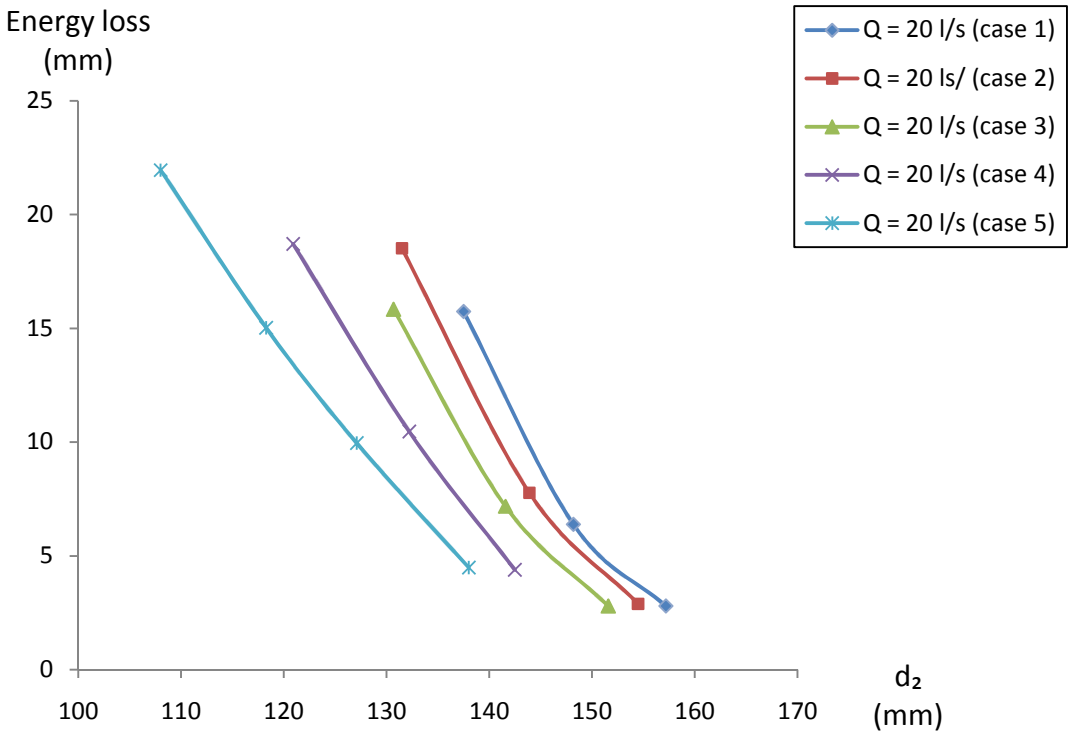

Figure (6 - 7): Energy head loss versus downstream water depth (Q = 20l/s for all cases)

6.3 Prediction of Energy Head Loss in Highly Submerged Conditions

By applying the Form Drag model stated in section 3.5.3, the theoretical prediction and experimental results are compared (α_1 = 1.2, β_1 = 1.03). In this study, the discharge per unit width over the weir is assumed to be equal to the upstream. The relative energy loss to the downstream water depth is selected to illustrate the accuracy of the method in Figure (6-8). The data was collected by three different discharges with a couple of high tail heights in overtopping condition. The results show that most predictions are within 19% error margin. The largest deviation occurs in case 5 in which undular waves were observed leading to some errors. Besides, the results are very sensitive to the accuracy of the measurement at the flow state with low values of $\Delta H / d_2$. Another reason to have the errors is the assumption of enqw2ergy conservation in the upstream. According to Bukreev *et al.* (2008) the energy loss at the entrance of the breach makes a significant contribution to the total loss. However, by applying the energy coefficient and the momentum coefficient in the model, the estimations fit well at the range of 0.04 to 0.1 regarding to the ratio of $\Delta H / d_2$.

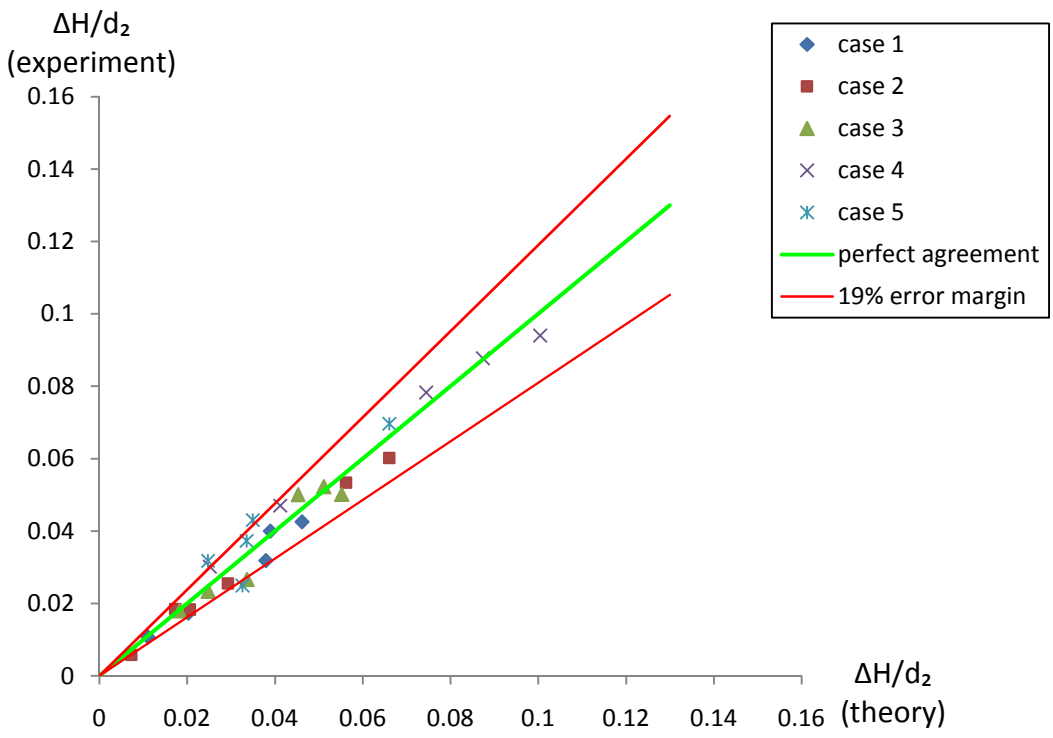

Figure (6 - 8): Comparison of experimental data and results predicted by Form Drag model

CHAPTER 7. ANALYSES OF RESULTS ON LOCAL HYDRAULIC CHARACTERISTICS

7.1 Upstream Water Depth and Discharge

In perfect weir situations, the upstream water depth-discharge rating curve is shown in Figure (7-1) for each case. As expected, the rating curves fall down from case 1 to case 5 due to the increase of flow conveyance capacity. An evident change of slope appears for each curve at the transition zone from emerged flow to overtopping flow. The area function in the process is discontinuous and as a result, a break in slope of the rating curve is generated. Before the slope break, the rate of the curve decreases from cases 1 to 5. After the transition from emerged flow to overtopping flow, on another hand, there is not much difference on the rates of curves for all cases. The present study also confirms the conclusions of Gögüs *et al*. (2006) and Wahl *et al.* (2006) on compound weir with a rectangular cross-section (see section 3.5.4).

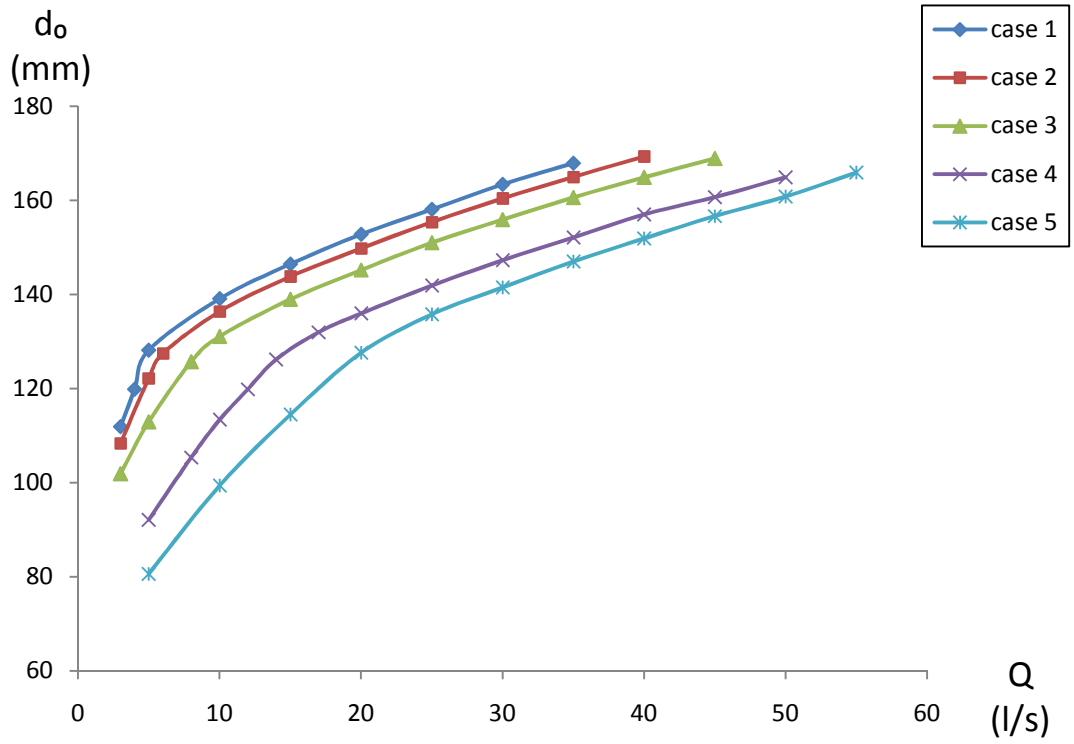

Figure (7 - 1): Upstream water depth - discharge rating curve

7.2 Velocity Distribution

The distribution of the flow velocity in a breach is of importance for the process of erosion and sediment transport. In this section, case 1 and case 5 which aim to present an initial stage and a final stage, respectively, have been selected to be studied. The distributions in the main flow direction, transverse direction as well as the vertical profiles are to be discussed. The data was collected at the middle cross-section of the weir model in perfect weir situations.

7.2.1 Velocity Distribution in Flow Direction

Figure (7-2) illustrates the situation at the low discharges when the flow only passes through the breach. As shown in the figure the flow close to the side is a bit faster than in the middle of the breach. Nevertheless, by increasing the discharge to the overtopping condition (Figure 7-3), it can be seen that the flow velocity in the breach is much larger than the flow velocity over the crest and the flow also speeds up in the near fields of the breach. After further increase of the incoming flow (Figure (7-4)), the maximum velocity in the breach does not change too much. However, the flow velocity over the crest increases significantly. Hence, the difference of velocity magnitude between the breach and crest is smaller compared to that with the lower discharges. In the ideal condition the profile should be symmetrical, but due to the complex flow patterns and the constriction of the weir model it is not the case.

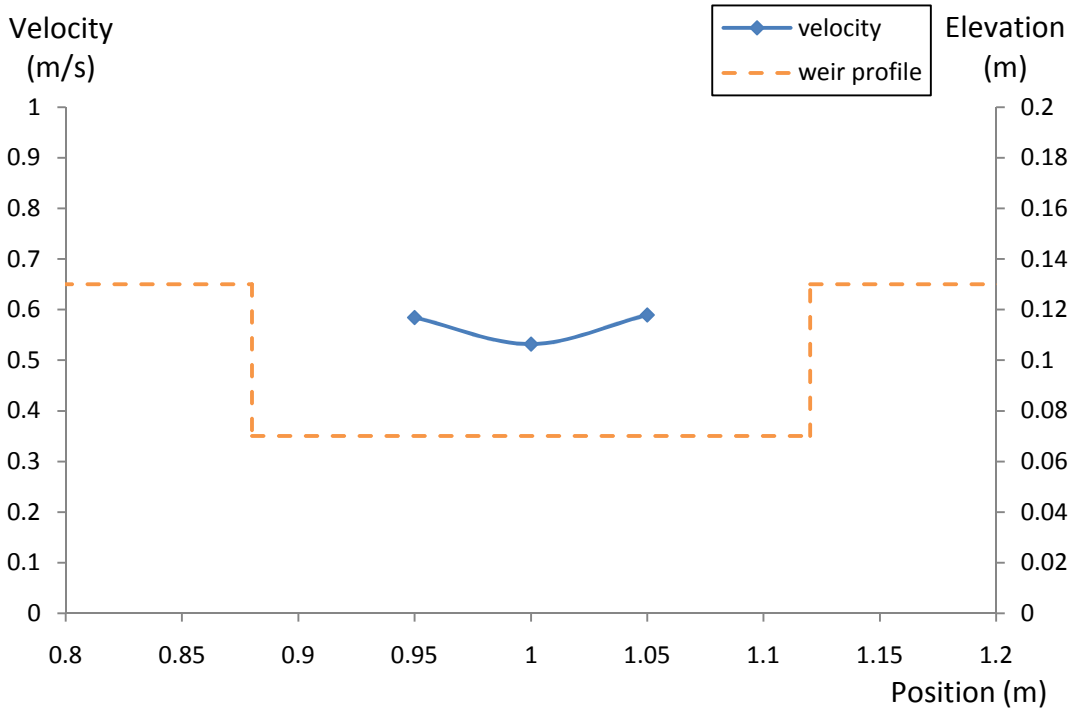

Figure (7 - 2): Velocity distribution in the flow direction (Q = 4/s, case 1)

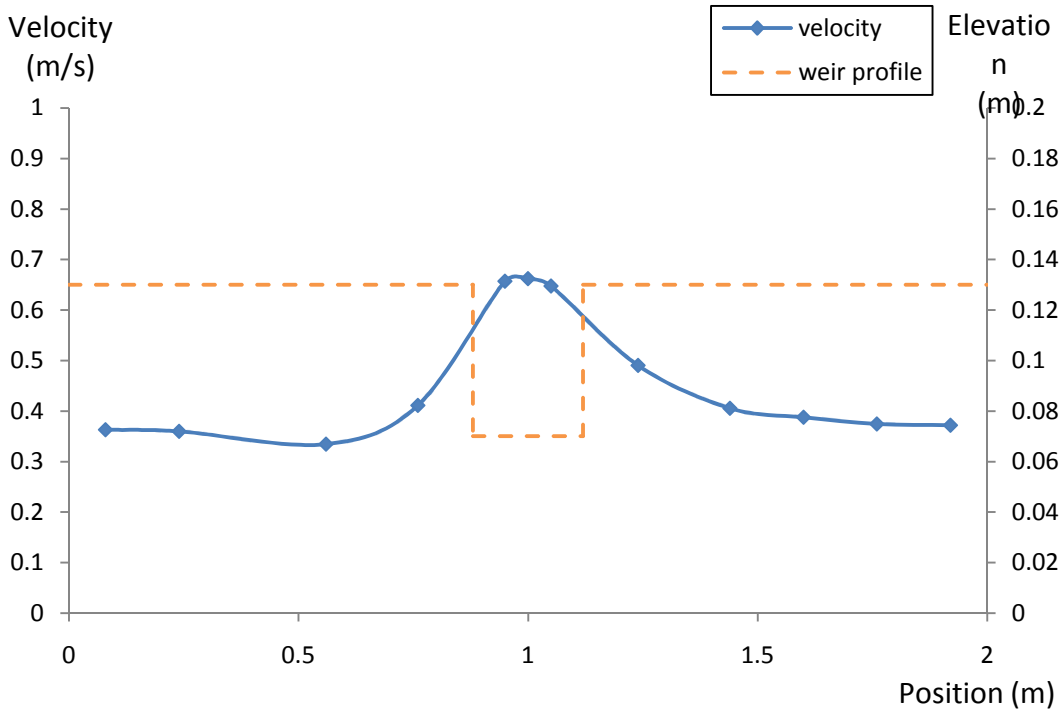

Figure (7 - 3): Velocity distribution in the flow direction (Q = 20 l/s, case 1)

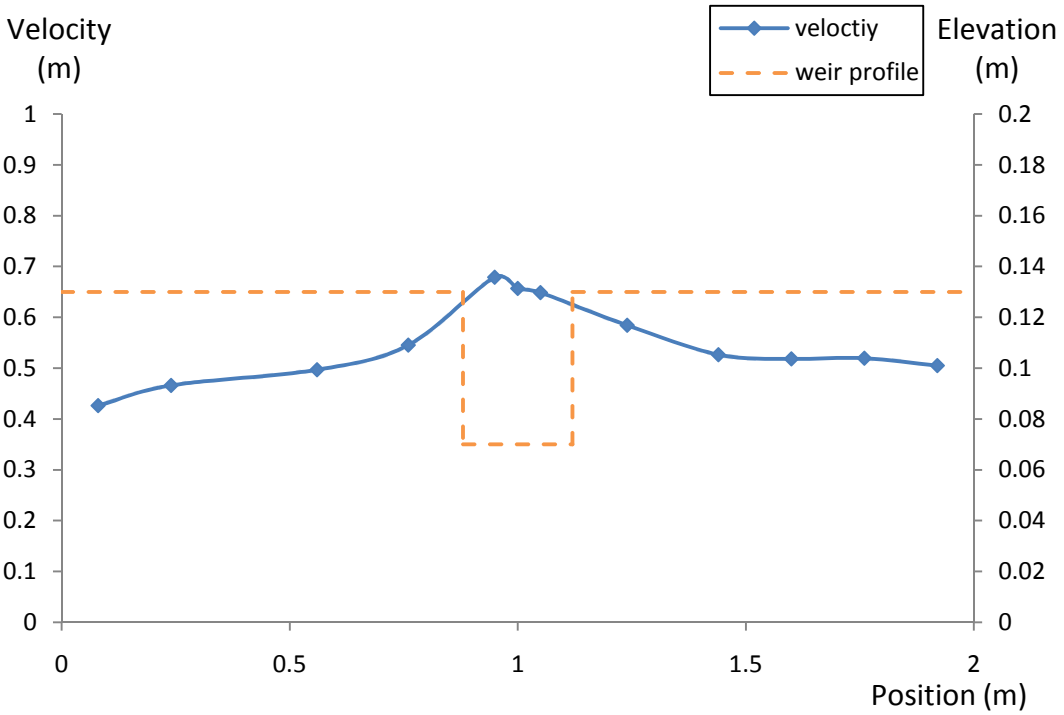

Figure (7 - 4): Velocity distribution in the flow direction (Q = 30 l/s, case 1)

Similar to case 1, the faster flow occurs close to the sides of the breach under the emerged condition in case 5 (see Figure (7-5)). In overtopping condition (Figure (7-6)), the velocity in the breach is much larger than at the crest and reaches its maximum value at the places close to the side slopes. If moving to the middle of the breach, the flow becomes slower.

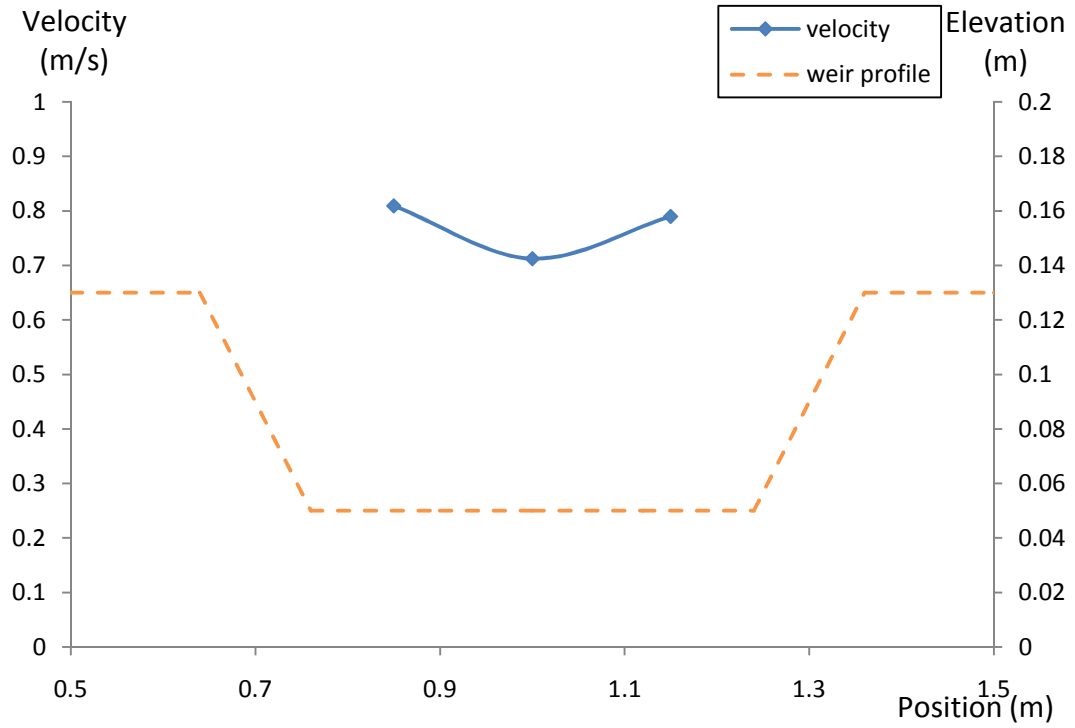

Figure (7 - 5): Velocity distribution in the flow direction (Q = 20 l/s, case 5)

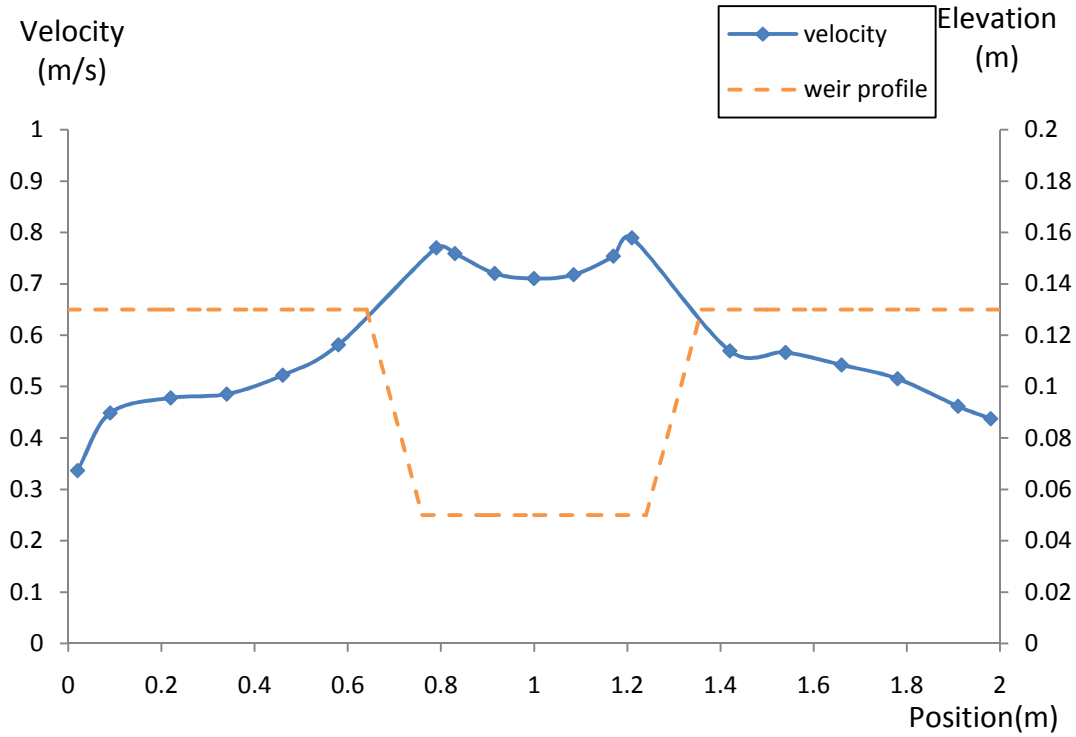

Figure (7 - 6): Velocity profile in flow direction (Q=50l/s, case 5)

The vertical profiles of the velocity in the flow direction are plotted below. When the weir is emerged (Figure (7-7)), the top flow is a little faster than the bottom flow. Due to the limitation of the measurement equipments, the velocity further close to the bottom or surface could not be collected. When the overtopping occurs (Figure (7-8)), the profiles are irregular because of the complex flow patterns in the breach. (y indicates the cross-sectional position along the 2 m wide weir model)

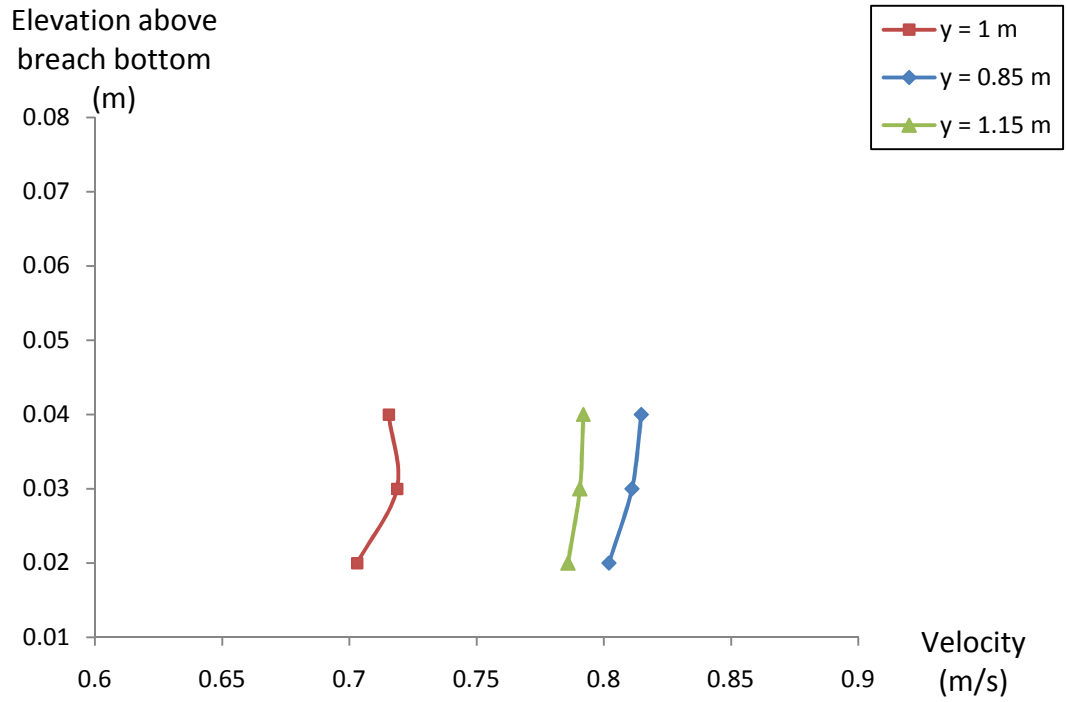

Figure (7 - 7): The vertical profile of the velocity in flow direction (Q = 20 l/s, case 5)

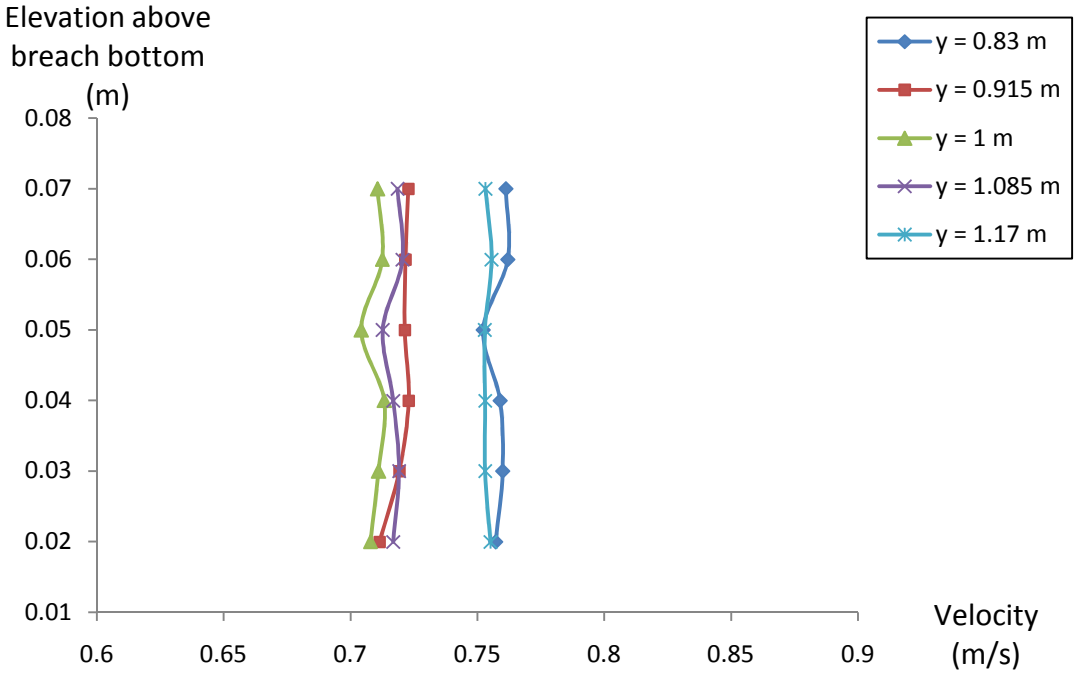

Figure (7 - 8): The vertical profile of the velocity in flow direction (Q = 50 l/s, case 5)

7.2.2 Transverse Velocity Distribution in the Breach

The transverse velocity components in the breach may play a role in the erosion of the breach. The results in emerged and overtopping conditions for case 5 are presented in Figure (7-9) and (7-10), respectively. As shown, the magnitude of the transverse velocity is much lower compared to the components in the main flow direction. In emerged condition, the flow has the transverse components to the sides and the upper flow has slightly higher velocity than the bottom. In the middle of the breach, there is a very small and constant transverse velocity over the water column. In overtopping condition, the flow has the transverse components to the middle of the breach and the magnitude becomes stronger from the top to the bottom, which may be caused by the transverse flow from the crest to the breach. (y indicates the cross-sectional position along the 2 m wide weir model)

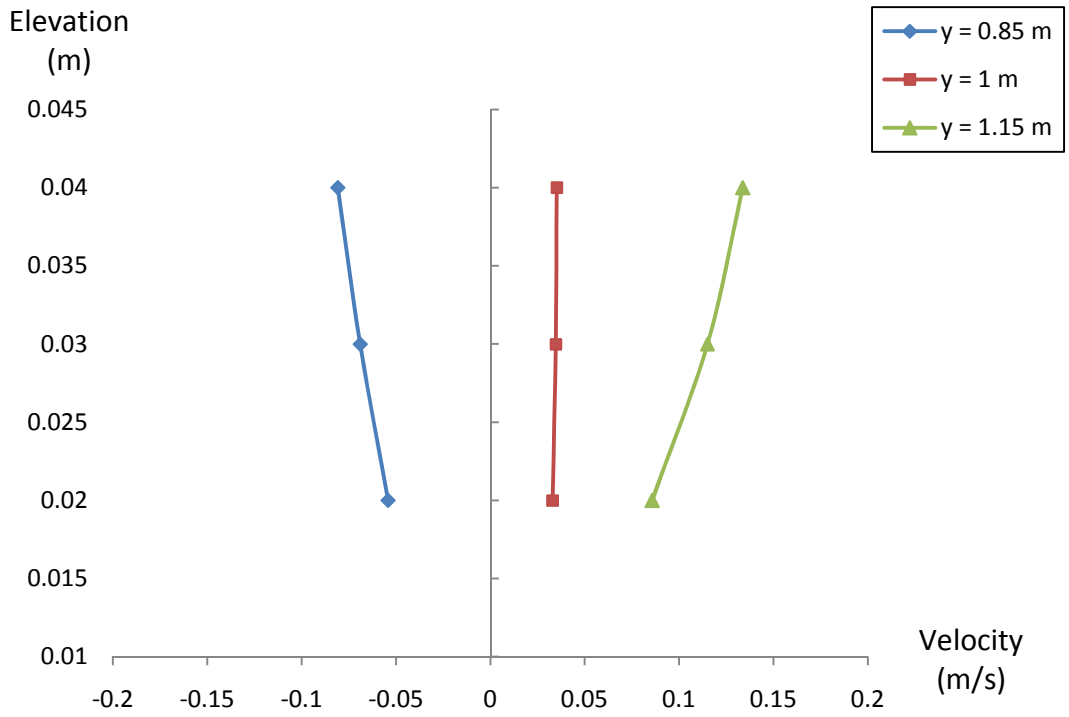

Figure (7 - 9): Velocity profile in transverse direction (Q = 20 l/s, case 5)

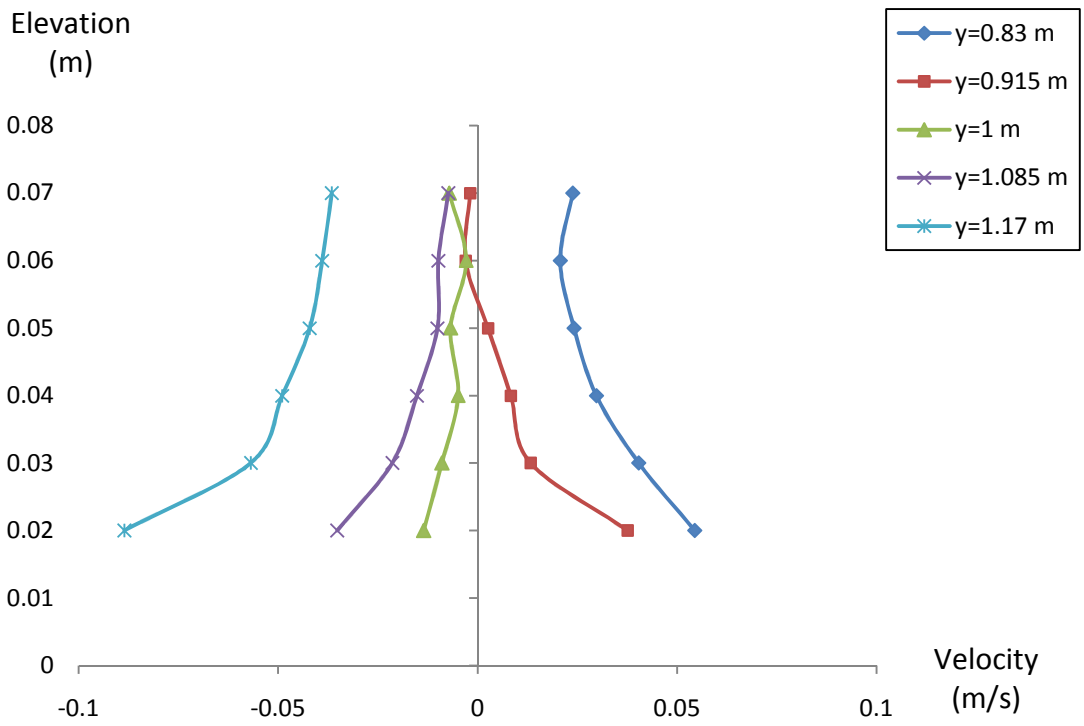

Figure (7 - 10): Velocity profile in transverse direction (Q = 50 l/s, case 5)

7.3 Water Level Elevation

Water level elevation provides the information for the estimation of the discharge and also importance for breach erosion processes. Based on Figures (7-11) and (7-12), it is found that in emerged condition, the water levels fluctuate with a bit higher level in the middle of the breach and lower at the sides. These fluctuations are related to waves and turbulence formed in the breach.

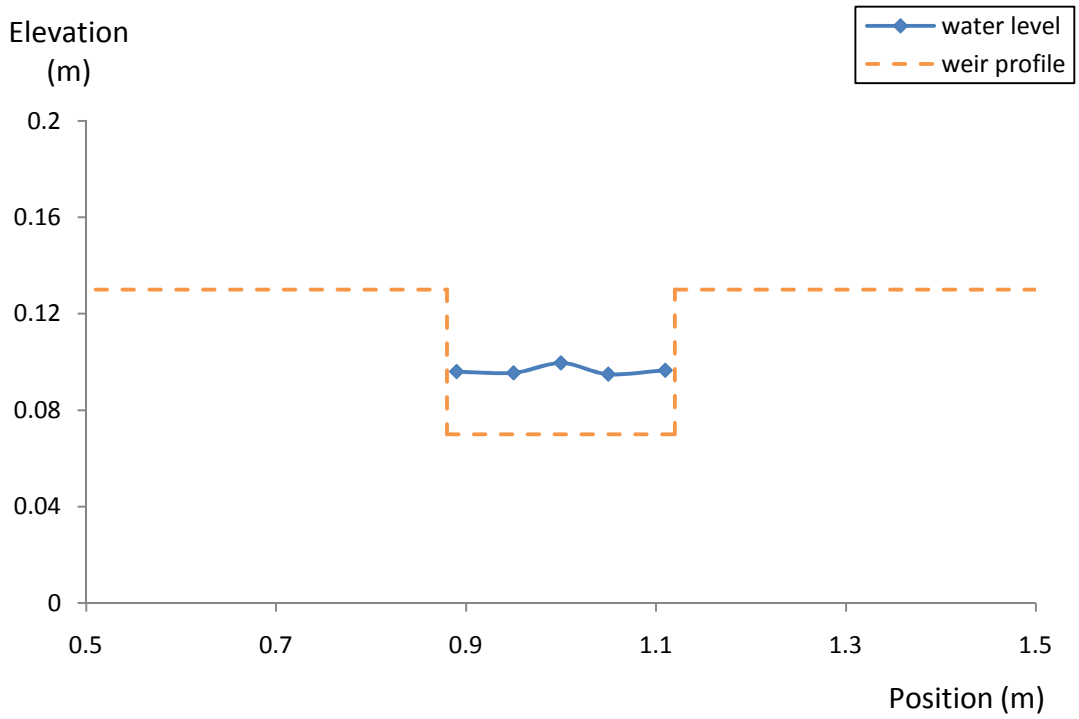

Figure (7 - 11): Water level in emerged condition (Q = 4 l/s, case 1)

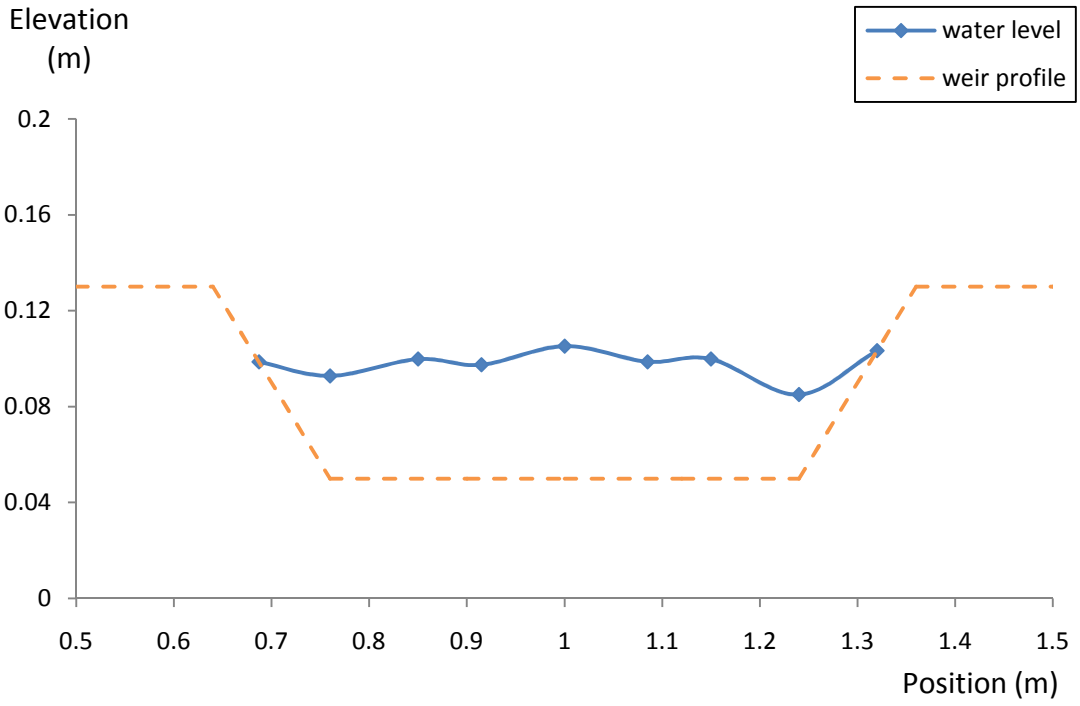

Figure (7 - 12): Water level in emerged condition (Q=20, case 5)

In overtopping condition the flow states are more complicated due to the interaction between the crest and the breach. Figures (7-13) and (7-14) shows the water level for the same breach property with different discharges. By comparisons, it can be observed from the two figures that the water level over the crest decreases gradually towards the breach in cross-sectional direction. As a part of the thin flow over the crest has transverse components to the breach where the flow has larger depth, hydraulic jumps would be formed. Therefore, there is a sharp drop occurring at the intersection of the crest and the breach. With a higher discharge, it can be found that the water level rises with a slight larger amount in the breach with respect to the crest where the water surface increases more or less equally. As a result, the sharp drop becomes smaller.

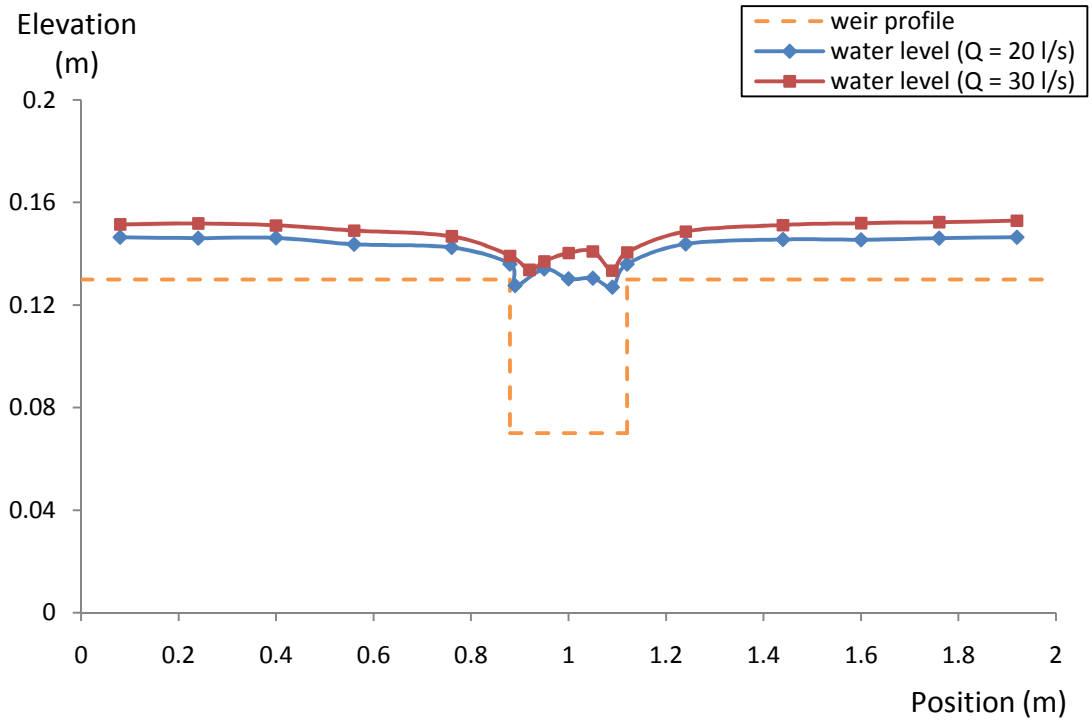

Figure (7 - 13): Water level in overtopping condition (case 1)

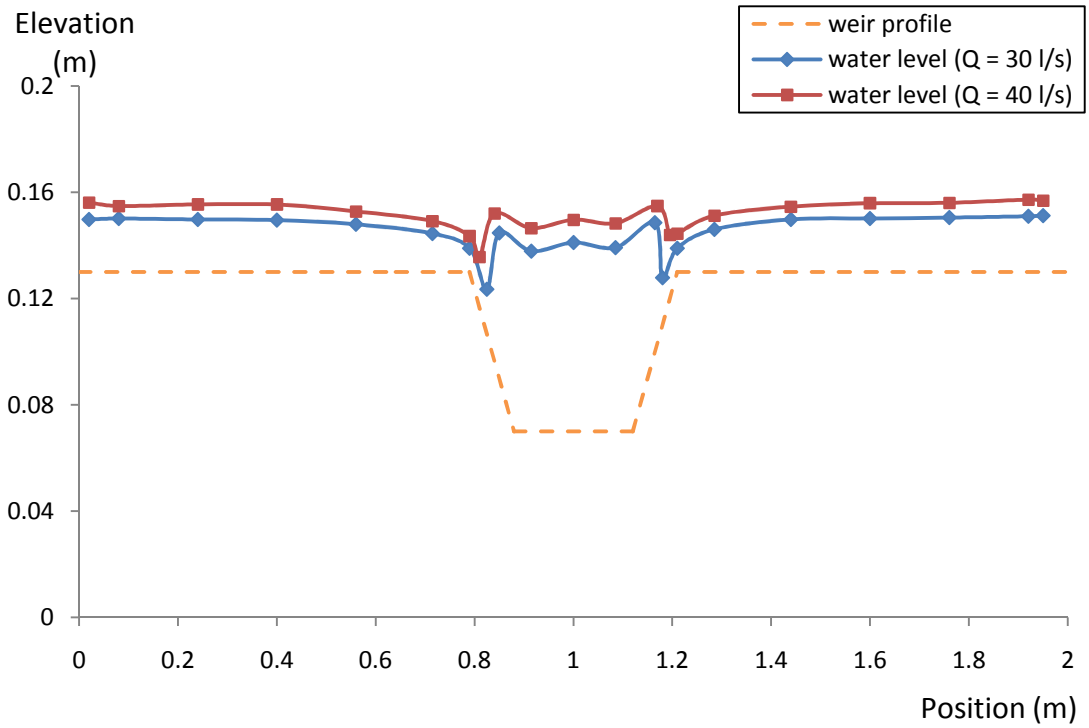

Figure (7 - 14): Water level in overtopping condition (case 2)

By applying the same discharges in the upstream, the water levels for different weir geometries are depicted in below figures. The transform from the rectangular breach (case 1) to trapezoidal breach (case 2) leads to a lower water level over the crest resulting in a stronger sharp drop over the breach slope (Figure (7-15)). The difference caused by weir geometry is significant around the breach. Similar results can also be gained from other cases, such as cases 4 and 5 (Figure (7-16)). Therefore, with the same discharge the lower the water level over the crest, the stronger jumps that are generated. Based on above, it can be stated that the hydraulic jumps occur at the intersection between the crest and the breach and are dependent on the water level over the crest.

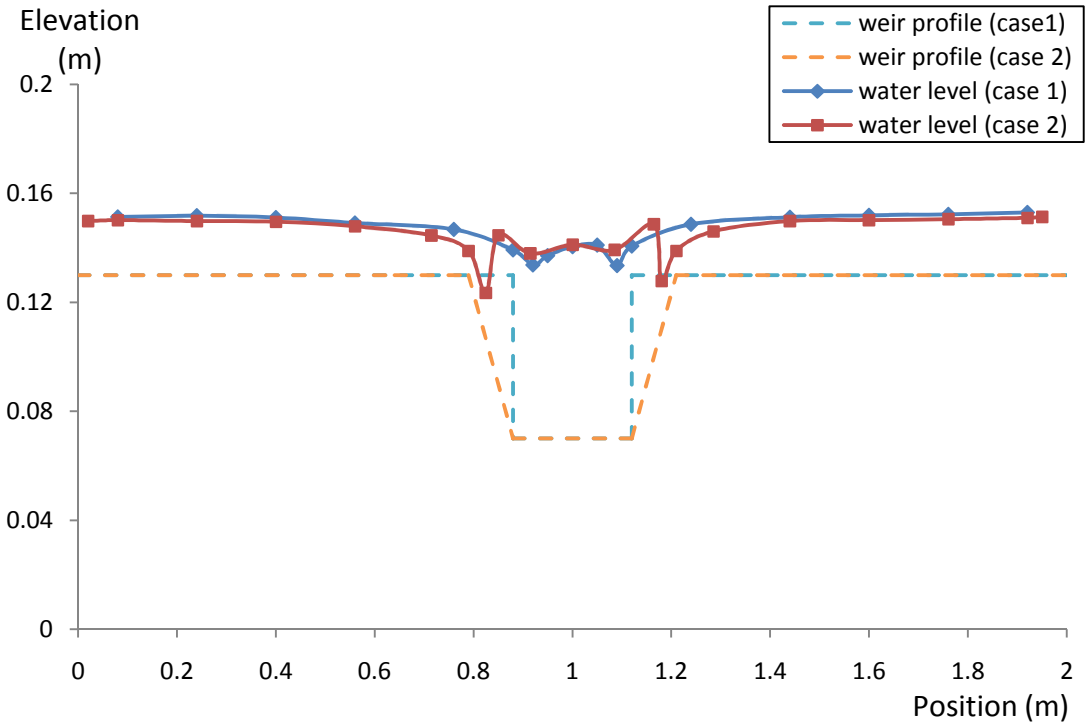

Figure (7 - 15): Water level in overtopping condition (Q = 30)

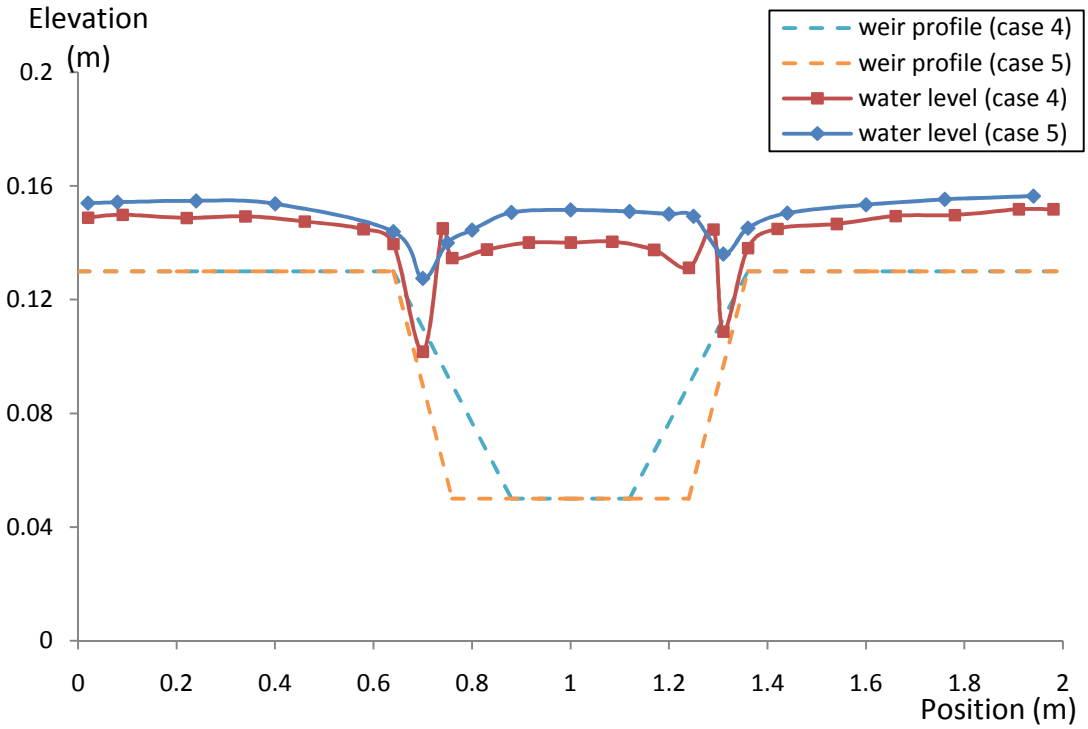

Figure (7 - 16): Water level in overtopping condition (Q = 50)

7.4 Downstream Eddies and Hydraulic Jumps

In this section, phenomena such as eddies and hydraulic jumps are to be described by comparing the photos taken during the experiment. Case 5 is selected to be tested with various flow conditions.

7.4.1 Constant Discharge

By fixing the upstream boundary with discharge Q = 20 l/s, the weir model is in emerged condition. It can be seen from Figure (7-17) that eddies and hydraulic jumps are generated behind the weir. In the figure eddies are indicated by the color line and black tracers. Hydraulic jumps are in a triangular shape at the downstream of the breach.

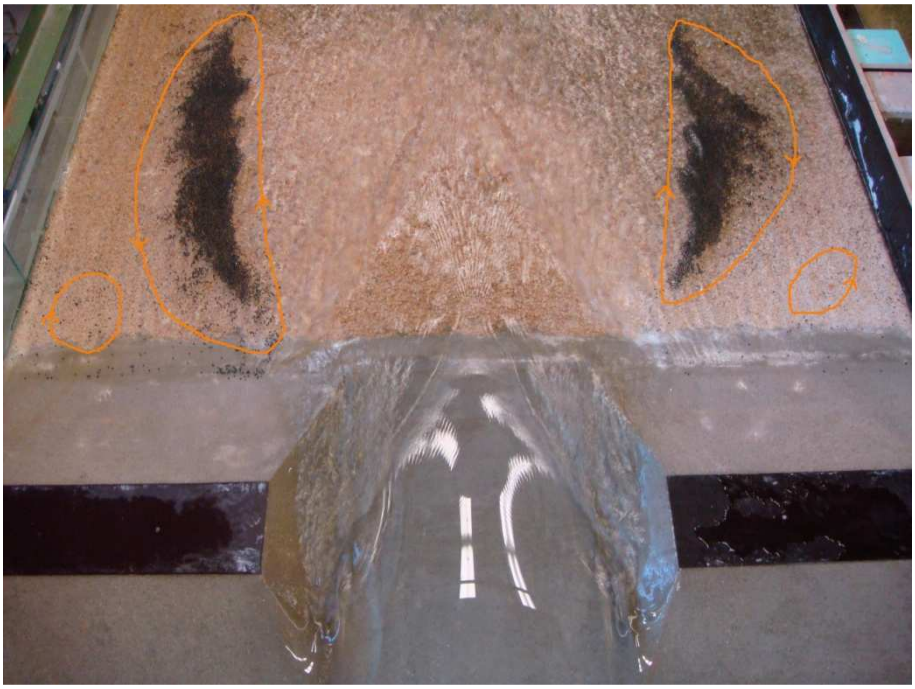

Figure (7 - 17): Downstream flow patterns (Q = 20 l/s, tail height 1, case 5)

However, by means of increasing the downstream gate height, it can be seen from Figures (7-18) that eddies become higher in refreshment (less black tracers) and larger in scale (area of black tracers). The hydraulic jumps in the downstream of weir are observed to move towards the breach forming a curved line surrounded the outlet of the breach.

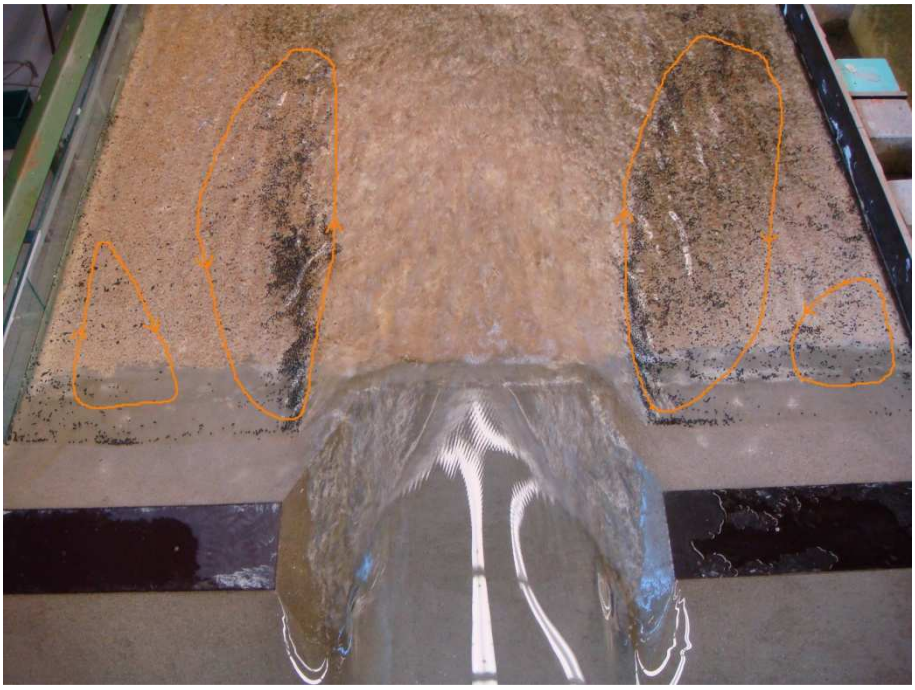

Figure (7 - 18): Downstream flow patterns (Q = 20 l/s, tail height 2, case 5)

Further increase of the tail gate results in even larger area of eddies and higher refreshment (Figure (7-19)). The hydraulic jumps in the downstream are hard to see, instead, shock waves appear. Finally, if the tail gate has reached a certain level, eddies would disappear and the flow in the breach becomes subcritical thus no hydraulic jump appears any more.

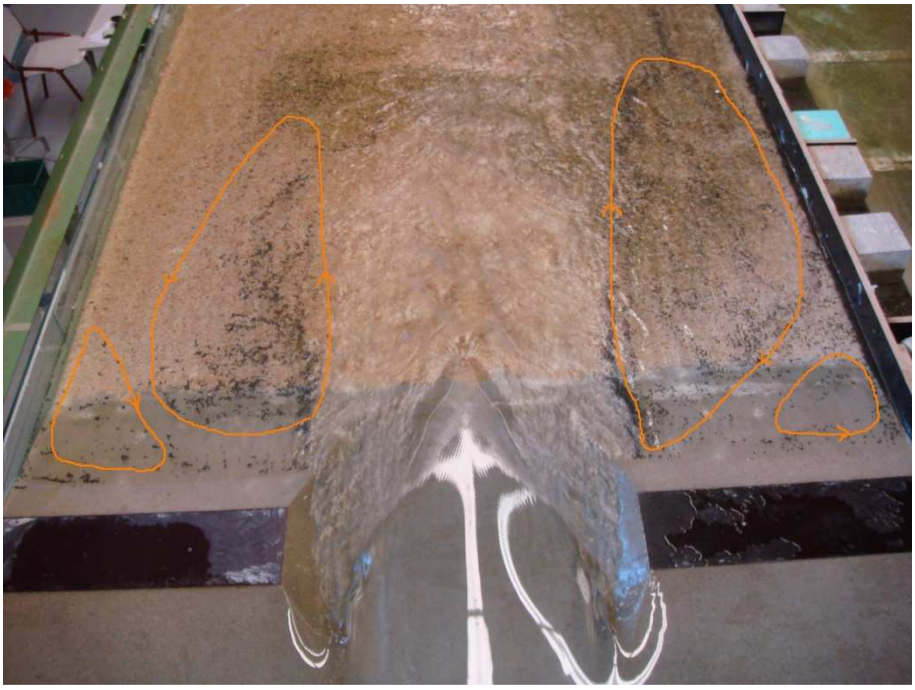

Figure (7 - 19): Downstream flow patterns (Q = 20 l/s, tail height 3, case 5)

For large discharges (e.g. 50 l/s), the weir is in overtopping condition. In the case of a low tail gate level (Figure (7-20)), the flow in the downstream is so fast that there is no eddy behind the weir at all. The hydraulic jumps are generated over the downstream weir slope behind the crest. Similar to the emerged condition, hydraulic jumps with a triangular shape are located in the downstream of breach.

Figure (7 - 20): Downstream flow patterns (Q = 50 l/s, tail height 1, case 5)

But after increasing the downstream to a higher water level (Figure (7-21)), the flow at the sides slows down and small-size eddies appear but at some distance away from the weir due to the push of overtopping flow. Still the hydraulic jumps shift a bit to the upstream with the increase of downstream water level.

Figure (7 - 21): Downstream flow patterns (Q = 50 l/s, tail height 2, case 5)

With continuing to lift the tail height, the no eddy exists because of the high downstream water level (Figure (7-22)). At the same time, the hydraulic jumps have gone as the flow becomes subcritical and undular waves are generated in the downstream.

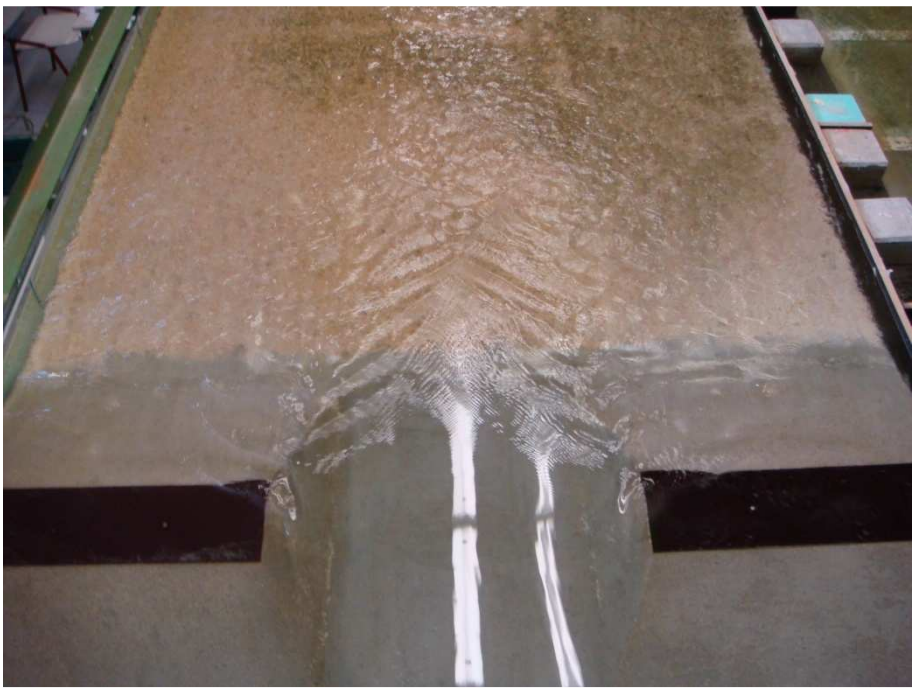

Figure (7 - 22): Downstream flow patterns (Q = 50 l/s, tail height 3, case 5)

7.4.2 Constant Tail Gate Height

In this condition, the tail gate is fixed but the discharge is varied. Figure (7-23) shows the picture of the situation with relatively low discharge (Q = 18l/s) in which the flow only passes through the breach. By increasing the discharge (to Q = 45l/s), the flow pattern is illustrated in Figure (7-24). By comparing the two figures, it can be concluded that eddies become smaller and further away from the weir if increasing the incoming discharge. Also, hydraulic jumps occur behind the weir rest due the overtopping flow.

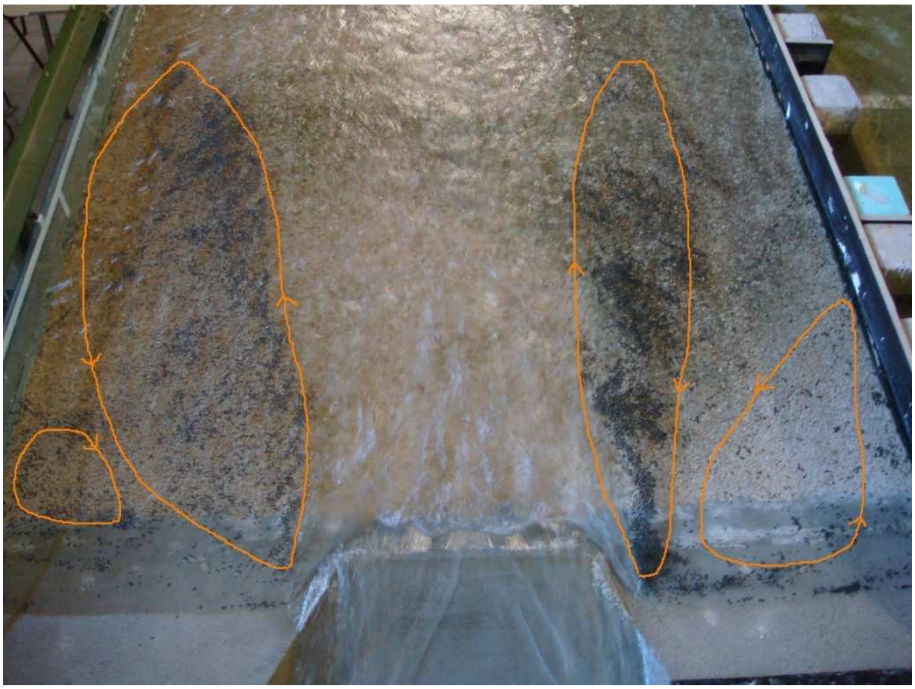

Figure (7 - 23): Downstream flow patterns (Q = 18 l/s, case 5)

Figure (7 - 24): Downstream flow patterns (Q = 45 l/s, case 5)

At the situation with extreme large discharge (Q = 60 l/s), eddies are gone and triangular shape of jumps shows again because the very fast flow through the breach (Figure (7-25)). In short, with fixed height of tail gate, the flow patterns behind weir depend on the upstream flow conditions.

Figure (7 - 25): Downstream flow patterns (Q = 60 l/s, case 5)

CHAPTER 8. NUMERICAL MODELING

8.1 Introduction

This chapter deals with numerical simulations of the flow over the weir with Delft3D. In order to verify the application of this numerical model to present study, the results of Delft3D are to be compared with the experimental data.

8.1.1 General background

Delft3D is fully integrated computer software for a multi-disciplinary approach and 3D simulations for coastal, river and estuarine areas. It can be used for the simulations of two-dimensional (2D, depth-averaged) or three-dimensional (3D) unsteady flow and transport phenomena. If the fluid is homogeneous in the vertical direction, the 2D approach is appropriate with one computational layer. In 3D simulations, multi-layers can be adapted and the vertical grid is defined following the co-ordinate in which the horizontal length and time scales are significantly larger than the vertical scales. Delft3D-FLOW solves the Navier Stokes equations for an incompressible fluid, under the shallow water and the Boussinesq assumptions. In the vertical momentum equation the vertical accelerations are neglected, which leads to the hydrostatic pressure equation. In 3D models the vertical velocities are computed from the continuity equation. Within the Delft3D-flow model, this hydrostatic pressure assumption has been adopted, which implies that the numerical model is based on the shallow-water equations. It has been applied successfully in many test cases in describing horizontal velocity profiles in vertical direction or stratified currents in predominantly horizontal flows. However, the application of hydrostatic approximation is disputable, when the non-hydrostatic pressure component cannot be neglected. In this study, since the curvature of flow streamlines occurs due to the contraction effect of the weir, 2D simulations are applied.

8.1.2 Approximations

In Delft3D some assumptions are made in 2D simulations:

Incompressibility

The flow is assumed to be incompressible.

Hydrostatic pressure assumption

In the sigma co-ordinate system the depth is assumed to be much smaller than the horizontal length scale. So, the vertical pressure distribution is considered to be hydrostatic and vertical accelerations are not taken into account.

Boussinesq approximation

The effect of variable density is only taken into account in the pressure term.

Boundary condition

At the bottom a slip boundary condition is assumed and a quadratic bottom stress formulations are applied. The boundary conditions for the turbulent

kinetic energy and energy dissipation at the free surface and bottom assume a logarithmic law of the wall. For large-scale flow simulations, the tangential shear-stress at lateral closed boundaries can be neglected (free slip). In case of small-scale flow partial slip is applied along closed boundaries.

8.2 Set-up of Delft3D model

The Delft3D model is set up based on the geometries of the laboratory experiment. 10 meters length of flume is simulated with the weir model located in the middle over the distance. But in case 1 due to the fact that only one value of bottom elevation can be set in Delft3D, a very large breach slope (1H : 20V) is built instead of a vertical breach side, which would generate small differences from the analytical and physical models. In the numerical model, 2D simulation is selected. The settings of Delft3D, e.g. for case 5 are presented in Table (8-1).

Table (8 - 1): Settings of Delft3D

Input	***Parameters***	***Values***
Time frame	*Simulation time*	*5 minutes*
	Time step	*0.024 s*
Domain	*Grid cells in M-direction*	*333*
	Grid cells in N-direction	*50*
	Delta X	*0.03 m*
	Delta Y	*0.04 m*
Initial conditions	*Water depth*	*0.04 m*
Boundary conditions	*Upstream discharge*	*0.05 m3/s*
	Reflection parameter alpha	*1.02 s*
	Downstream water level	*0.04 m*
	Reflection parameter alpha	*1.02* s^2
	Rriction formula	*White-Colebrook*
	U	*0.005*
	V	*0.005*
	Wall roughness	*Partial*
	Roughness length	*0.002 m*
Physical parameters	*Horizontal eddy viscosity (fixed)*	*0.005* m^2/s
Numerical parameters	*Drying and flooding check at*	*cell centers and faces*
	Depth specified	*cell corners*
	Depth at grid cell centers	*Max*
	Depth at grid cell faces	*Min*
	Threshold depth	*0.01 m*
	Smoothing time	*1 minute*
	Advection scheme	*Flooding*

8.3 Verification of Delft3D Model

One of the advantages of a numerical model is that simulations can be done with relatively little effort and that it can solve problems that physical models may have due to the limitations of measurement, time, etc. However, whether the set-up of the numerical model is appropriate and reliable to the subject should be discussed first. In this section, the Delft3D models are to be verified by comparing the numerical results with the laboratory data. In the aspect of hydraulic characteristics, velocity distribution and water depth over the weir are selected for the comparison of the Delft3D results with the experimental data. The comparisons are made for cases 1 and 5.

As is shown in Figures (8-1) and (8-2), the overall profile of depth averaged velocity is in line with the experimental data. Particularly over the crest, the difference is small on average. However, the results from Delft3D are lower in the magnitude of the velocity in the breach where the flow is very turbulent and variable. It shows the weakness of the numerical model on the simulations with sudden change of topography.

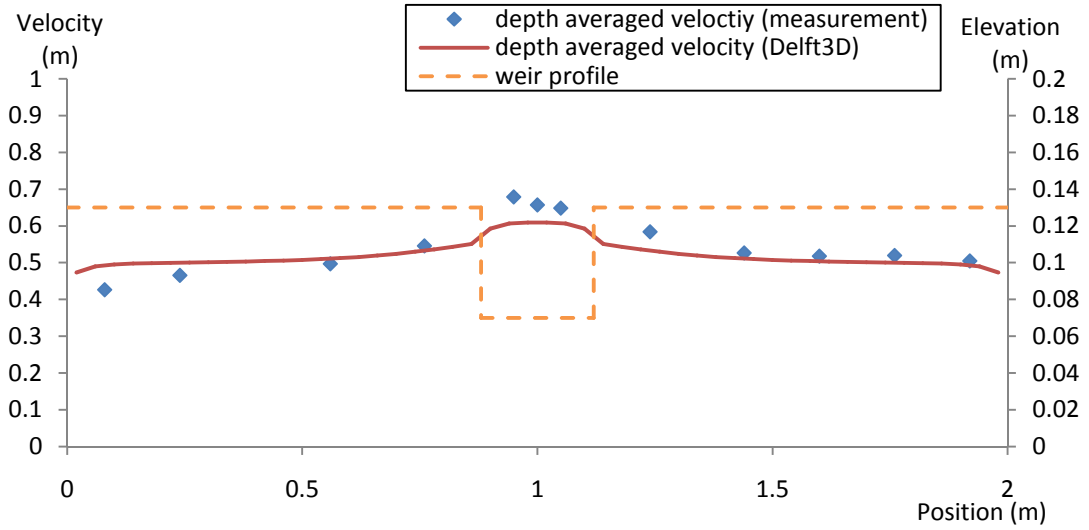

Figure (8 - 1): Comparison of laboratory measurement and Delft3D on depth averaged velocity over weir (case 1, Q = 30 l/s)

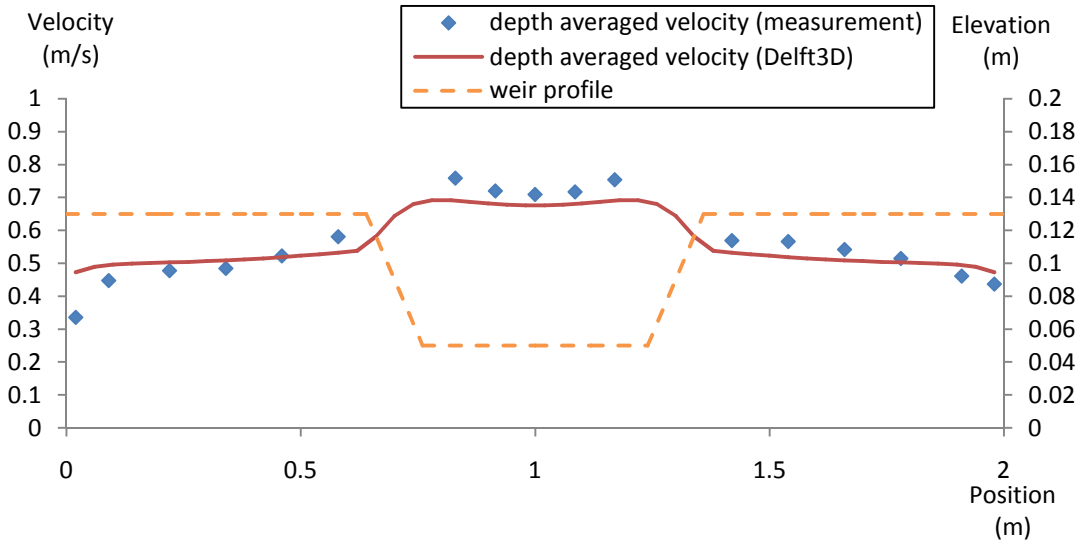

Figure (8 - 2): Comparison of laboratory measurement and Delft3D on depth averaged velocity over weir (case 5, Q = 50 l/s)

The comparisons of water level over the weir are illustrated in Figures (8-3) and (8-4). It shows that the results of measurements and numerical model fit well over the crest where the flow is thin and relatively streamlined. In the breach, a difference can be seen especially close to the breach slopes. For instance, in case 5, instead of the sharp drop over the side slope, a relatively smooth decrease of water level is generated in the numerical model.

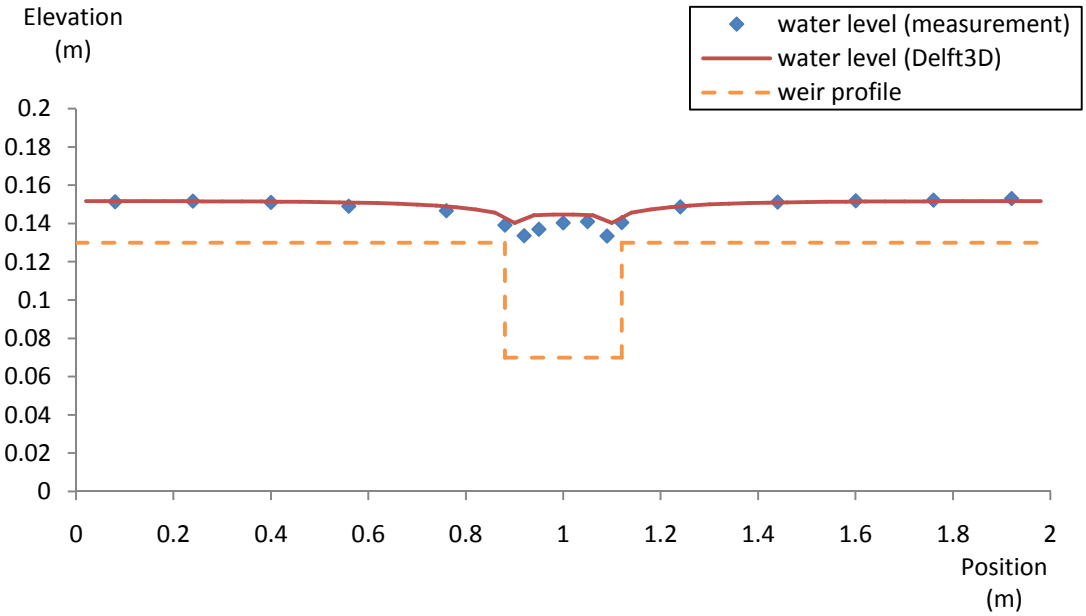

Figure (8 - 3): Comparison of laboratory measurement and Delft3D on water level over weir (case 1, Q = 30 l/s)

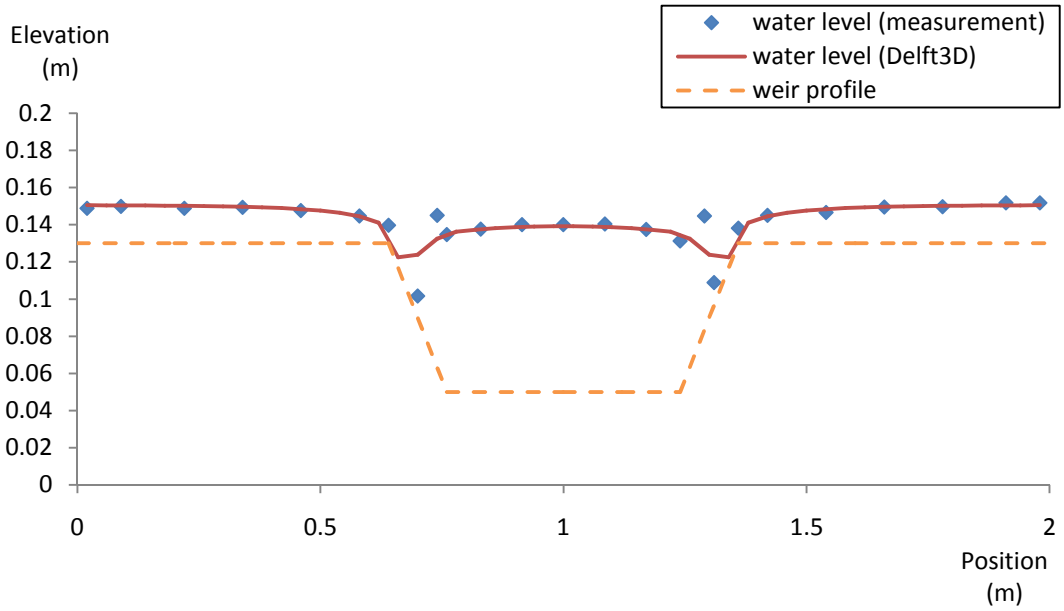

Figure (8 - 4): Comparison of laboratory measurement and Delft3D on water level over weir (case 5, Q = 50 l/s)

Furthermore, the discharge distribution based on the physical, analytical and numerical models is presented in Figure (8-5). It can be concluded that the results are rather comparable for cases 2 to 5. The numerical model owns the lower values with respect to the analytical predictions and the laboratory measurements in case 1 as the side slope cannot be set vertical leading to less water through the breach in Delft3D. Overall, the analytical solution performs a bit better than Delft3D in the domain of present study.

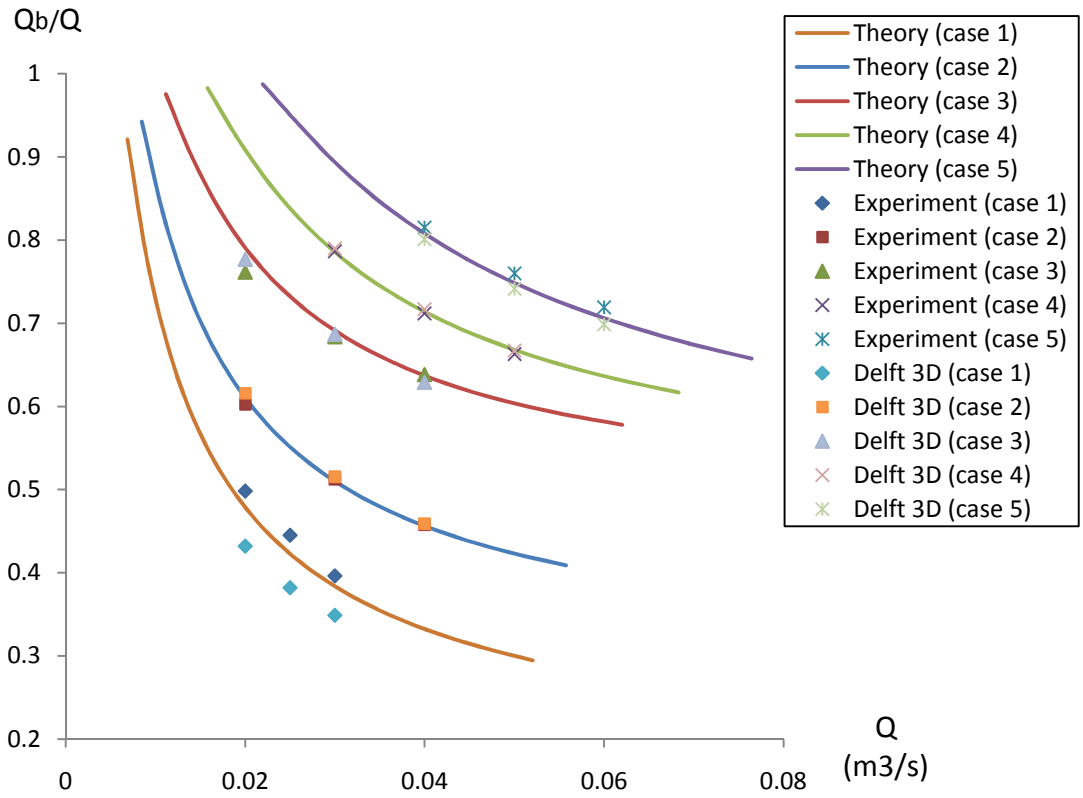

Figure (8 - 5): Comparison of laboratory measurement, analytical solution and Delft3D on discharge distribution

In conclusion, except of the inaccuracy in the fields close to the breach slopes, Delft3D model is able to provide appropriate simulations for the subject of the breach flow over broad-crested weir in two-dimensional simulation. Some simulations based on Delft3D model are done in Appendix A.

CHAPTER 9. CONCLUSIONS AND RECOMMENDATIONS

9.1 Conclusions

In breach models often broad-crested weir formulae are used to simulate the flow through the breach. In order to understand the effects of breach properties on the breach flow, five tests with different breach properties were performed. Delft3D calculations were performed for the comparison with the experimental data. The results of the investigation are useful for the development of breach models and the design of compound weirs. The conclusions regarding to the objectives of the thesis are given below.

9.1.1 Upstream Water Depth and Discharge

A break in slope caused by the sudden change of flow area was shown in each upstream water depth-discharge rating curve. In emerged condition, the slope of the curves decreases in the processes of top widening, deepening and bottom widening of the breach. After overtopping, there is not much difference on the slopes for all the cases.

9.1.2 Discharge Coefficient

The study of the discharge over a weir with a breach was carried out both in perfect and imperfect weir situations. Two flow conditions (emerged and overtopping) were taken into consideration.

Emerged Condition

In this condition, the flow only passes through the breach. The values of discharge coefficient are more or less constant with the increase of the upstream head. With small discharges relatively low values of the discharge coefficient (smaller than 1) were obtained as the bottom friction and flow contraction played a role. The effects of breach properties on the flow in perfect weir situations are:

(a). In the case of a small top width of the breach, a strong contraction occurs resulting in relatively low discharge coefficient.
(b). Keeping the top width of the breach constant, breach deepening and bottom widening might lead to higher values of the discharge coefficient.
(c). Therefore, with a constant breach slope, the combined effects of bottom widening and deepening result in a significantly increase in the discharge coefficients.

In imperfect weir situations, the values of the discharge coefficients would be reduced. A submergence coefficient was introduced for emerged flow to account for the reduction. The comparison of theory and experimental results shows a good agreement.

Overtopping Condition
In this condition, the flow passes through the whole width of the weir. The significant difference with the emerged condition in terms of the discharge coefficients is the interactions between the flow over the crest and the flow through the breach. A linear combination of traditional discharge formulae was applied. The conclusions can be summarized as below:

(a). The values of the discharge coefficients are higher than for emerged flow but still lower than 1. By increasing the upstream energy head, the discharge coefficients increase for all cases.
(b). The difference on the values of the discharge coefficients are small for the process of top widening of the breach. However, the breach deepening results in obviously higher values and the breach bottom widening leads to lower values.

Emerged and Overtopping Condition
Both for emerged and overtopping conditions, the breach discharge can be computed simply with the formula for broad-crested weirs (for overtopping condition the formula for a compound weir), with a proper estimation of the discharge coefficient.

9.1.3 Energy Head Loss
The energy head loss was studied in imperfect weir situations. For given heights of the tail gate, the energy loss increase with the increase of the discharges. This is the same case for the flow over weirs in general. Nevertheless, the dissipation rates are different in emerged and overtopping flow conditions. In emerged flow, the dissipation rates decrease in the processes of top widening, deepening and bottom widening of the breach. In overtopping flow, the dissipation rates are constant for all cases.

Just as the energy loss for general weir flow, the energy loss decreases with the increase of the downstream water depth for given discharges. With the increase of submergence, the energy loses at a decreasing rate. In present study, however, the energy dissipation rate decreases during the processes of top widening, deepening and bottom widening of the breach for the constant upstream discharges.

The form drag model has been proved to be applicable in the case of a weir with a breach for predicting the energy loss by the downstream water depth in highly submerged conditions.

9.1.4 Local Hydraulic Characteristics
Velocity Distribution
The velocity signals in the middle cross-section of the weir were measured. The magnitudes of transverse velocities are rather small compared to the velocity

components in the main flow direction. For emerged flow, the depth averaged flow velocities in the main flow direction are a bit larger close to the sides of breach than the middle of the breach. For vertical profiles, the flow at the top is a little faster than the flow at the bottom. In the transverse direction, the flow has the components to the sides of the breach which are slightly higher in the upper flow.

For overtopping flow, the depth averaged velocities in the breach are much larger than the velocities over the crest in the main flow direction. With the increase of discharges, the maximum velocity in the breach does not change too much. However, the flow velocities over the crest increase significantly. The vertical profiles are irregular because of the complex flow patterns happening there. The flow has the transverse components to the middle of the breach and the magnitude become stronger from the top to the bottom.

Water Level

In emerged condition, the water level fluctuates with a bit higher level in the middle of the breach than at the sides. In overtopping condition, the water level over the crest decreases gradually towards the breach. Sharp drops occur over the breach slopes due to the form of jumps caused by transverse flow from crest to breach. The drops occurring over the breach slopes depend on the water levels over the crest. The lower the water levels over the crest, the larger drops would be generated.

Downstream Eddies and Hydraulic Jumps

Eddies are formed behind the weir with a low downstream water level and disappear at relatively high downstream water levels. With the increase of the downstream water depth in emerged condition, eddies become higher in refreshment and larger in size. The increase of the discharges in overtopping condition would push eddies away from the weir.

A triangular shape of hydraulic jumps is generated in the downstream of the breach at the low gate level. Hydraulic jumps (see Figure (9-1)) also occur over the downstream slope of the weir in overtopping condition. Increasing the tail height forces the jumps move towards the breach forming a curved line around the outlet of the breach. If the downstream water level further increases, the flow in the breach becomes subcritical and no jumps appear any more.

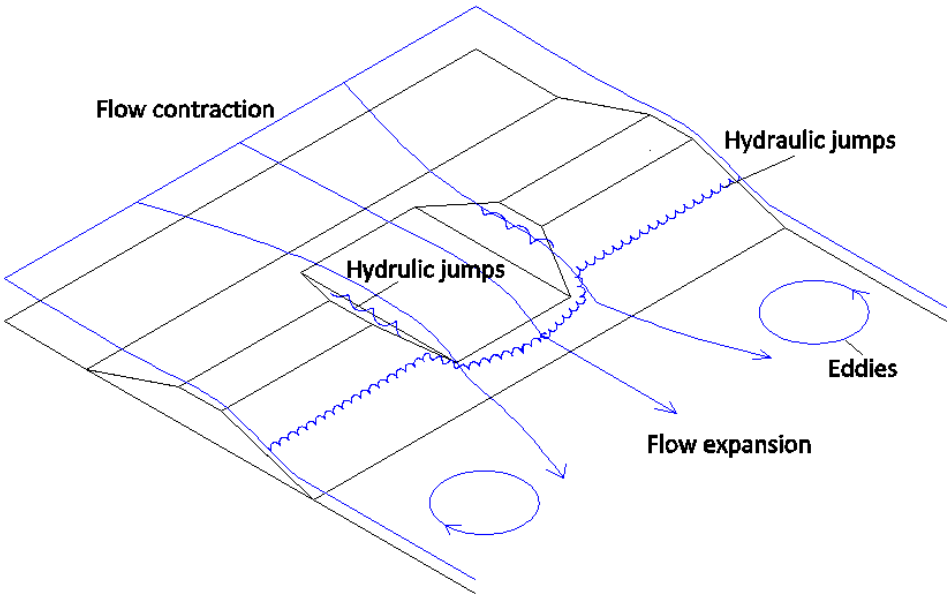

Figure (9 - 2): Sketch of breach flow modeled as flow over a weir

9.1.5 Numerical Modeling

A numerical model as Delft3D has been verified to simulate the present laboratory experiment by comparing its predictions with the experimental results with respect to the local hydraulic characteristics, e.g. the velocity distribution and the water level elevation. It can be concluded that the numerical model can provide appropriate 2D simulations of the flume-scale experiment. However, inaccurate results can be found in the near fields of breach slopes where the sudden change of flow section occurs. With respect to the discharge distribution, Delft3D does not give better results than the formula for broad-crested weirs.

9.2 Recommendations

The effect of breach geometry to breach flow has been investigated. Nevertheless, further research needs to be done to complete the subject of breach flow over weirs. The following suggestions are given:

(a). More shapes of breach needs to be tested, e.g. parabolic breach.
(b). Larger size of breach is required for further study on breach properties and flow characteristic in the breach.
(c). Research on the morphology changes of the weir caused by the breach flow is recommended.

REFERENCES

Ackers, P., White, W.R., Perkins, J.A and Harrison, A.J.M (1978): Weirs and flumes for flow measurement. *John Wiley & Sons*

Ali, S. and Uijttewaal, W.S.J. (2009): The Form drag due to vegetated weir-like obstacles interpreted as expansion losses. *Proceedings of the 33rd IAHR congress Water Engineering for a sustainable environment*, 140-146

Ali, S. and Uijttewaal, W.S.J. (2010): Flow resistance of vegetated weir-like obstacles during high water stages. *River Flow 2010*

Andrews, D.P., Coleman, S.E., Webby, M.G., and Melville, B.W. (1999): Noncohesive embankment failure due to overtopping flow. *Proceedings of the 28th Congress of the International Association for Hydraulic Research*, 7

Azimi, A.H. and Rajaratnam, N. (2009): Discharge characteristics of weirs of finite crest length. *Journal of Hydraulic Engineering*, 135, 12, 1081-1085

Beffa, C. and Connell, R.J. (2000): Two-dimensional flood plain flow. I: model description. *Journal of Hydrologic Engineering*, 6, 5

Biscarini, C., Francesco, S.D. and Manciola, P. (2010): CFD modeling approach for dam break flow studies, *Hydrology and Earth System Sciences*, 14, 4, 705-718

Bos, M.G. (1985): Long-throated flumes and broad-crested weirs. *Martinnus Nijhoff/Dr W. Junk Publishers*

Bos, M.G. (1989): Discharge measurement structures. *ILRI publication 20*, 3rd edition

Bukreev, V. I., Degtyarev, V. V. and Chebotnikov, A. V. (2008): Discharge and energy-loss coefficients in flow through a breach in a trapezoidal dam. *Journal of Applied Mechanics and Technical Physics*, 49, 1, 53-57

Chang, D. S. and Zhang, L. M. (2010): Simulation of the erosion process of landslide dams due to overtopping considering variations in soil erodibility along depth. *Natural Hazards and Earth System Sciences*, 10, 933-946

Chanson, H. (2004): The hydraulics of open channel flow: An Introduction. *Elsevier Butterworth-Heinemann*, 2nd edition

Chaudhry, M.H. (2008): Open-channel flow. *Springer,* 2nd edition

Chow, V.T. (1986): Open-channel hydraulics, *McGraw-Hill Book Company,* International edition

Coleman, S.E., Andrews, D.P. and Webby, M.G., (2002.): Overtopping breaching of noncohesive homogeneous embankments. *Journal of Hydraulic Engineering*, 128(9), 829-838

Deltares (2009): Delft3D-FLOW user manual, Delft, the Netherlands

Endress+Hauser: Proline Prosonic Flow.

Ervine, D. A. and MacLeod, A. B. (1999): Modelling a river channel with distant. Floodbanks. *Proceedings of Institution of Civil Engineers, Water Maritime and Energy*, 136, 21-33

Fread, D.L. (1984): DAMBRK: The NWS dam-break flood forecasting model. *Office of Hydrology, National Weather Service Report,* Silver Spring, Maryland

Fread, D.L. (1988, revised in 1991): BREACH: An erosion model for earthen dam failures, *Hydrologic Research Laboratory, National Weather Service, NOAA*

Fritzi, M. and Hager, W.H. (1998): Hydraulics of embankment weirs. *Journal of Hydraulic Engineering*, 124, 9

Fujita, Y. and Tamura, T. (1987): Enlargement of breaches in flood levees on alluvial plains. *Journal of Natural Disaster Science*, 9(1), 37-60

Gögüs, M., Defne, Z. and Özkandemir, V. (2006): Broad-crested weirs with rectangular compound cross sections. *Journal of Irrigation and Drainage Engineering*, 132, 3, 272-280

Gonzalez , C.A. and Chanson, H. (2007): Experimental Measurements of Velocity and Pressure Distribution on a Large Broad-Crested Weir. *Flow Measurement and Instrumentation,* 18, 3-4, 107-113

Hager, W. H., and Schwalt, M. (1992): Broad-crested weir. *Journal of Irrigation and Drainage Engineering*, 120(1), 13-26

Han, K.-Y., Lee, J.-T., and Park, J.-H. (1998): Flood inundation analysis resulting from levee break. *Journal of Hydraulic Research*, 36, 5

Heller, V. (2011): Scale effects in physical hydraulic engineering models. *Journal of Hydraulic Research*, 49, 3, 293-306

Jain, S.C. (2001): Open-channel flow. *John Wiley & Sons*

Jan, C., Chang, C., and Kuo, F. (2009): Experiments on discharge equations of compound broad-crested weirs. *Journal of Irrigation and Drainage Engineering*, 135, 4

Kuiry, S.N., Sen, D. and Bates, P.D. (2010): Coupled 1D-Quasi-2D flood inundation model with unstructured grids. *Journal of Hydraulic Engineering*, 136, 8

Leeuwen, K.C. van. (2006): Modeling of submerged groynes in 1D hydraulic computations. MSc thesis, *University of Twente*, Enschede, the Netherlands

Li, B., Phillips, M., and Fleming, C. A. (2006): Application of 3D hydrodynamic model to flood risk assessment. *Proceedings of the Institution of Civil Engineers, Water Management*, 159, 63-75

Macchione, F. (2008): Model for predicting floods due to earthen dam breaching. I: Formulation and evaluation. *Journal of Hydraulic Engineering*, 134, 12

Mark, C.F. van der (2009): A semi-analytical form drag model for river bedforms. PhD thesis, *University of Twente*, Enschede, the Netherlands

Mark, C.F. van der, Blom, A., Uijttewaal, W. S. J., Hulscher, S. J. M. H. and Hoeijmakers, H. W. M. (2009): An analytically-based form drag model for river dunes. *Proceedings of the 6th IAHR Symposium on River, Coastal and Estuarine Morphodynamics*, 21-25, 845-852

Morris, M.W., Hassan, M.A.A.M. and Vaskinn, K.A. (2007): Breach formation: Field test and laboratory experiments, *Journal of Hydraulic Researc*h, 45:S1, 9-17

Munson, B.R, Young, D.F., and Okiishi, T.H. (2002): Fundamentals of fluid mechanics. *John Wiley & Sons*

Nguyen, B.T., (2006): Flow over oblique weirs. MSc thesis, *Delft University of*

Technology, Delft, the Netherlands

Nikolov, N.A., Minkov, I.N., Dimitrov, D.K., Mincheva, S.K. and Mirchev, M.A. (1978): Hydraulic calculation of a submerged broad-crested weir. *Power Technology and Engineering*, 12, 6, 631-634

Ramamurthy, A.S., Tim, U.S., and Rao, M.V.J. (1988): Characteristics of square-edged and round-nosed broad-crested weirs. *Journal of Irrigation and Drainage Engineering*, 114, 1

Rijn, L.C. Van (1994): Principles of fluid flow and surface waves in rivers, estuaries, seas and ocean. *Aqua Publications*, 2nd edition

Sargison, J.E. and Percy, A. (2009): Hydraulics of broad-crested weirs with varying side slopes. *Journal of Irrigation and Drainage Engineering*, 135, 1,115-118

Schmocker, L. and Hager, W.H. (2010): Overtopping and breaching of dikes - Breach profile and breach flow. *River Flow 2010*

Schiereck, G.J. (2007): Concise overview of scale rules in coastal engineering, Hanoi, Vietnam

Singh, V.P. (1996): Dam breach modeling technology. *Kluwer Academic Publishers*, Dordrecht, the Netherlands

Singh, V.P., and Quiroga, C.A. (1987): A dam-breach erosion model: I. Formulation. *Water Resources Management*, 1, 3, 177-197

Singh, V.P., Scarlatos, P.D., Collins, J.G. and Jourdan, M.R. (1988): Breach erosion of earthfill dams (BEED) model. *Natural Hazards*, 1, 2, 161-180

Visser, P.J. (1998): Breach growth in sand-dikes. PhD thesis, *Delft University of Technology*, Delft, the Netherlands

Vuik, V. (2010): Numerical modeling of sediment transport over hydraulic structures. MSc thesis, *Delft University of Technology,* Delft, the Netherlands

Wahl, T. L. (2010): Dam breach modeling - an overview of analysis methods. *Proceedings of Joint Federal Interagency Conference on Sedimentation and Hydrologic Modeling*, Las Vegas, USA

Wahl, T.L., Clemmens, A.J., Replogle, J.A., and Bos, M.G. (2007): Discussion of "Broad-Crested Weirs with Rectangular Compound Cross Sections" by M. Göğüş, Z. Defne, and V. Özkandemir. *Journal of Irrigation and Drainage Engineering*

Wurbs, R.A. (1987): Dam-breach flood wave models. *Journal of Hydraulic Engineering,* 113, 29

Yen, B.C. (2001): Open channel flow resistance. *Journal of Hydraulic Engineering*, 128, 1

Ying, X., and Wang, S.S.Y. (2005): Modeling flood inundation due to dam and levee breach. *Proceedings of US-China Workshop on Advanced Computational Modelling in Hydroscience and Engineering*, Oxford, Mississippi, USA

Zhang, H. and Wen, K. (2001): Flood control and management for large rivers in China. *Presented during the Workshop on Strengthening Capacity in Participatory Planning and Management for Flood Mitigation and Preparedness in Large River Basins: Regional Cooperation in Flood Control*

and Management in Asia and the Pacific, Bangkok, 20-23

Zhang, J., Li, Y., Xuan, G., Wang, X., and Li, J. (2009): Overtopping breaching of cohesive homogeneous earth dam with different cohesive strength. *Science in China Series E-Technological Sciences*, 52(10): 3024-3029

Zhu, Y., P.J. Visser and Vrijling, J.K. (2006): Laboratory observations of embankment breaching. *Proceedings of the 7th International Conference on Hydroscience and Engineering,* Philadelphia, USA

Zhu, Y. (2006): Breach growth in clay-dikes. PhD thesis, *Delft University of Technology*, Delft, the Netherlands

APPENDIX A: NUMERICAL RESULTS

A.1 Constant Upstream Water Level

It is a research option to keep the same upstream water level to see the flow behaviors for different cases. But in the laboratory experiment, it is not easy to do this in an efficient way. Therefore, the numerical model (Delft3D) is set-up for the situation. In the settings of Delft3D (Table (8-1)), the upstream boundary is changed to water level (0.16 m).

The outputs of water level distribution and corresponding depth averaged velocity for all cases are depicted in Figures (A-1) to (A-10). The following conclusion can be made:

(a). The effect of the breach to the upstream can be clearly seen from the area in front of the breach where the water level starts to drop. The water level difference is indicated by colors. Instead of straight streamlines, flow curvature caused by the breach occurs due to the contraction effect which is shown by the directions of arrows in the velocity distribution. Based on these indictors, one can conclude that with the same upstream water level, the enlargement of the breach would result in stronger contraction effects in overtopping condition, hence larger influenced area in the upstream.

(b). In the breach, the water level is lower than that over the crest, but at the end of the breach the flow acts as a jet flow which has a higher water level in the cross-section. Also, transverse flow components from crest to breach can be observed. These are confirmed by the present laboratory observations.

(c). As the breach is larger from cases 1 to 5, the discharge conveyance capacity through the weir also increases. For large breach sizes, the area of fast flow in the downstream also large. This may be taken into consideration when studying the downstream erosion or flood propagation. As can been seen, the relative fast flow occurs over the downstream weir slope and hydraulic jump forms at the zone with low water levels (dark blue) in the water level distribution. The hydraulic jumps are located at the end of the downstream slope and have a triangular shape behind the breach. The large discharges push the positions of hydraulic jumps further away from the weir, which is in line with the conclusion made before (see section 7.4). In the model, the upstream head is enough high that no eddy appears behind the weir.

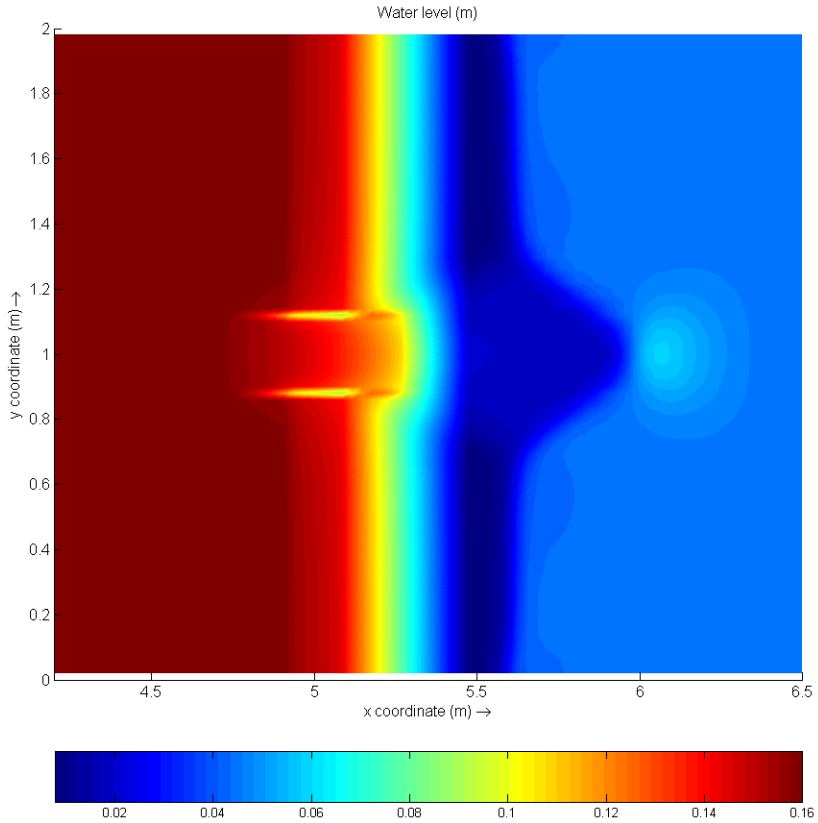

Figure (A - 1): The distribution of water level (case 1, upstream water level 0.16 m)

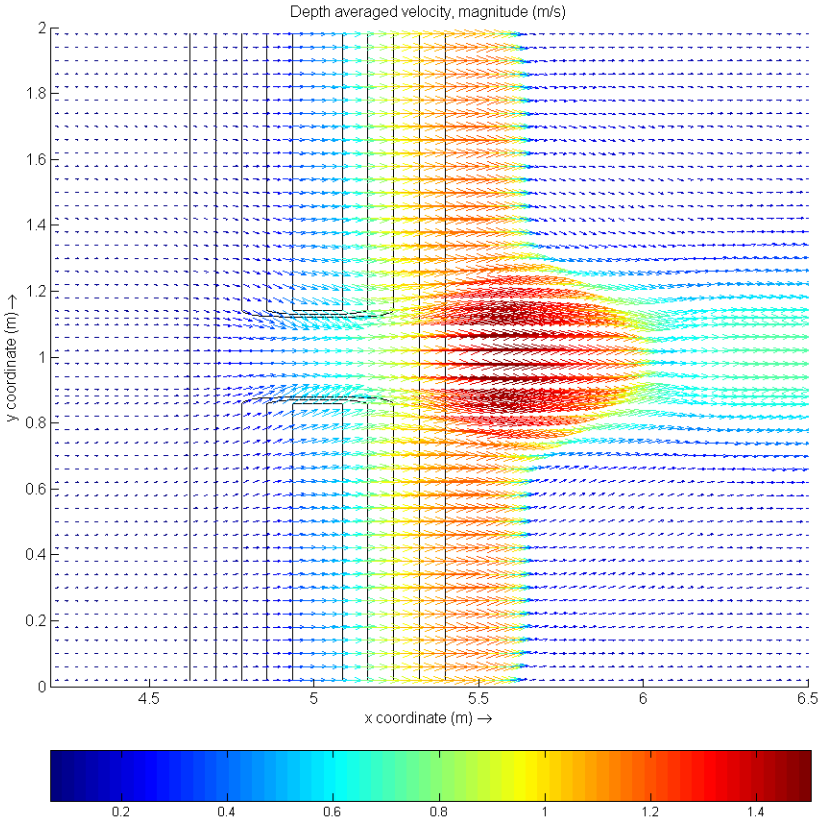

Figure (A - 2): The distribution of depth averaged velocity (case 1, upstream water level 0.16 m)

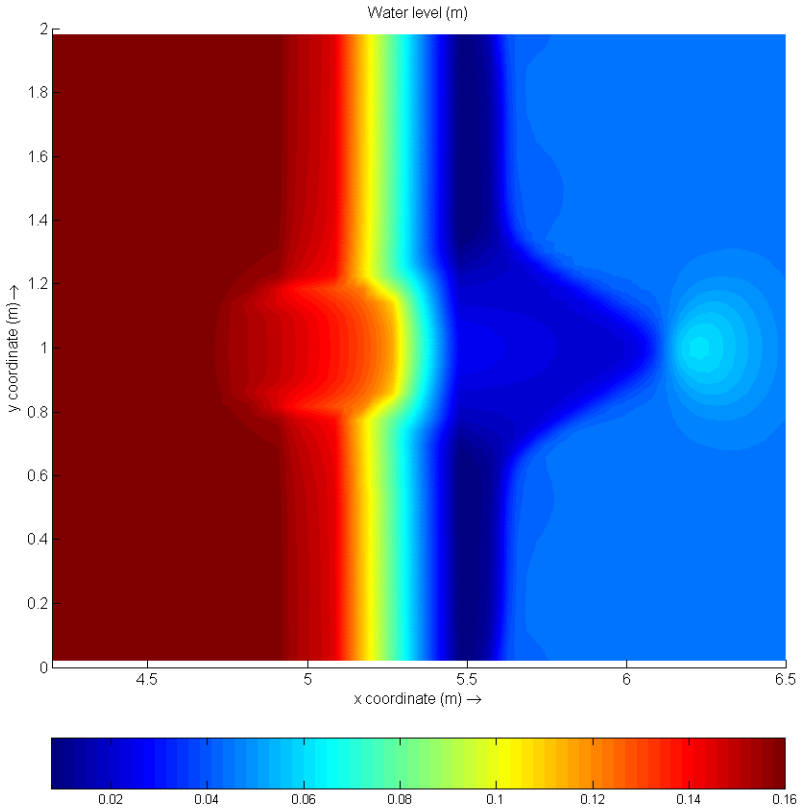

Figure (A - 3): The distribution of water level (case 2, upstream water level 0.16 m)

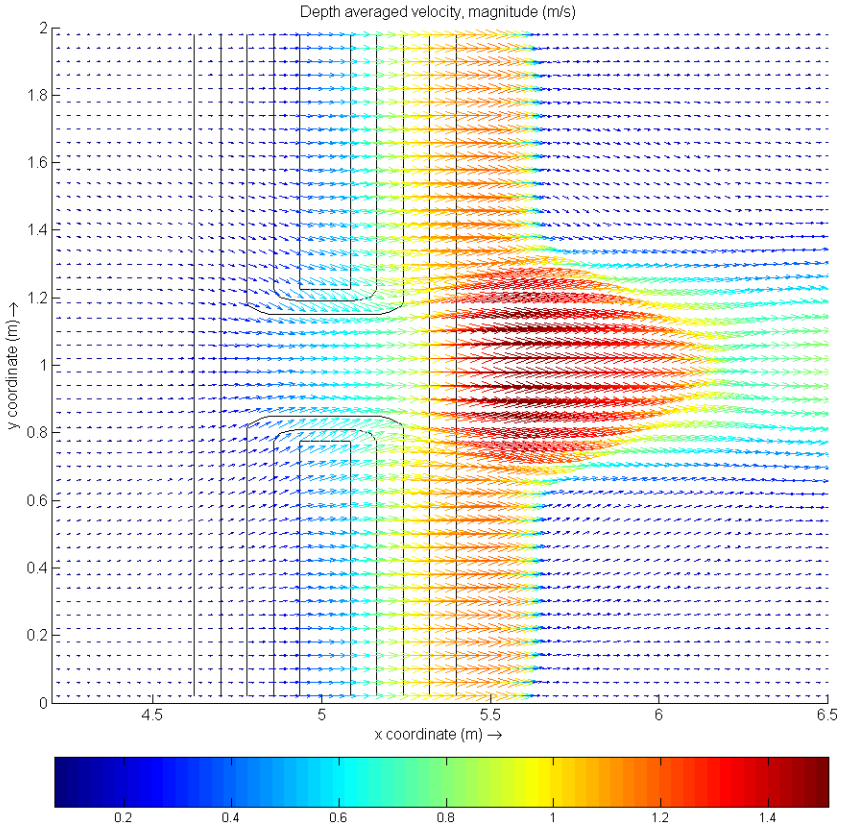

Figure (A - 4): The distribution of depth averaged velocity (case 2, upstream water level 0.16 m)

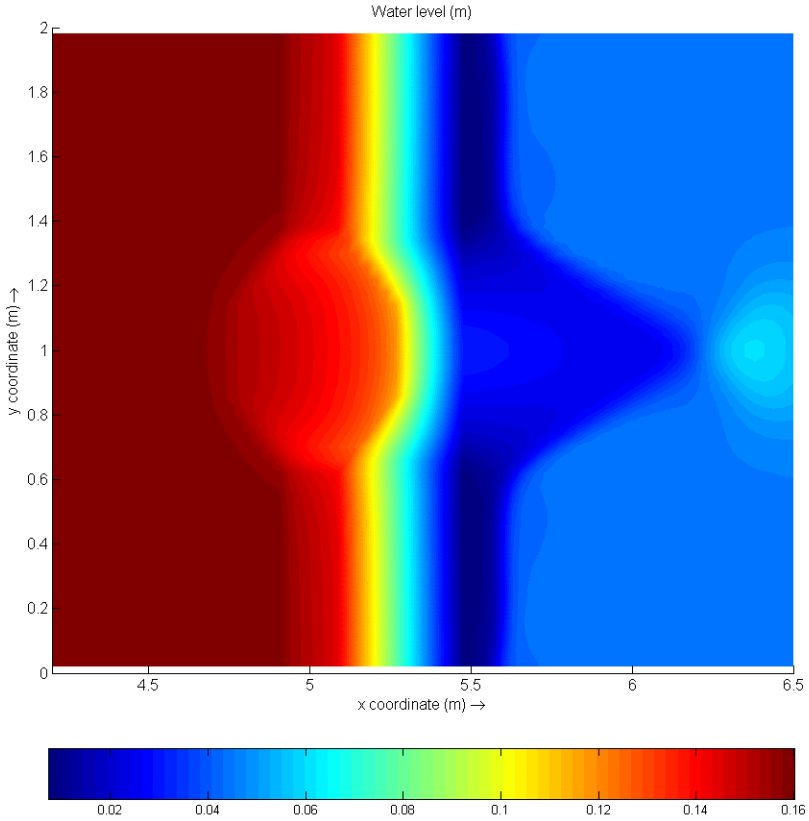

Figure (A - 5): The distribution of water level (case 3, upstream water level 0.16 m)

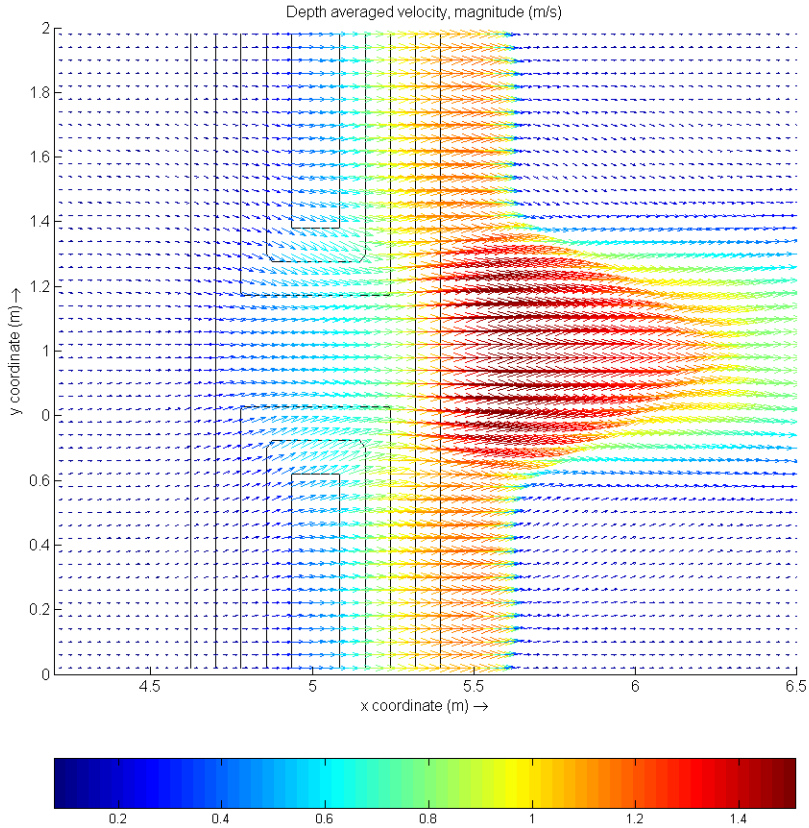

Figure (A - 6): The distribution of depth averaged velocity (case 3, upstream water level 0.16 m)

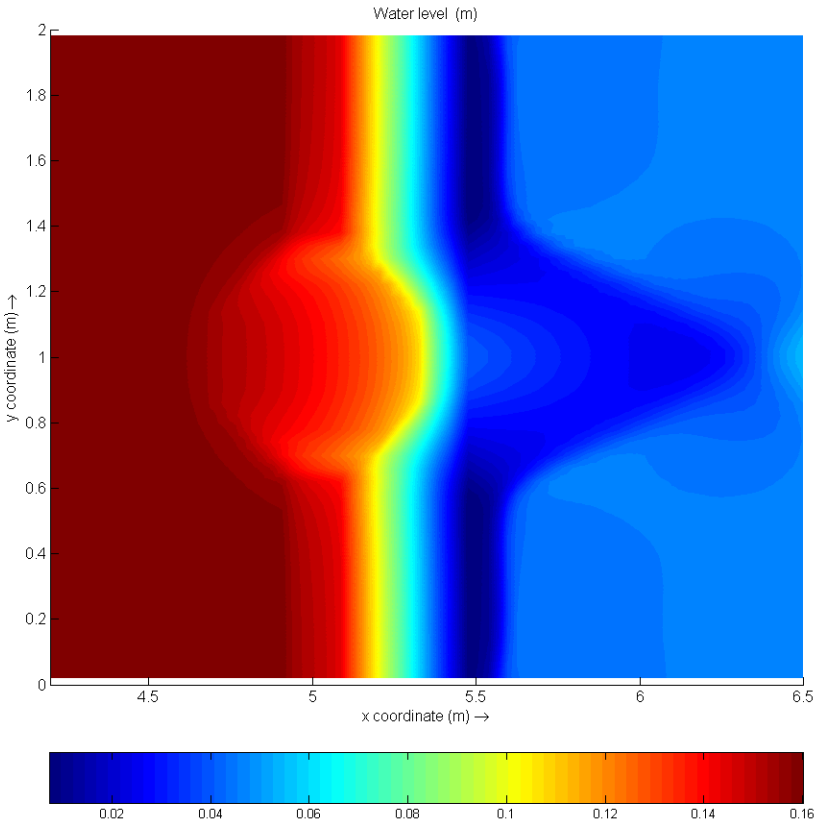

Figure (A - 7): The distribution of water level (case 4, upstream water level 0.16 m)

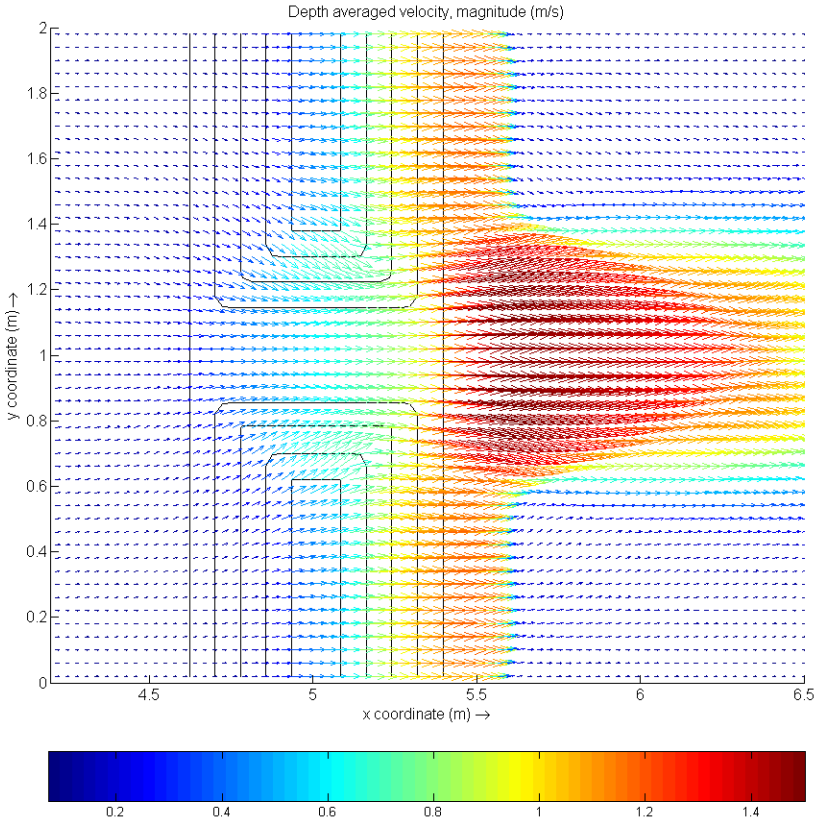

Figure (A - 8): The distribution of depth averaged velocity (case 4, upstream water level 0.16 m)

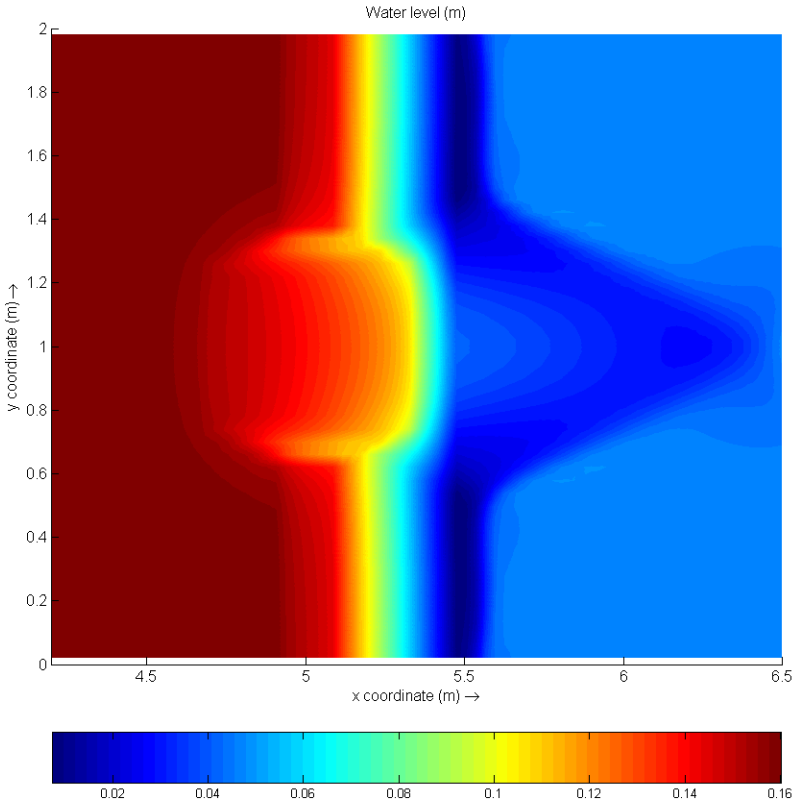

Figure (A - 9): The distribution of water level (case 5, upstream water level 0.16 m)

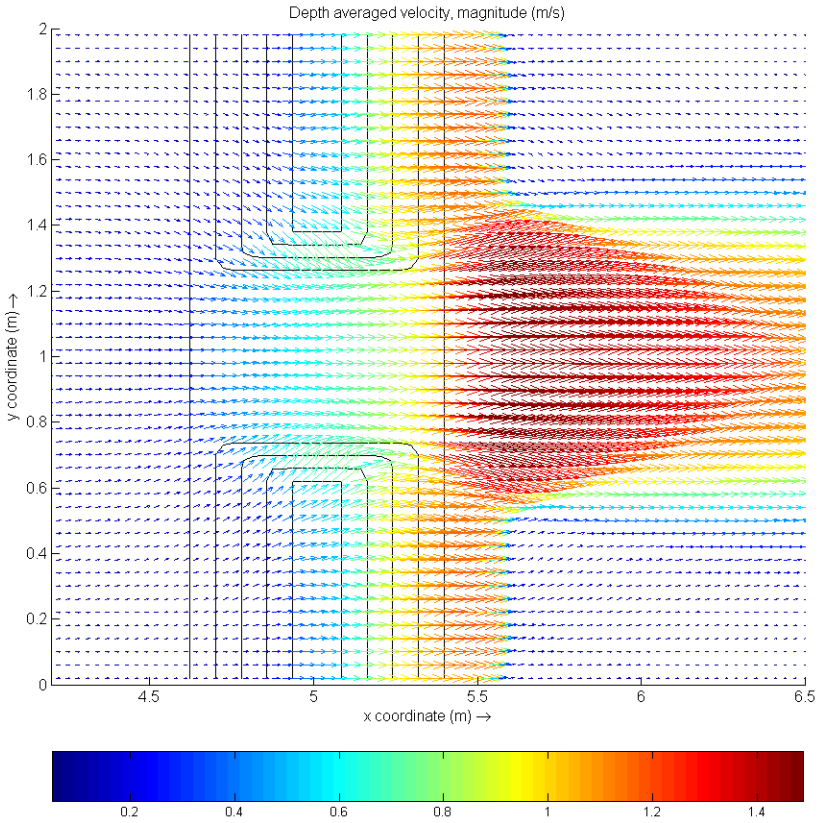

Figure (A - 10): The distribution of depth averaged velocity (case 5, upstream water level 0.16 m)

A.2 Constant Upstream Discharge

In addition to set same upstream water level, constant discharge (Q = 30 l/s) is applied at the upstream boundary for all cases. The distributions of water level and depth average velocity are presented in Figures (A-11) to (A-20). According to the figures, one can find that:

(a). At the same discharge, small sizes of breach lead to a higher upstream water level due to the low flow conveyance capacity. Still, the largest influence of breach to the upstream is caused by case 5. For large size of breach geometries (e.g. cases 4 and 5), the discharge over the weir crest are relatively low. As a result, the flow behind the breach is much faster compared to the surroundings and some eddies at the boundary wall can be seen from figures.

(b). Due to the small size of breach in case 1, the velocity over the weir quite high, especially at the end of breach where the flow is concentrated with really large speed. Moreover, the maximum velocity in the downstream of breach decreases with the enlargement of the breach. It is due to the increase of flow discharging capacity for larger breach size and reduced effect of sudden expansion.

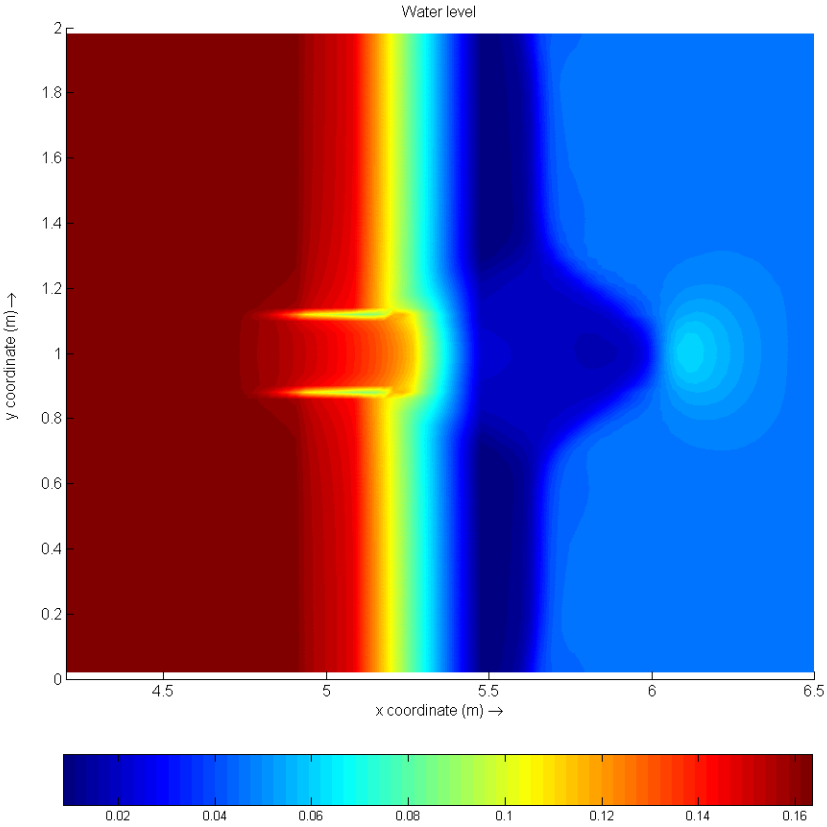

Figure (A - 11): The distribution of water level (case 1, Q = 30l/s)

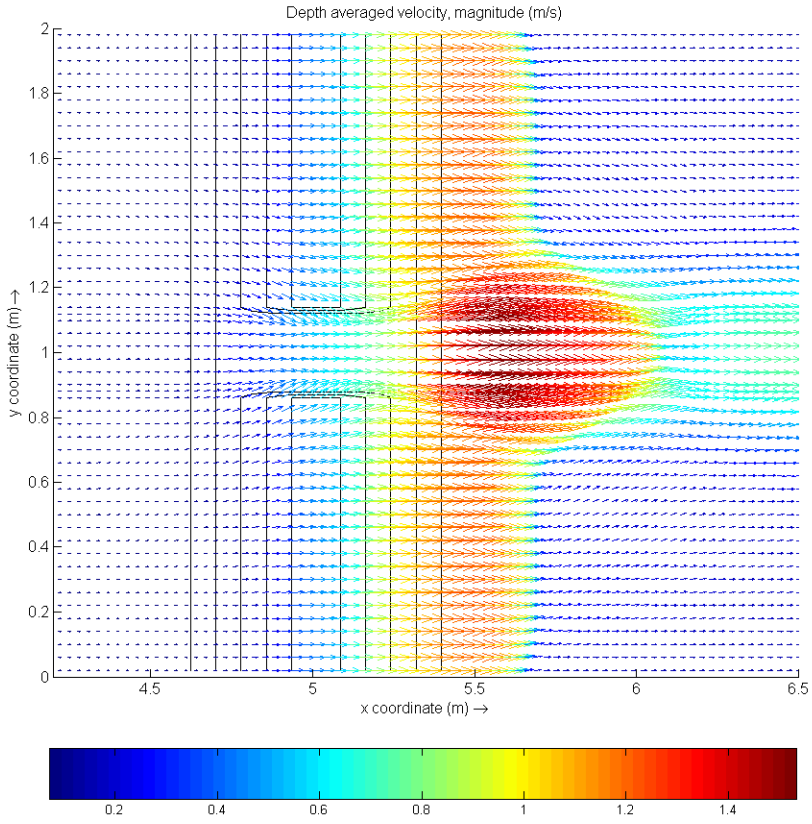

Figure (A - 12): The distribution of depth averaged velocity (case 1, Q = 30l/s)

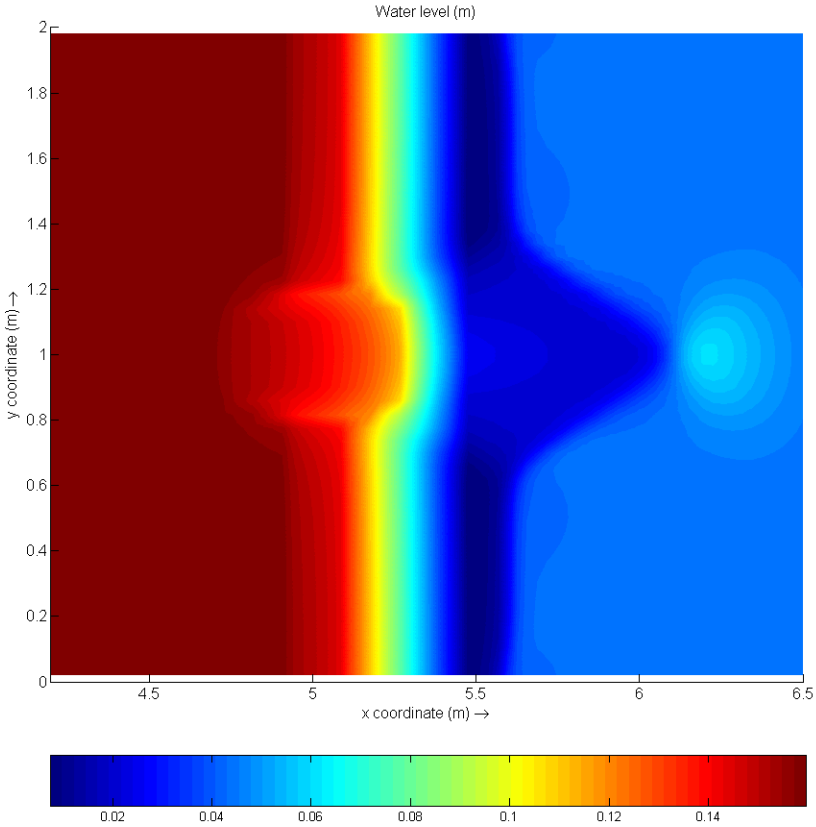

Figure (A - 13): The distribution of water level (case 2, Q = 30l/s)

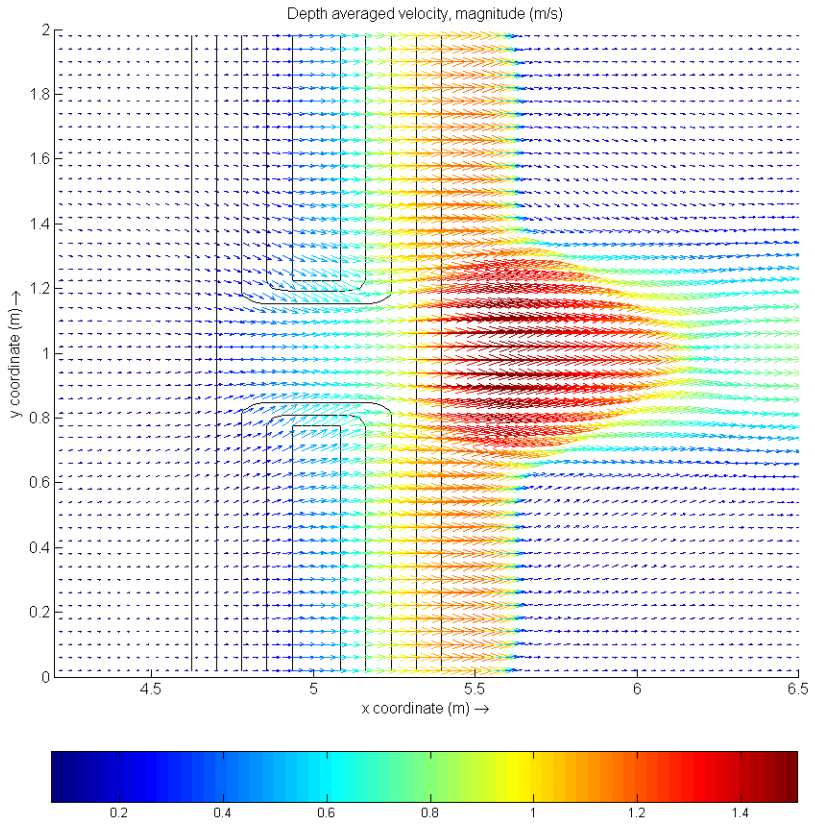

Figure (A - 14): The distribution of depth averaged velocity (case 2, Q = 30l/s)

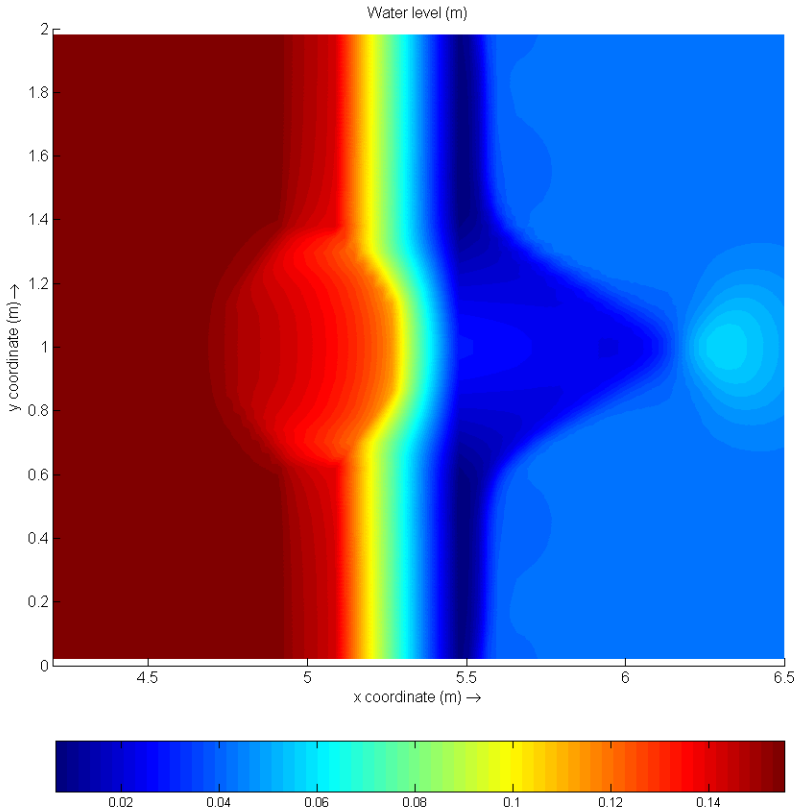

Figure (A - 15): The distribution of water level (case 3, Q = 30l/s)

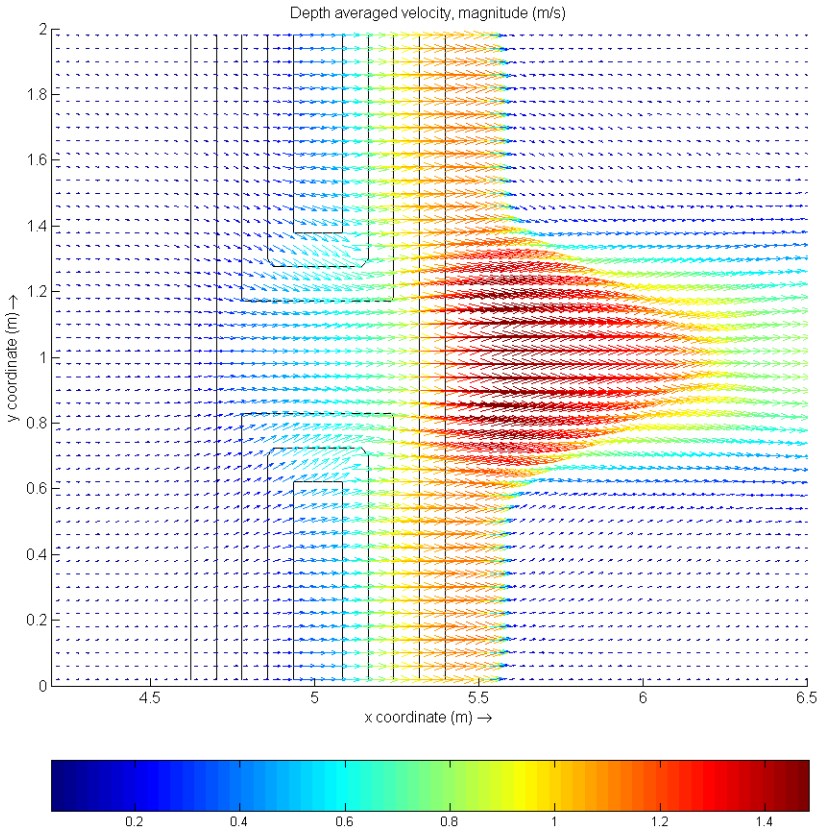

Figure (A - 16): The distribution of depth averaged velocity (case 3, Q = 30l/s)

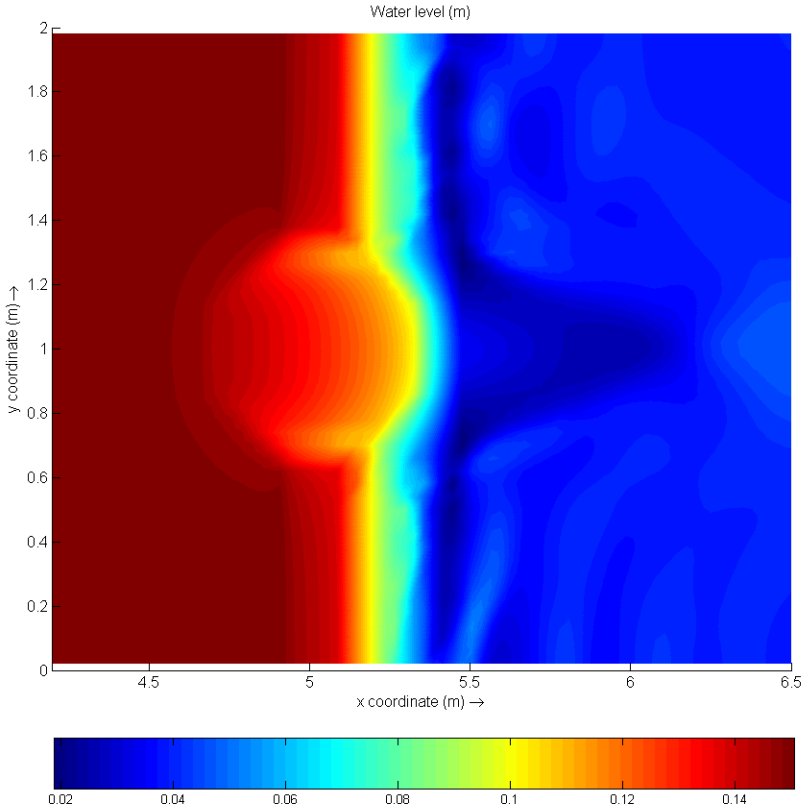

Figure (A - 17)：The distribution of water level (case 4, Q = 30l/s)

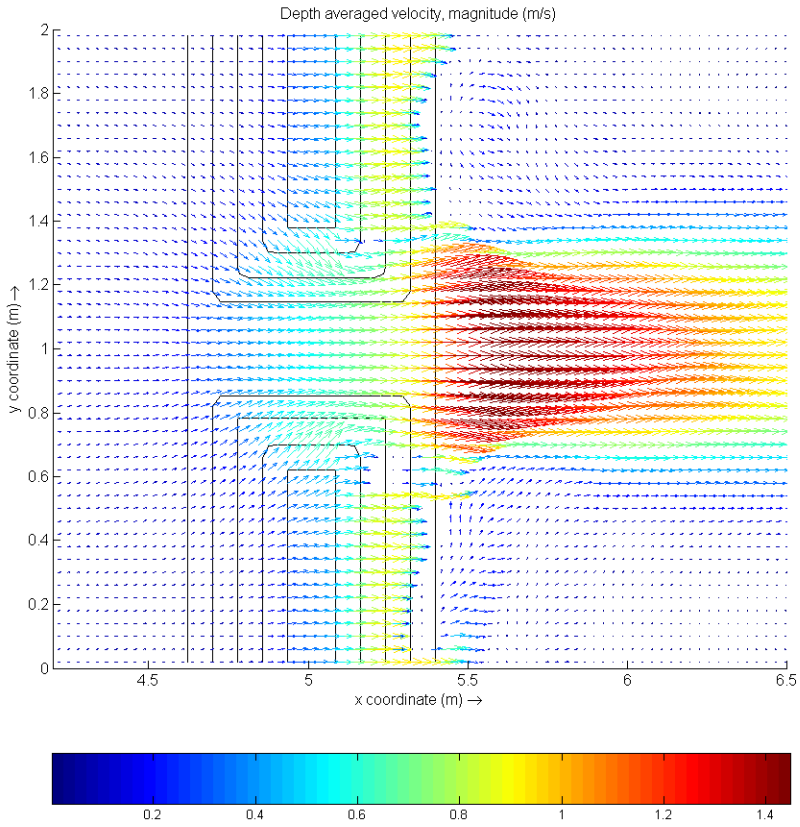

Figure (A - 18)：The distribution of depth averaged velocity (case 4, Q = 30l/s)

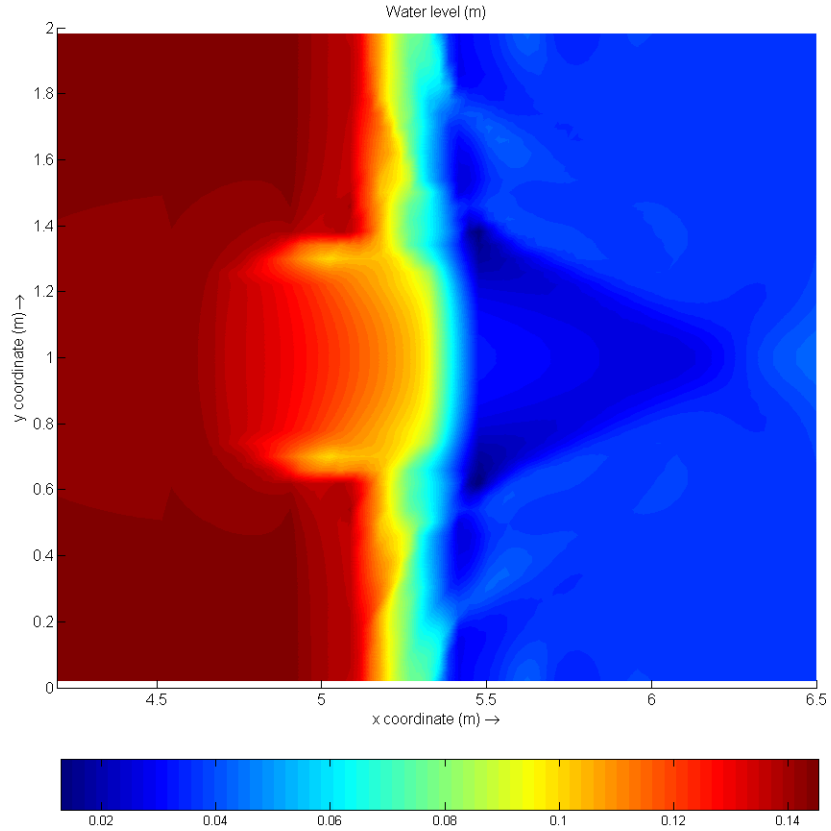

Figure (A - 19)：The distribution of water level (case 5, Q = 30l/s)

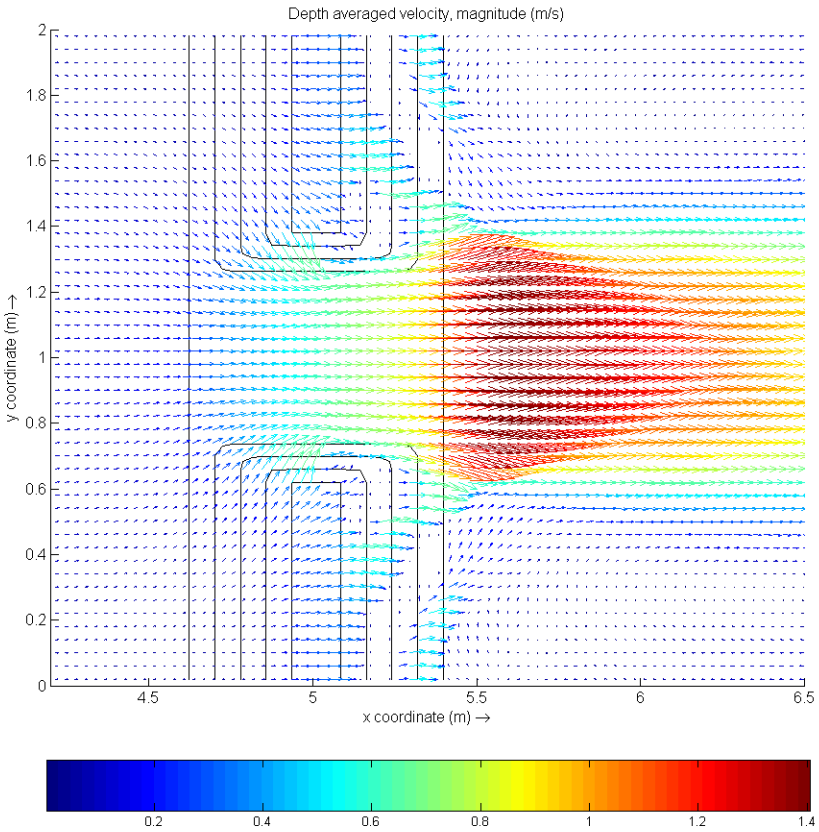

Figure (A - 20)：The distribution of depth averaged velocity (case 5, Q = 30l/s)

APPENDIX B: DATA COLLECTED IN THE LABORATORY EXPERIMENT

Table (B - 1): Discharges and water level differences in imperfect situation

Case 1	Q (l/s)	3	4	5	10	15	20	25	30	35				
	d_0 (mm)	121.8	126.8	130.9	140.5	147.2	153.2	158.8	163.6	168.3				
	d_2 (mm)	116.2	118.6	121.1	129.5	134.2	138.5	142.9	146.6	150.6				
	Δd (mm)	5.5	8.2	9.8	11	13	14.7	15.8	17	17.7				
Case 2	Q (l/s)	3	5	6	10	15	20	25	30	35	40			
	d_0 (mm)	115.9	125	129.7	137.4	144.4	150.2	155.8	160.6	165.4	169.7			
	d_2 (mm)	110.9	114.4	117.2	122.7	127.4	131.5	135.9	139.6	143.2	146.9			
	Δd (mm)	5	10.6	12.6	14.7	17	18.7	19.9	21.1	22.2	22.8			
Case 3	Q (l/s)	3	5	8	10	15	20	25	30	35	40	45		
	d_0 (mm)	109.4	116.7	127.5	132.5	139.7	146.1	151.9	156.5	161.4	165.6	169.9		
	d_2 (mm)	106	110.4	113.2	115.3	119.9	124.5	128.9	132.3	136.2	139.2	143.4		
	Δd (mm)	3.4	6.3	14.3	17.2	19.8	21.6	23	24.2	25.2	26.4	26.5		
Case 4	Q (l/s)	5	8	10	12	14	17	20	25	30	35	40	45	50
	d_0 (mm)	106.6	113	118.5	124.7	130.4	134.9	138.8	144.6	149.8	154.9	159.1	163.4	167.1
	d_2 (mm)	102.5	105.4	107.4	107.9	109.8	112.5	115.5	119.4	123.3	127.1	130.2	133.7	136.6
	Δd (mm)	4.1	7.5	11.1	16.8	20.6	22.3	23.3	25.1	26.4	27.8	29	29.8	30.6
Case 5	Q (l/s)	5	10	15	20	25	30	35	40	45	50	55	60	
	d_0 (mm)	104.8	113.8	124.4	132.8	138.9	144	148.8	153.6	157.7	161.9	166.2	169.7	
	d_2 (mm)	103.1	107.7	113.3	116.6	120.6	124.7	128.5	132.1	135.1	138.4	141.7	144.4	
	Δd (mm)	1.8	6.2	11	16.2	18.2	19.3	20.2	21.6	22.6	23.4	24.5	25.2	

Table (B - 2): Water levels with increasing tail gate height in imperfect situation

case 1	Q (l/s)	10	10	10	20	20	20	30	30	30						
	h_0 (mm)	140	142.3	148.4	153.3	154.6	160	163.2	163.5	166.6						
	h_2 (mm)	125.8	136.8	146.8	137.5	148.2	157.2	140.2	151.4	161.3						
	Δh (mm)	14.2	5.5	1.6	15.8	6.4	2.8	23	12.2	5.3						
case 2	Q (l/s)	10	10	10	20	20	20	30	30	30						
	h_0 (mm)	138.1	142.6	150.5	150.1	151.7	157.4	160.8	161.8	166.6						
	h_2 (mm)	128.2	140	149.6	131.5	143.9	154.5	141.8	152.4	162.3						
	Δh (mm)	9.9	2.6	1	18.6	7.8	3	19	9.4	4.3						
case 3	Q (l/s)	20	20	20	30	30	30	40	40	40						
	h_0 (mm)	146.6	148.8	154.4	157.1	159	164.4	166.1	167.5	171.9						
	h_2 (mm)	130.7	141.6	151.6	138.6	150.9	160.5	147.3	159.2	167.2						
	Δh (mm)	15.7	7.1	2.8	18.5	8.1	3.8	18.8	8.3	4.6						
case 4	Q (l/s)	20	20	20	30	30	30	40	40	40	40	50	50	50	50	50
	h_0 (mm)	139.7	142.7	146.9	150.7	152.6	155.4	159.3	159.6	160.4	162.2	166.3	166.8	167.1	167.4	167.9
	h_2 (mm)	120.9	132.2	142.5	130.2	139.2	148.2	118.6	128.5	138.6	148.7	93.6	106.8	118.3	129.1	141.2
	Δh (mm)	18.8	10.5	4.4	20.6	13.4	7.3	40.6	31.1	21.8	13.4	72.7	60	48.8	38.3	26.7
case 5	Q (l/s)	20	20	20	20	30	30	30	40	40	40	50	50	50	50	
	h_0 (mm)	130.1	133.4	137.1	142.5	144.44	148	151.9	153.6	155.6	160.7	161.4	162.9	166.4	171.9	
	h_2 (mm)	108	118.3	127.1	138	124.8	136.4	145.4	134.7	141.3	156.5	132.5	143.6	155	165.3	
	Δh (mm)	22.1	15	10	4.6	19.6	11.6	6.5	18.8	14.3	4.2	28.9	19.4	11.3	6.6	

Table (B - 3): Depth averaged velocity over weir

case 1	*Q = 4 l/s*	u (m/s)	0.58436	0.53217	0.589225						
		cross-sectional position (m)	0.95	1	1.05						
	Q = 20 l/s	u (m/s)	0.362887	0.359531	0.334433	0.411254	0.656938	0.661967			
		cross-sectional position (m)	0.08	0.24	0.56	0.76	0.95	1			
		u (m/s)	0.647494	0.490454	0.405706	0.387462	0.374592	0.371511			
		cross-sectional position (m)	1.05	1.24	1.44	1.6	1.76	1.92			
	Q = 30 l/s	u (m/s)	0.426438	0.465748	0.496684	0.545451	0.678692	0.656977			
		cross-sectional position (m)	0.08	0.24	0.56	0.76	0.95	1			
		u (m/s)	0.648609	0.58437	0.526672	0.517974	0.519636	0.504924			
		cross-sectional position (m)	1.05	1.24	1.44	1.6	1.76	1.92			
case 5	*Q = 20 l/s*	u (m/s)	0.789538	0.712425	0.809313						
		cross-sectional position (m)	1.15	1	0.85						
	Q = 50 l/s	u (m/s)	0.336229	0.448337	0.477787	0.485293	0.52228	0.581189	0.758664	0.719905	0.709992
		cross-sectional position (m)	0.02	0.09	0.22	0.34	0.46	0.58	0.83	0.915	1
		u (m/s)	0.717436	0.75387	0.569382	0.566512	0.541974	0.514973	0.461301	0.437136	
		cross-sectional position (m)	1.085	1.17	1.42	1.54	1.66	1.78	1.91	1.98	

APPENDIX C: ADDITIONAL TABLES AND FIGURES USED IN THE REPORT

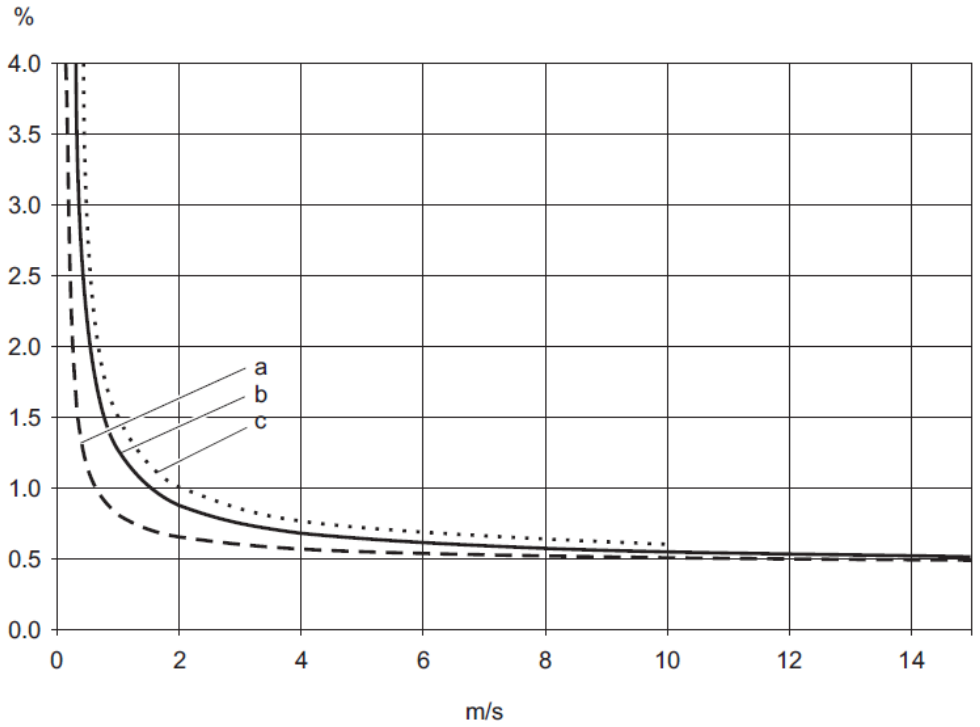

Figure (C - 1): Maximum measured error for wet calibration and verification of accuracy in % of reading (Endress+Hauser)

Table (C - 1): Values of the ratio d_c / H_0 as a function of m and H_0 / b for trapezoidal control sections (Bos, 1989)

		Side slopes, ratio of horizontal to vertical (*m:1*)								
H_0/b	vertical	0.25:1	0.5:1	0.75:1	1:1	1.5:1	2:1	2.5:1	3:1	4:1
0.000	0.667	0.667	0.667	0.667	0.667	0.667	0.667	0.667	0.667	0.667
0.010	0.667	0.667	0.667	0.668	0.668	0.669	0.670	0.670	0.671	0.672
0.020	0.667	0.667	0.668	0.669	0.670	0.671	0.672	0.674	0.675	0.678
0.030	0.667	0.668	0.669	0.670	0.671	0.673	0.675	0.677	0.679	0.683
0.040	0.667	0.668	0.670	0.671	0.672	0.675	0.677	0.680	0.683	0.687
0.050	0.667	0.668	0.670	0.672	0.674	0.677	0.680	0.683	0.686	0.692
0.060	0.667	0.669	0.671	0.673	0.675	0.679	0.683	0.686	0.690	0.696
0.070	0.667	0.669	0.672	0.674	0.676	0.681	0.685	0.689	0.693	0.699
0.080	0.667	0.670	0.672	0.675	0.678	0.683	0.687	0.692	0.696	0.703
0.090	0.667	0.670	0.673	0.676	0.679	0.684	0.690	0.695	0.698	0.706
0.100	0.667	0.670	0.674	0.677	0.680	0.686	0.692	0.697	0.701	0.709
0.120	0.667	0.67 1	0.675	0.679	0.684	0.690	0.696	0.701	0.706	0.715
0.140	0.667	0.672	0.676	0.681	0.686	0.693	0.699	0.705	0.711	0.720
0.160	0.667	0.672	0.678	0.683	0.687	0.696	0.703	0.709	0.715	0.725
0.180	0.667	0.673	0.679	0.684	0.690	0.698	0.706	0.713	0.719	0.729
0.200	0.667	0.674	0.680	0.686	0.692	0.701	0.709	0.717	0.723	0.733
0.220	0.667	0.674	0.681	0.688	0.694	0.704	0.712	0.720	0.726	0.736
0.240	0.667	0.675	0.683	0.689	0.696	0.706	0.715	0.723	0.729	0.739
0.260	0.667	0.676	0.684	0.691	0.698	0.709	0.718	0.725	0.732	0.742
0.280	0.667	0.676	0.685	0.693	0.699	0.711	0.720	0.728	0.734	0.744
0.300	0.667	0.677	0.686	0.694	0.701	0.713	0.723	0.730	0.737	0.747
0.320	0.667	0.678	0.687	0.696	0.703	0.715	0.725	0.733	0.739	0.749
0.340	0.667	0.678	0.689	0.697	0.705	0.717	0.727	0.735	0.741	0.751
0.360	0.667	0.679	0.690	0.699	0.706	0.719	0.729	0.737	0.743	0.752

Table (C - 2): Values of the ratio d_c / H_0 as a function of m and H_0 / b for trapezoidal control sections (Bos, 1989) (continued)

H_0/b	vertical	0.25:1	0.5:1	0.75:1	1:1	1.5:1	2:1	2.5:1	3:1	4:1
0.380	0.667	0.680	0.691	0.700	0.708	0.721	0.731	0.738	0.745	0.754
0.400	0.667	0.680	0.692	0.701	0.709	0.723	0.733	0.740	0.747	0.756
0.420	0.667	0.681	0.693	0.703	0.711	0.725	0.734	0.742	0.748	0.757
0.440	0.667	0.681	0.694	0.704	0.712	0.727	0.736	0.744	0.750	0.759
0.460	0.667	0.682	0.695	0.705	0.714	0.728	0.737	0.745	0.751	0.760
0.480	0.667	0.683	0.696	0.706	0.715	0.729	0.739	0.747	0.752	0.761
0.500	0.667	0.683	0.697	0.708	0.717	0.730	0.740	0.748	0.754	0.762
0.600	0.667	0.686	0.701	0.713	0.723	0.737	0.741	0.754	0.759	0.167
0.700	0.667	0.688	0.706	0.718	0.728	0.742	0.752	0.758	0.764	0.771
0.800	0.667	0.692	0.709	0.723	0.732	0.746	0.756	0.762	0.767	0.774
0.900	0.667	0.694	0.713	0.727	0.737	0.750	0.759	0.766	0.770	0.776
1.000	0.667	0.697	0.717	0.730	0.740	0.754	0.762	0.768	0.773	0.778
1.200	0.667	0.701	0.723	0.737	0.747	0.759	0.767	0.772	0.776	0.782
1.400	0.667	0.706	0.729	0.742	0.752	0.764	0.771	0.776	0.779	0.784
1.600	0.667	0.709	0.733	0.747	0.756	0.767	0.774	0.778	0.781	0.786
1.800	0.667	0.713	0.737	0.750	0.759	0.770	0.776	0.781	0.783	0.787
2.000	0.667	0.717	0.740	0.754	0.762	0.773	0.778	0.782	0.785	0.788
3.000	0.667	0.730	0.753	0.766	0.773	0.781	0.785	0.787	0.790	0.792
4.000	0.667	0.740	0.762	0.773	0.778	0.785	0.788	0.790	0.792	0.794
5.000	0.667	0.748	0.768	0.777	0.782	0.788	0.791	0.792	0.794	0.795
10.000	0.667	0.768	0.782	0.788	0.791	0.794	0.795	0.796	0.797	0.798
∞		0.800	0.800	0.800	0.800	0.800	0.800	0.800	0.800	0.800